

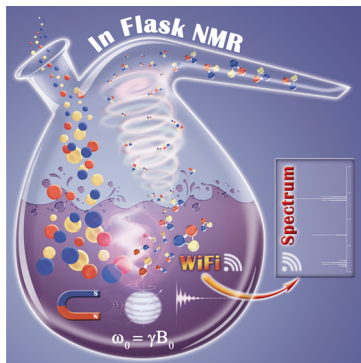
Miniaturization of NMR Systems: Desktop Spectrometers, Microcoil Spectroscopy, and “NMR on a Chip” for Chemistry, Biochemistry, and Industry

Sergey S. Zaleskiy,[†] Ernesto Danieli,[‡] Bernhard Blümich,^{*,‡} and Valentine P. Ananikov^{*,†,§}

[†]Zelinsky Institute of Organic Chemistry, Russian Academy of Sciences, Moscow, 119991, Russia

[‡]Institut für Technische Chemie und Makromolekulare Chemie, RWTH Aachen University, Worringerweg 1, D-52074 Aachen, Germany

[§]Department of Chemistry, Saint Petersburg State University, Stary Peterhof, 198504, Russia



CONTENTS

1. Introduction	5641
2. Development of Equipment for NMR Miniaturization	5642
2.1. Magnet Development and Design	5643
2.2. Electronics and Radiofrequency Transmission Part	5649
2.3. Probes and Microcoil Systems Development	5652
2.4. New Designs and Alternative Detection Methods	5661
2.5. Perspectives of Hardware Miniaturization	5663
3. Properties and Applications of Miniaturized NMR	5665
3.1. Flow Systems and LC-NMR	5665
3.2. NMR on a Chip and Total Analysis Systems (TAS)	5669
3.3. In Vivo Studies	5673
3.4. Industrial Applications	5676
3.4.1. Rubber and Polymer Materials	5676
3.4.2. Concrete and Building Materials	5678
3.4.3. Cultural Heritage	5679
3.4.4. Plant Phenotyping	5680
3.4.5. Pharmaceutical Industry	5680
3.4.6. Food Industry	5681
3.4.7. Process Analysis and Control	5683
4. Conclusions	5686
Author Information	5687
Corresponding Authors	5687
Notes	5687
Biographies	5687
Acknowledgments	5688
References	5688

1. INTRODUCTION

Nuclear magnetic resonance spectroscopy (NMR) nowadays is one of the most powerful and versatile analytical methods for modern organic chemistry,¹ catalysis,² biology,³ medicine,⁴ and industry.⁵ Rapid development of hardware equipment, experimental methodology, and processing software in the recent decades enabled numerous applications and led to breakthrough discoveries in the field of chemical reaction mechanisms.

The unique feature of the NMR approach is the diversity of chemical and physical properties at different structural levels that can be accessed using a single instrument. On the basis of a few measured fundamental characteristics (chemical shifts, coupling constants, relaxation times), one can deduce complete chemical structures at the level of interatomic bonds,⁶ rapidly identify the molecules of interest in complex mixtures,⁷ study dynamics of molecules,⁸ and characterize conformational behavior.⁹ Moving to the upper molecular organization level, it is possible to discriminate the phase composition of the sample,¹⁰ study reactions in media with varying polarity,¹¹ characterize the mobility of catalysts or certain catalytic sites,¹² and get high-resolution images of the internal structure of an object in real time even if the object is a living organism.¹³

The state-of-the-art of modern science brings a number of outstanding research challenges. In the field of chemistry, these include green chemistry procedures, especially cost-efficient and sustainable production of chemicals and pharmaceuticals. Highly efficient, selective, stable, and recyclable catalysts as well as protocols for asymmetric transformations are key requirements for modern catalysis. NMR spectroscopy has been recognized as a valuable tool for promoting research in organic synthesis and catalysis.^{14,15} Moreover, NMR has become a proven instrument for metabolomic¹⁶ and structural studies¹⁷ in biology. An emerging area is the application of NMR for “in cell” biological studies where a variety of fascinating findings have been reported.¹⁸ One of the most well-known applications of NMR to medicine is magnetic resonance imaging (MRI).^{4,19} Beyond that, NMR is widely used to study drug distributions *in vivo*²⁰ or to control product quality in pharmaceuticals.²¹ For industry-oriented applications, an important goal is the implementation of nondestructive analysis and control, which can be combined with high throughput quality control

Received: February 1, 2013

Published: April 29, 2014

procedures. Equally important are analytical applications for purity control, adequate risk assessment, and safe production of chemicals.

To address these global challenges, it is necessary to rethink existing NMR equipment all along and to create fundamentally new tools and approaches. There are several requirements that need to be fulfilled to meet the contemporary developments of chemical science.

NMR has the important advantage of simplicity when identifying chemical structures in liquid and solid samples, and, together with X-ray analysis and mass spectrometry, it is a primary research tool (Table 1).²² However, achievement of

Table 1. Sample Amounts and Concentrations Required To Carry Out X-ray, NMR, and MS Studies of Organic and Organoelement Compounds in Regular Laboratory Applications (Including Sample Preparation and Analysis)²²

method	minimal amount of sample, mg		concentration range (mol/L)
	routine	advanced	
X-ray single-crystal analysis	50	10	not applicable
NMR spectroscopy	0.01–5	10^{-6} – 10^{-2}	10^{-6} –1
mass spectrometry	10^{-6} – 10^{-3}	10^{-12} – 10^{-6}	10^{-12} – 10^{-5}

high sensitivity in standard NMR experiments is of paramount importance. It is well-known that the intrinsic sensitivity of NMR is quite low as compared to other analytical techniques such as mass spectrometry.²³ This situation arises from the fact that even at the highest magnetic field available (23.5 T), the relative population difference between the energy levels of the NMR transitions is still about 10^{-4} . One way to accommodate the low sensitivity is to use large amounts of samples. However, for each magnet geometry, the ratio between magnet size and the size of the sensitive volume is roughly constant. So, when the size of the magnet is reduced, a smaller volume of high field homogeneity is generated, and thereby sensitivity is sacrificed. Moreover, advanced applications require operation of NMR instruments at the level of 10^{-6} – 10^{-2} mg of sample, which severely challenges the detection capabilities of NMR devices.

Another significant factor that still limits the widespread application of NMR in medicine, biology, and industrial settings is the size of the currently available NMR equipment. The particular demands for site planning and the lack of mobility complicate the integration of NMR into clinical *in vivo* cell and tissue studies, and the implementation of such devices as quality control tools in industrial production lines. Compact and portable NMR and MRI scanners are required for effective use in the field.

Additionally, another argument favoring NMR miniaturization is the cost of modern hardware. For some applications, using permanent magnets instead of superconducting magnets decreases not only the magnet size by 1 or 2 orders of magnitude, but also dramatically reduces the operational cost due to the absence of cryogenic coolants. Upgrading the radiofrequency (RF) part with modern integrated high-performance electronics is another way to further decrease the size and total cost of the system.

Indeed, landmark discoveries have demonstrated proof of principle for NMR miniaturization, microcoil, and microchip NMR. Small benchtop NMR machines based on permanent magnets have been developed during the last years with varying

performance covering applications involving relaxometry, imaging, and even spectroscopy studies with hand-held systems.^{24–31,69} An impressive reduction of the size of permanent magnets was possible because of extensive research oriented to control the homogeneity of the magnetic field generated by arrays built from permanent magnet blocks. The control of magnet homogeneity was the main limiting factor for the miniaturization of the magnets in the past. Although rare earth alloys, such as neodymium iron boron (NdFeB) or samarium cobalt (SmCo), will generate magnetic fields lower than those obtained with superconducting technology, the possibility to have compact and robust magnets that can be installed where the measurements need to be performed justifies their use for many scientific and industrial applications. Moreover, the magnetic field is generated without consumption of external power, and the magnet does not generate maintenance costs.

Another milestone en route to reducing the size of NMR equipment was the improvement of sensitivity obtained with the development of miniature radio frequency coils used to excite and detect the NMR signals of mass-limited samples.^{32–35} Because the sensitivity of the coil is inversely proportional to its diameter, by decreasing the coil size, sample volumes of the order of nanoliters could be analyzed by high-resolution NMR spectroscopy in just a few minutes. Applications in combinatorial chemistry, the characterization of extracts from natural products, as well as the chance to hyphenate NMR with other analytical methods have been demonstrated.^{36,37} Moreover, MRI of single neurons and cells is possible.³⁸

Recent advances in microelectronics technology opened the door to scale down the size of the spectrometer electronics, which represent another key component of the NMR system. It is now possible to integrate the pulse programmer, the transmitter, receiver, and digital signal processor (DSP) on a circuit platform such as a field-programmable gate array (FPGA)^{39,40} or custom complementary metal–oxide–semiconductor (CMOS).⁴¹ This technology leads to hand-held NMR devices. In this Review, we address state-of-the-art of NMR miniaturization paying special attention to particular chemical, biological, and industrial applications that become possible with the equipment discussed.

2. DEVELOPMENT OF EQUIPMENT FOR NMR MINIATURIZATION

The use of NMR is based on the magnetic properties of the nuclei that compose different materials and tissues. Nuclei with magnetic moments, such as ^1H , ^{13}C , ^{15}N , ^{19}F , etc., when placed in an external magnetic field B_0 , can be excited with an electromagnetic wave whose frequency (Larmor frequency) is proportional to the strength of B_0 . The response of the nuclei to this excitation provides information concerning: (1) the local magnetic field that each nucleus experiences; this feature is fundamental to both molecular structure determination in chemical analysis and MRI in medical diagnostics; (2) interactions of the nuclei with its surrounding electrons, neighbor nuclei, and molecules, which affect the build-up time of the magnetic order of the nuclei (characterized by the longitudinal relaxation time T_1) and the lifetimes of the coherences generated by the RF waves (characterized by transverse relaxation times T_2); (3) the density or the amount of nuclei within the detection volume; and (4) molecular mobility. As NMR can access this information noninvasively, it

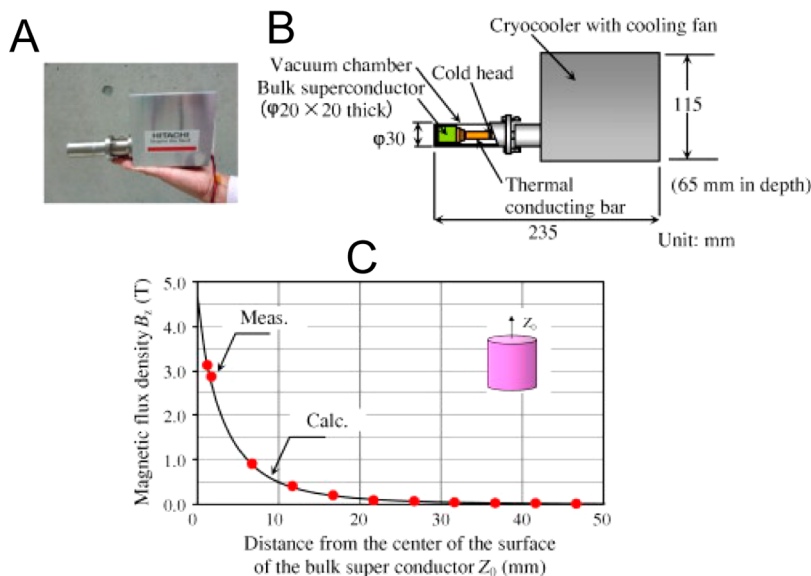


Figure 1. Miniature HTS bulk magnet system: (A) hand-held superconducting magnet; (B) drawing of the system showing the magnet, vacuum chamber, and cryocooler; and (C) magnetic field strength measured along the cylinder axis at different z positions. Reprinted with permission from ref 54. Copyright 2012 Elsevier.

is a powerful technique widely used for studying molecular and material properties in chemistry, biology, medicine, physics, and material science.

In general terms, a typical NMR sensor consists of a magnet that generates a stable magnetic field B_0 , an RF generator, a probe with an RF coil close to the sample to generate a variable magnetic field B_1 that interacts with the nuclear spins in the sample, a receiver that amplifies the weak signal generated in the sample, and further electronics responsible for synchronizing the different components and to store the data.⁴² The characteristics of each of these components depend on the particular application. Within the present section, the most commonly used NMR system components will be highlighted stressing the different approaches for their size reduction as well as their corresponding advantages for the applications in mind.

2.1. Magnet Development and Design

One of the most straightforward ways to improve both spectral resolution and NMR sensitivity is the design of new ultrahigh field magnets. Typically, these magnets consist of multi layer solenoids, that is, multicoil arrays wound in helix form and made of superconducting wire. However, a serious and partly insurmountable obstacle for superconducting magnets is the critical magnetic field that can be achieved without loss of the superconductivity. For the originally developed NbTi multifilament superconducting wire, the maximum field strength achieved at liquid He temperature (4.2 K) is about 10 T, which is slightly above 400 MHz in terms of proton frequency. Changing NbTi to Nb₃Sn in 1979 allowed pushing the maximal field limit up to 13 T (~550 MHz for ¹H).⁴³ One of the possible solutions to achieve higher fields without changing the material of the wire was to lower the temperature of the superconducting coil. This would allow increasing the critical current in the wire at certain frequency, which has two main benefits. First, this would allow reducing the cross-section of the superconducting wire resulting in significant reduction of overall magnet size. Second, it would allow increasing the maximum critical field, giving access to higher-field instruments. This solution was employed in ultrahigh-field magnets ranging

from 750 to 900 MHz proton frequency.⁴³ By reducing the temperature of the inner dewar with the superconducting coil from 4.2 to 1.8 K by Joule–Thomson cooling, the limit of 21 T (900 MHz for ¹H) could be reached.

Extensive studies in the field of high-temperature superconductors (over 6500 of publications about HTS for the last 10 years according to *Web of Science*) lead to the development of new superconducting materials, which are able to withstand larger current density at higher working temperatures. The first examples of this approach were demonstrated by Kiyoshi and co-workers in 1999.⁴⁴ Their project was based on a regular LTS-based 900 MHz magnet, which was equipped with an additional HTS inner coil. The combination of the magnetic fields from the two coils was aimed to reach 23.5 T (1 GHz) of field strength. However, ongoing studies showed that one of the main problems of an HTS-based system was insufficient field stability (field drift more than 0.01 ppm/h). This problem was solved by an HTS insert operating in the driven mode (with a power supply unit permanently connected to the superconducting coil).^{45,46} In this case, field instabilities due to the intrinsic physical properties of the superconducting wire could be compensated by the active power supply. It was demonstrated that residual inhomogeneities arising from power supply ripple are efficiently eliminated by careful adjustment of an internal ²H lock system.⁴⁷ Similar studies were conducted by Hahn and co-workers.⁴⁸ It was shown that for a hybrid LTS/HTS design, it is essential to reduce the magnetic coupling between the LTS and HTS coils to improve the temporal and spatial field stability.⁴⁹ The most recent reports advertise a 1.3 GHz system based on the LTS/HTS design with an inner HTS coil consisting of two parts made from different superconducting materials.⁵⁰ At the same time, ongoing research on the new superconducting alloys promises new materials for HTS magnets, which are capable of sustaining up to 480 A/mm² current density to produce 24 T magnetic field with a hybrid design.⁵¹

Considering currently installed NMR systems, the utilization of bismuth strontium calcium copper oxide (BSCCO) HTS wire allowed one to reach the practical limit of 1 GHz proton

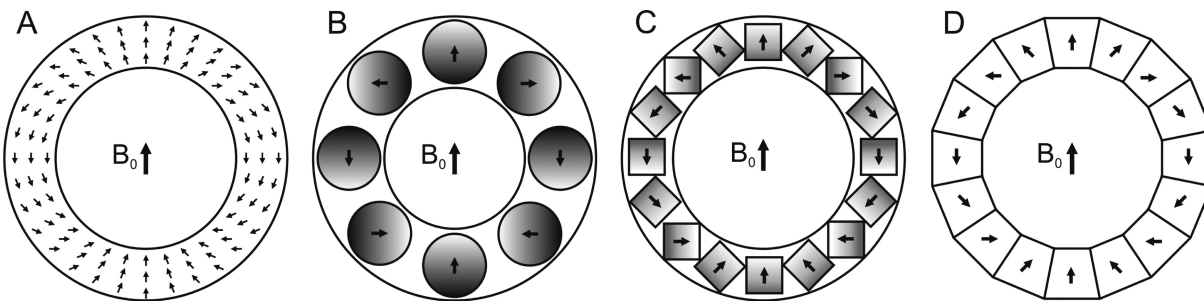


Figure 2. Cylindrical Halbach arrays: (A) ideal Halbach magnet in which the polarization varies continuously along the circumference of the ring; (B) discrete approximation of a Halbach array built from identical cylindrical rods;⁵⁹ (C) identical cubic magnets (MANDHaLa) used to build the array;⁶⁰ and (D) Halbach magnet built from trapezoidal pieces polarized in different directions.⁶⁴ Adapted from ref 28.

frequency for NMR magnets. The first 1 GHz NMR system was installed in December 2009 in Lyon, France.⁵²

Kitagawa and co-workers have reported an NMR system based on a split superconducting magnet type geometry.⁵³ Besides the use of more sensitive solenoid RF coils instead of birdcage coils, this magnet configuration allows conducting NMR measurements of different type, such as flow-through experiments, due to its free access to the probe area.

Recently, a miniature HTS bulk magnet system was demonstrated, which weighs about 2 kg and generates a magnetic field of the order of 3 T (Figure 1A,B).⁵⁴ It is assembled with a rotary microcooler, consuming 23 W when working in a steady operation state. The magnet consists of a cylinder 20 mm in diameter and 20 mm in length that is polarized along the axis, with a field gradient close to the top surface of the cylinder of about 400 T m⁻¹. The spatial dependence of the magnetic field is depicted in Figure 1C. This is the first step in superconducting magnet miniaturization with a great potential for mobile NMR or MRI.

Another promising area that has emerged in the past years is the design of compact portable magnet assemblies for a wide range of R&D and industrial applications,⁵⁵ which are mainly based on permanent magnetic materials. Using permanent magnets for NMR is as old as this technique itself.⁵⁶ Originally the systems explored the so-called C-magnet geometry, where two magnetic blocks generate the main magnetic field. The blocks were positioned one in front of the other and attached to an iron frame closing the magnetic field lines and defining geometry similar to the letter "C". The surfaces of both blocks forming the magnet gap were covered by iron poles properly designed to homogenize the magnetic field within the gap. Such permanent magnet systems, however, competed with electromagnets and were later replaced by superconducting technology because superconductors of similar size achieved higher magnetic fields.

Nevertheless, improved new permanent magnetic materials provided the chance to scale the size of the magnet down to the limit of millimeter size structures rekindling the interest of NMR in permanent magnets, despite the fact of the lower field strength achieved (and consequently sensitivity loss) in comparison with superconducting magnets. In the process of magnet miniaturization, to avoid further compromising the signal-to-noise (S/N) ratio, a first approach would be to start reducing the size of the magnet while keeping the sample volume V_s and field strength B_0 constant. This can be achieved by removing portions of magnetic materials located in the periphery of the magnet array and replacing them inside the magnet bore, closer to the sensitive volume. Because the

strength of the magnetic field depends on the spatial distance to the source, thinner internal layers replace thicker external ones. The ideal limit of this process would be the one in which the internal parts of the magnet are as close as possible to the sample to reach the minimum magnet size. However, as long as the magnetic sources get closer to the sensitive volume, it is harder to achieve a homogeneous field, that is, a magnetic field free from contamination of higher harmonic terms, across the entire sample volume. The different harmonics characterizing the spatial dependence of the magnetic field are integer powers of the ratio $(r_{\text{sample}}/R_{\text{source}})^n$,⁵⁷ where r_{sample} stands for any position at the sample or sensitive volume and R_{source} is the position of the magnetic source both measured from the center of the sensitive volume. For the case of magnets made from permanent magnetic materials, R_{source} can be associated with an average radius characterizing the magnet size. A compromise then should be obtained in terms of homogeneous volume, field strength, and magnet size. Once this limit is achieved, further magnet size reduction would be possible, but at the expense of S/N ratio loss because of a reduction of either B_0 or V_s . In this last case, the loss of sensitivity obtained through the reduction of V_s can be partially compensated by the use of more efficient RF coils. A detailed description of the sensitivity of miniaturized RF probes can be found elsewhere.³²

An alternative and promising magnet design for NMR miniaturization is the Halbach array.⁵⁸ The ideal cylindrical Halbach magnet (Figure 2A) is a cylinder magnet, which requires a magnetic material whose polarization varies continuously along the circumference to generate a magnetic field in the central region and which has the following properties: (1) the field strength is proportional to the ratio of its outer and inner radii; (2) the field is perfectly homogeneous inside the magnet bore; and (3) there is no stray field outside the magnet. The advantages of this magnet are that it offers a generous volume for sample positioning (large bore-size to magnet-size ratio) and, at the same time, generates relatively strong magnetic fields (1–2 T) using conventional magnetic materials such as SmCo or NdFeB. Moreover, it generates a magnetic field perpendicular to the axis of symmetry of the magnet, allowing the use of sensitive solenoid RF coils to detect NMR signals.

Practical realizations of this geometry were obtained with cylindrical rods polarized transverse to the axis⁵⁹ (Figure 2B) and with cubic blocks arranged in rings (Figure 2C);⁶⁰ several of them are stacked in a Halbach cylinder. The orientation of the polarization for each rod or cube in the ring is adjusted depending on the angular position of that piece. The use of many identical pieces to build the Halbach array is convenient

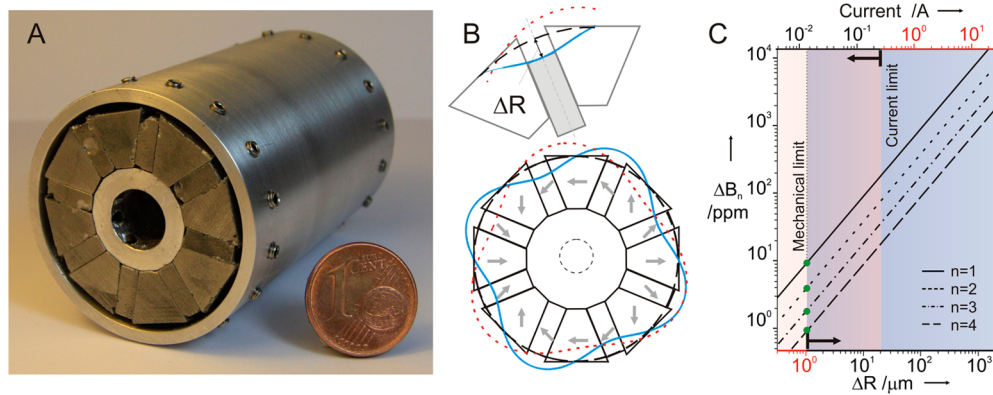


Figure 3. Modern Halbach array magnet for NMR applications: (A) picture of a modified Halbach array comparing its size with a 1 cent euro coin; (B) modulation of the movable pieces required to generate third- and fourth-order corrections (the control variable ΔR is shown in the enlargement); and (C) efficiency of the different mechanical shim corrections and their comparison with equivalent terms generated by resistive coils. Reprinted with permission from ref 68. Copyright 2010 Wiley-VCH.

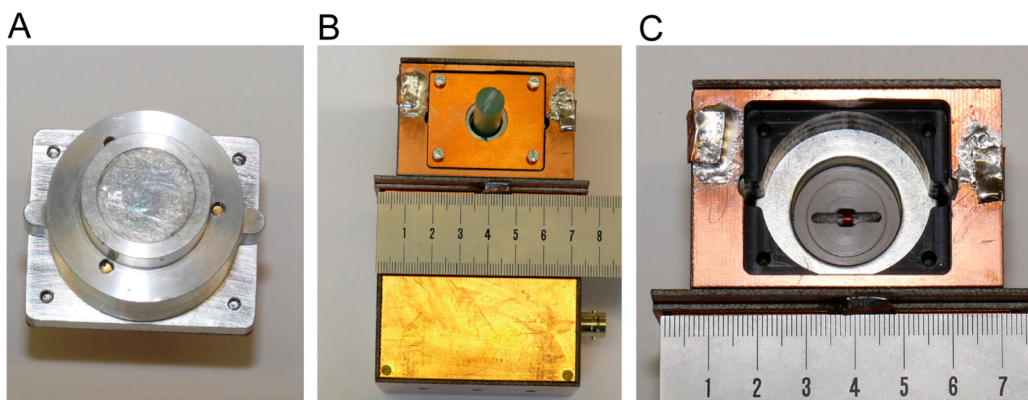


Figure 4. Pocket-size magnet and microcoil assembly: (A) the magnet assembly (top view); (B) whole probe (top) and tuning box (bottom); and (C) the probe with the top magnet removed to show the RF coil. Reprinted with permission from ref 71. Copyright 2008 Elsevier.

as it reduces the cost of acquiring the magnet blocks from the manufacturer. Furthermore, formally identical magnet pieces can be sorted and classified according to criteria by which the best magnets are positioned in the critical locations when the magnet is assembled.⁶¹ The use of identical pieces with transverse trapezoidal geometry but each of them polarized in different directions (Figure 2D) is also commonly used to build such magnets.^{62–64}

Despite the advantages of the Halbach geometry and its practical realization by assembling blocks with identical geometries, the homogeneity typically obtained in the final array is about 100 ppm in a volume with a diameter on the order of 1/10th of the size of the magnet bore.⁶¹ Under these conditions, applications involving MR imaging and NMR spectroscopy should be discarded. The origin of the problem resides in the physical properties of the magnetic material itself (typically SmCo, NdFeB, AlNiCo). The magnetization generated by identical blocks presents deviations that range from 0.1% to 1% (1% = 10 000 ppm). Additionally, the errors in positioning the pieces in the final array also contribute to the final field inhomogeneity. In this scenario, the conventional approach to homogenize the magnetic field through resistive shim coils⁶⁵ is useless, as excessive current would be required. Different alternative approaches were followed to reduce the inhomogeneities of the magnetic field up to a limit that allows implementing shim coils. Examples involve the inclusion of thin iron sheets inside the magnet bore,⁶⁶ the use of shim units

made from small and movable permanent blocks assembled inside the main Halbach magnet,⁶⁷ or varying the angular orientation of the pieces in the case of cylindrical Halbach magnets made from cylindrical rods.⁵⁹

An effective approach to reduce the magnet size while simultaneously keeping its field homogeneity under control has been presented by Danieli and co-workers⁶⁸ (Figure 3). In their miniature Halbach design, they combine trapezoidal and rectangular elements to build the rings (Figure 3A,B). The trapezoidal pieces are fixed forming parallel gaps between them. These gaps guide the rectangular magnet blocks, which can be moved radially in- and outward to mechanically shim the magnetic field in a highly efficient and accurate way. To minimize border effects introduced by the truncation of the ideal infinite Halbach cylinder, the present design combines rings with different geometric proportions. By displacing the rectangular blocks in each ring with defined angular modulations and amplitudes ΔR (Figure 3B), it is possible to independently generate the set of spherically harmonic corrections to the magnetic field up to order $N/2$, where N is the number of blocks with the same geometry in the ring. The efficiencies of this shimming approach and the shimming procedure based on the use of conventional resistive coils are compared in Figure 3C.

After the magnet blocks are assembled, the mechanical shim procedure goes as follows: (1) the field is scanned using a fast MRI method, and it is projected into the spherical harmonic

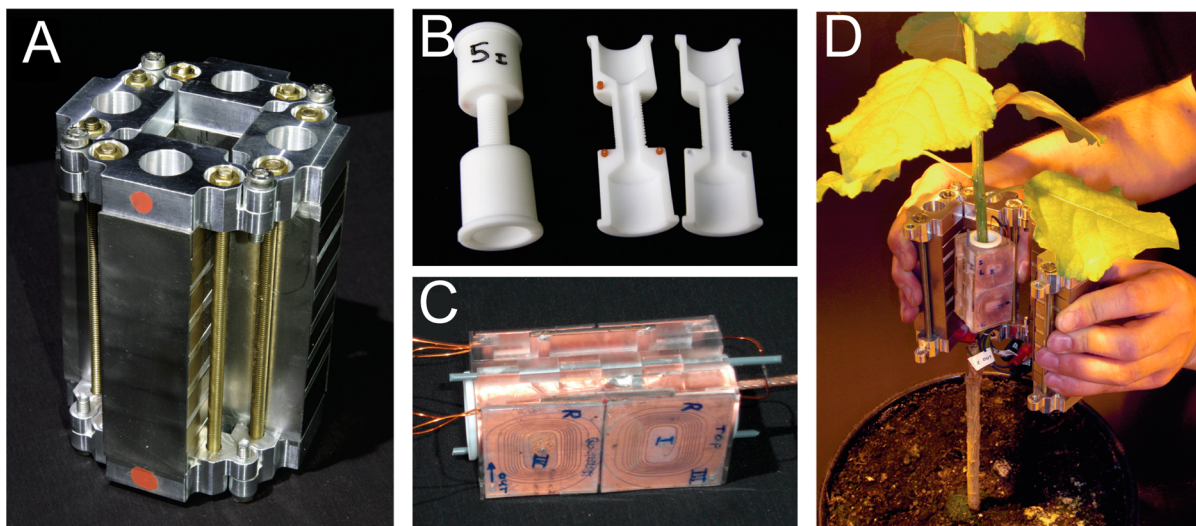


Figure 5. Dismountable portable magnet system (NMR-CUFF): (A) NMR-CUFF when it is closed; (B) PTFE holder for the RF coil; (C) plane parallel gradient system; and (D) NMR-CUFF when open at the moment of being mounted on a plant stem. The RF coil and the gradient coils system are already in place. Reprinted with permission from ref 66. Copyright 2011 Elsevier.

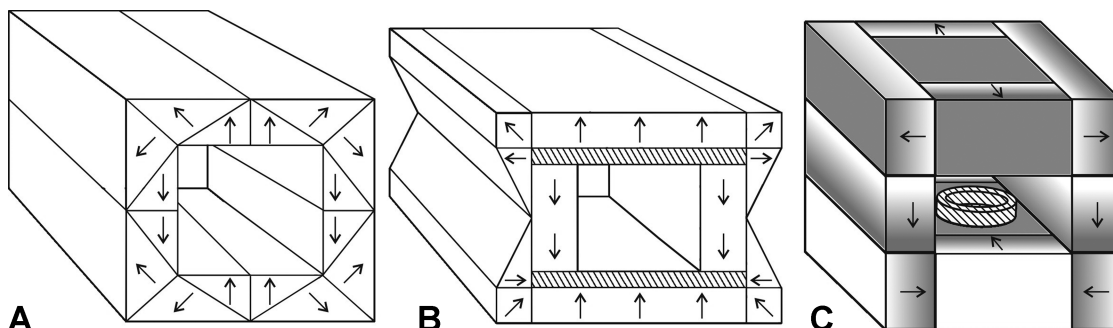


Figure 6. Magnets with rectangular cross sections. (A) Yokeless magnet consisting of a long tube of squared cross section. Arrows indicate the direction of polarization of individual blocks; (B) Same as (A), but with the inclusion of iron poles (dashed regions); (C) Magnet design which allows the realization of a compact NMR magnet with improved homogeneity. The direction of the polarization of the different pieces is indicated with arrows and grey scale color gradient.

terms; and (2) the required movements to cancel the measured terms are determined via computer simulations and then implemented. These steps are repeated in an iterative way until the field is shimmed. Using this approach, deviations of the magnetic field on the order of 10^{-7} (0.1 ppm) were reached in a volume corresponding to a 5 mm NMR tube.

As noticed above, the drawback of the Halbach magnets is poor field homogeneity, which may be attributed to slightly variable magnetization of individual magnetic blocks.⁶⁹ During the last years, various permanent magnet geometries concurrent to Halbach arrays were extensively tested in experimental studies and computer simulations. A variety of new designs suitable for different applications and with differing performance were reported.^{66,70,71}

One such design is illustrated in Figure 4. This pocket-size assembly⁷¹ consisted of only three individual magnetic elements, a ring magnet and two cylindrical bar magnets, which are located coaxially above and below the ring. The orientation of the polarization of the ring and the two bar magnets coincides with the axis of the system, but the polarization direction of the ring opposes that of the cylindrical bar magnets. By adjusting the gap between the two bar magnets, a homogeneity of 50 ppm was obtained with a field

strength of 1 T. The RF probe consisted of a solenoid coil with a diameter of 1.9 mm and a length of 1.8 mm (Figure 4C).

Recently, an attractive design of a magnet that can be opened and closed at a particular angular position using minimum force was presented by Windt and co-workers.⁶⁶ The NMR CUFF (cut-open, uniform, force free) magnet (Figure 5) weighs 3 kg and generates a magnetic field of 0.57 T. In combination with two sets of plane-parallel gradient coils (Figure 5C), the system allowed imaging of intact plants (Figure 5D) and measuring water (xylem) flow within a region of about 1 cm in diameter in a nondestructive way.

Examples of magnet geometries consisting of long tubular structures with squared cross sections have also been reported.⁷² The orientation of the polarization in the plane perpendicular to the axis of the tube shows the same distribution as in a Halbach ring (Figure 6A). This squared geometry exhibits certain advantages to include iron poles,⁷³ as shown in Figure 6B, which are effective to average out field inhomogeneities. When the length of the tube is reduced to obtain portable devices, it is possible to include, at the ends of the magnet tube, pieces with proper polarization direction to compensate border effects, which would compromise the homogeneity of the magnet (Figure 6C).⁷⁴ This geometry has been shown to be effective for shrinking a magnet. Cubic boxes

of about 16 and 30 cm³ with gaps of 2.5 and 4 cm, respectively, have achieved homogeneity on the order of 10 ppm across one-half of the gap.⁷⁵

A magnet design similar to that shown in Figure 6C, the one with poles and steel flux return as described above, has been used by McDowell and Fukushima to build a system suitable for NMR spectroscopy of limited sample volumes.⁶⁹ In this case, by confining the sample within a reduced spatial region where the variations of the magnetic field are of the order of some Hertz, it is possible to measure NMR spectra with high resolution. Reasonable results (0.24 ppm FWHM; S/N ratio = 61 for ¹H) were achieved with a compact (685 g) magnet with poles and steel flux return generating a field strength of 1 T, using a microcoil probe assembly with 0.3 mm inner diameter and 0.3 mm length without any shim system, temperature stabilization, and RF shield (Figure 7).

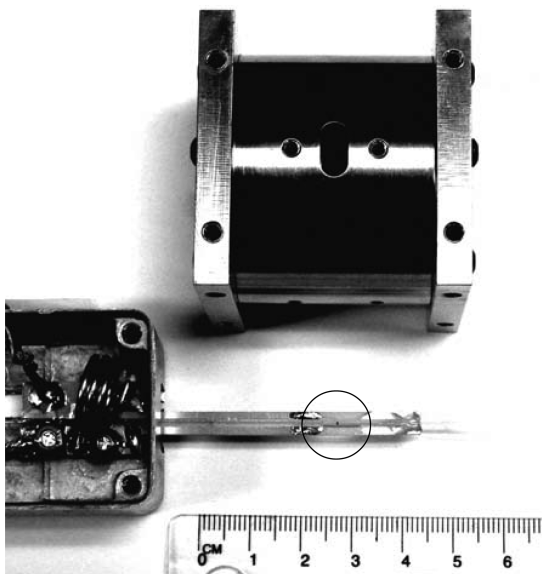


Figure 7. Picture of a pocket-sized magnet with a microcoil to record ¹H NMR spectra from samples confined in narrow capillaries. Reprinted with permission from ref 69. Copyright 2008 Springer.

In the permanent magnet arrays reported so far, the sample needs to be placed inside the bore to conduct the measurement. For some applications, this is not always possible because it may involve destruction of the object or simply because the objects cannot be brought to the NMR laboratory. Nevertheless, NMR has been applied to the study of such systems by means of single-sided or unilateral magnets. This idea was first proposed by the oil industry in the early 1980s. By compacting the entire equipment into a tube that is part of the drill string, it is possible to determine from a real-time NMR relaxation analysis of the borehole wall critical information on the fluid and formation properties needed to decide on the drilling direction. To accomplish this task, different arrays of permanent magnets were developed that generate magnetic fields outside the sensor, which, in combination with suitable surface RF coils, serve to excite and detect signals from samples in the stray field outside the instrument.⁷⁶

The invention of the NMR-MOUSE (MOBILE Universal Surface Explorer)⁷⁷ was inspired by the advent of these well-logging tools. The small stray-field magnet of the NMR-MOUSE allows detecting NMR signals ex situ when the sensor is placed at one side of a target object. It is then possible to perform nondestructive material testing of arbitrarily large samples or conduct in situ measurements that otherwise would be impossible using closed superconducting magnets. These characteristics spread the use of single-sided NMR devices into different research areas and gave rise to new industrial applications.^{24,27,30} The original sensor (Figure 8A) consists of two permanent magnet blocks with antiparallel polarizations placed on an iron yoke separated by a gap between them forming what is called a U-shaped magnet. Near the surface of the magnet, the stray magnetic field is oriented parallel to it and has the largest strength, which decreases as one moves away from the magnet. This spatial field variation is characterized by a field gradient G_0 , which for the NMR-MOUSE was about 20 T m⁻¹.

From this first prototype up to now, many efforts have been focused on optimizing the spatial variation of the magnetic field profile outside the magnet using different techniques, to satisfy particular applications. One important approach focused on improving the uniformity of the stray-field gradient along a large region over the magnet. This was motivated by the fact

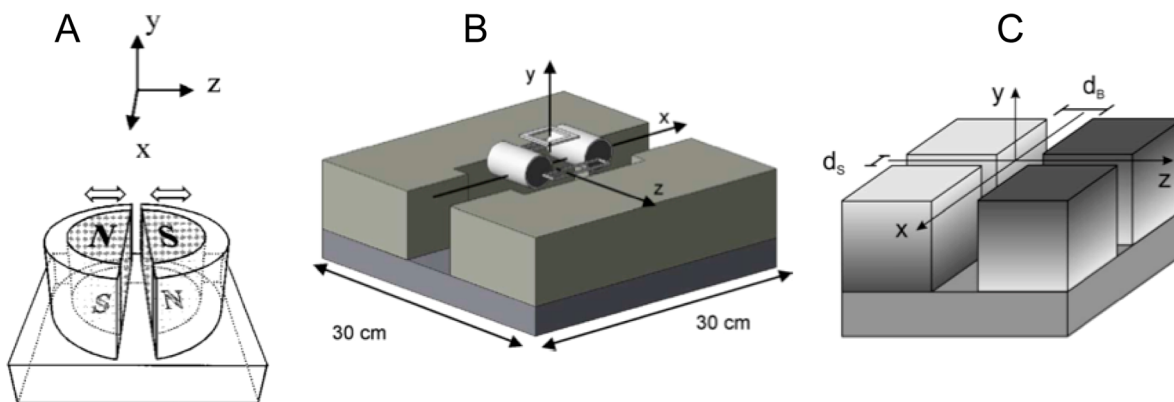


Figure 8. The prototypes of NMR magnets for one-side detection: (A) NMR-MOUSE original prototype. Reprinted with permission from ref 77a. Copyright 1995 Elsevier. (B) Open tomograph. The original blocks forming the U-shaped magnet were enlarged at both sides of the gap to improve the field gradient uniformity. The single-sided gradient system is also visible. Reprinted with permission from ref 78d. Copyright 2004 Elsevier. (C) Profile-NMR-MOUSE suitable to measure extended 1D profiles with high spatial resolution by displacing the magnet with the help of a repositioning system. Reprinted with permission from ref 80. Copyright 2005 Elsevier.

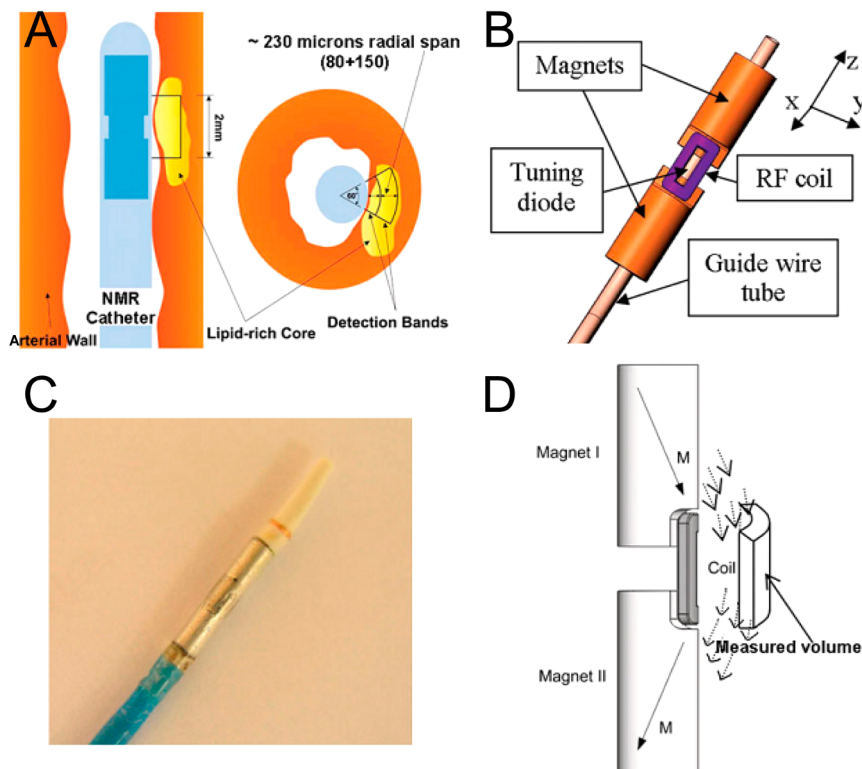


Figure 9. NMR catheters: (A) sketch of the system inside a blood vessel showing the detection region on the wall of the vessel; (B) drawing of the miniature sensor with a diameter of 1.3 mm; (C) photograph of the miniaturized sensor inside the catheter tube; and (D) drawing showing the polarization direction of the magnets, the RF coil, the orientation of the B_0 field, and the sensitive volume. Reprinted with permission from ref 83. Copyright 2005 Wiley-VCH.

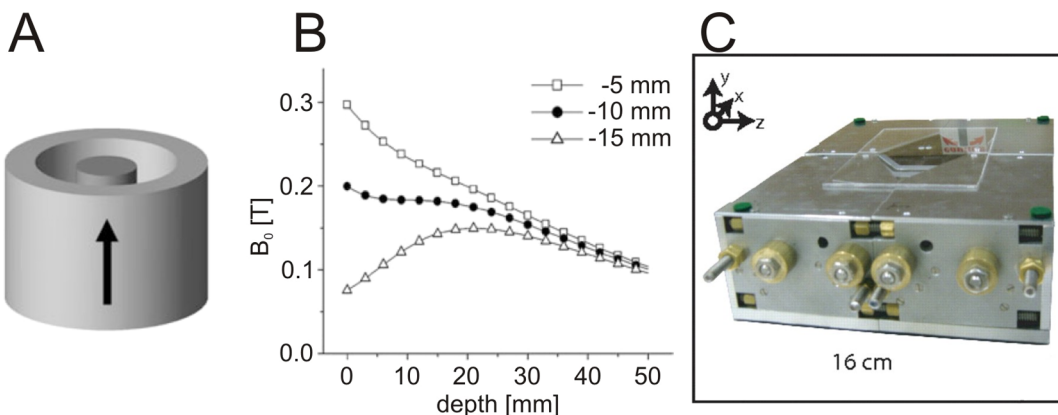


Figure 10. Sweet-spot magnets: (A) Original barrel magnet assembled with a small magnetic disc in its bore close to the top. (B) Strength of the magnetic field as a function of depth (z) corresponding to the magnet in (A) with the small disc placed at different axial positions ($z_1 = -5$ mm; $z_2 = -10$ mm; $z_3 = -15$ mm). $z = 0$ corresponds to the top of the barrel. Reprinted with permission from ref 30. Copyright 2011 Springer-Verlag. (C) Imaging magnet with an adjustable sweet spot. Reprinted with permission from ref 88. Copyright 2008 National Academy of Sciences.

that by using a stray field with constant values confined in planes parallel to the magnet surface and varying its strength along the depth direction, it is possible to measure one-dimensional images of objects that are located close to the magnet. By combining these magnets with proper gradient field coils, it is possible to gain spatial encoding along the lateral directions to measure 2D and 3D images of objects close to the magnet surface,⁷⁸ or to conduct single-sided velocimetry studies.⁷⁹ An example of such a magnet is shown in Figure 8B.

Other studies focused on optimizing the magnet geometry to obtain highly uniform and large field gradient strength of about 20 T m^{-1} , which is suitable to measure 1D profiles with spatial

resolution on the order of a micrometer.^{80,81} Figure 8C shows a drawing of the profile NMR-MOUSE, consisting of a U-shaped magnet but with an additional gap which splits the original NMR-MOUSE in two magnet blocks. With this modification, the magnet array generates a magnetic field with constant value in a flat region parallel to the magnet surface ($y = 0$) located at a certain distance y_0 . Next, by combining this kind of system with a repositioning device, which adjusts the relative distance between the sample and the magnet, the sensitive volume scans different regions of the sample recording extended profiles like in high-field STRAFY experiments.⁸²

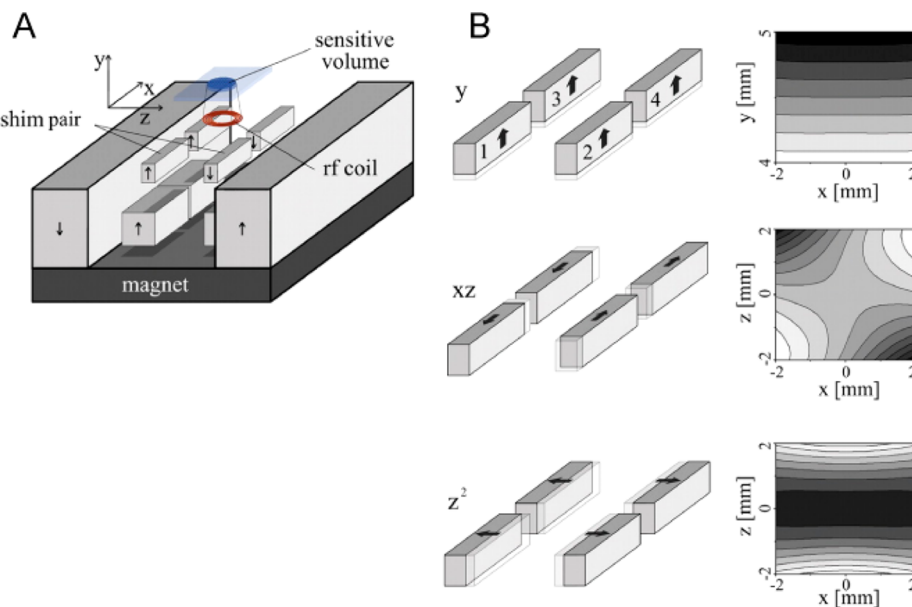


Figure 11. The concept of magnetic field shimming with moveable magnetic inserts: (A) U-shaped magnet assembled with an upper and a lower shim unit made of small magnetic blocks which allow obtaining a magnetic field with sub-ppm homogeneity on top of the magnet; (B) by moving the small magnet as shown in the examples, it is possible to generate corrections with defined spatial variations. Reprinted with permission from ref 87. Copyright 2007 AAAS.

The concept used by well-logging tools to inspect the walls of the holes from oil wells can be extended to study body tissues such as vessel walls or the prostate gland by developing NMR-catheters⁸³ or NMR-endoscopes.⁸⁴ A miniature single-sided sensor has been designed to work as a catheter and measure relaxation and diffusion properties of blood vessel walls (Figure 9B).⁸³ The sensor is composed of two cylindrical 1.7 mm diameter permanent magnets separated by a gap (Figure 9B). The magnets are polarized at 45° with respect to the cylinder axis and are arranged as shown in Figure 9C. Because of the reduced dimensions of the tool, the field gradient is about 150–200 T m⁻¹, which spreads the resonance frequency of the ¹H spins confined within a 250 μm thick vessel wall into a 2.5 MHz wide frequency band with a center frequency of 9 MHz. A small portion of the magnet that is facing the gap is removed to accommodate the surface RF coil (Figure 9B,C). Both magnet and RF coil are covered by a thin aluminum layer (Figure 9D), which effectively shields the device from external noise but nevertheless allows one to transmit the RF pulses and to receive the NMR signal.

When the sample under study is homogeneous, there is no need to spatially resolve any structure in it, but instead there is a need to maximize the sensitivity of the sensor to speed up the measurements. An approach for this is to increase the size of the excited volume, which is achieved by designing a single-sided magnet array with a sweet-spot. A sweet-spot is the spatial region over the magnet array in which the field gradient strength is zero ($G_0 = 0$).^{85–88} Figure 10A shows a pioneering design exploiting this principle.⁸⁶ The so-called barrel magnet consists of a hollow cylinder polarized along the cylinder axis assembled in combination with a magnetic disc placed inside its bore close to one of the barrel ends. By adjusting the axial position of the disc, it is possible to cancel the field gradient at a particular distance outside the magnet (Figure 10B). These magnets are suitable for moisture content measurements or relaxometry experiments.

Pines and co-workers introduced a portable MRI system consisting of four pairs of cylindrical magnetic rods held together on an aluminum frame as shown in Figure 10C, which generates a sweet-spot region. An optimization algorithm determined the overall magnet geometry and positions of the rods. The magnet construction allowed for adjusting the position of the sensitive volume (sweet-spot) of about 10 cm³ away from the sensor's surface by controlling the angular position of the rods. The magnet was assembled with gradient coils, with which MR images of objects placed at different positions above the magnet could be recorded.⁸⁸

An approach, which was really effective to control the stray magnetic field of single-sided devices, is the use of small movable magnets forming a so-called shim unit.⁸⁷ The working principle of this method was demonstrated on a single-sided sensor (Figure 11A), and it is based on copying the field inhomogeneities of the main magnet with the shim unit, while at the same time generating the smallest average field strength possible. By setting the polarization of the shim unit opposite to that of the main unit, the inhomogeneities of the main field can be corrected while the total field strength is maintained at an acceptable magnitude. After initial magnet assembly, the obtained magnetic field deviates considerably from the theoretical calculations due to unavoidable inaccuracies in the polarization, size, and positions of the magnet pieces. Small displacements of the magnet blocks around their calculated positions allow one to generate corrections with defined spatial variations (Figure 11B), thereby reaching in the experiments the performance calculated numerically. Following this concept, the stray field of an open magnet could be shimmed to sub-ppm homogeneity, allowing the measurement of proton spectra from liquids outside the magnet.⁸⁷

2.2. Electronics and Radiofrequency Transmission Part

The extensive development of programmable logic chips^{89,90} allowed most of the modules of a modern NMR spectrometer to be implemented in several integrated circuits (ICs)⁹¹ on a

single printed-circuit board (PCB). One of the most important steps was the development of high-precision radiofrequency sources, that is, direct digital synthesizers, capable of wide-band (hundreds of MHz) tuning.^{92,93} The pioneering work in the area of development of a single-PCB NMR spectrometer was done by Kazuyuki Takeda.³⁹ The system developed consisted of several modules that were joined together in a laptop-size assembly (Figure 12). Most of the functions were implemented

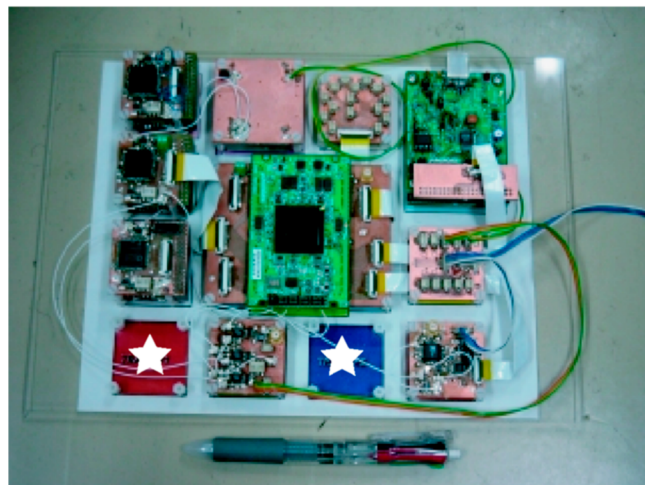
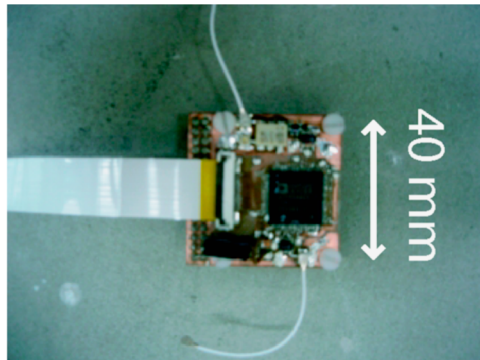


Figure 12. The first single-board spectrometer assembly. The external AD9858-based high-speed DDS (top) and the whole assembly (bottom). Reprinted with permission from ref 39. Copyright 2007 American Institute of Physics.

inside the Altera Cyclone II series FPGA chip. The FPGA held all interface functions, pulse programmer logics, receiver interface, and low-frequency direct digital synthesis (DDS) channel (DDS-I) for RF generation. The analogue part of the spectrometer consisted of a low-pass filter and mixer (AD9740 from Analogue Devices) for DDS-I, while DDS-II was based on the dedicated 1Gs/s DDS chip AD9858 (Analogue Devices) capable of generating frequencies up to 400 MHz. The second DDS channel was driven from the main FPGA with a clock frequency 1 GHz. The receiver consisted of an 80 Ms/s AD9245 analogue-to-digital converter from Analogue Devices and a digital demodulation circuit implemented inside the FPGA. In total, the whole system consisted of only 4 ICs, and its size did not exceed the size of medium laptop.

Connection of the RF part to a home-built microcoil probe and magnet allowed the author to measure NMR signals from water. The only external components needed were the magnet and probe assembly and the RF preamplifier/amplifier stages.

On the basis of this setup, the OPENCORE NMR project was developed in 2008 (Figure 13).⁴⁰ The project documentation

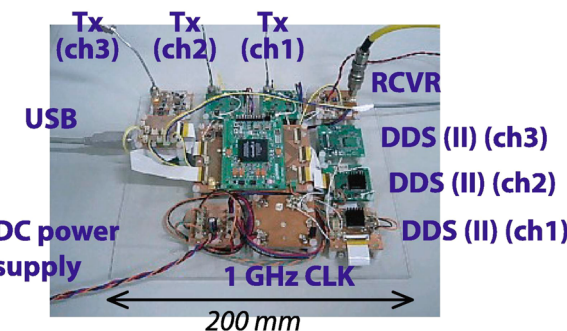


Figure 13. The OPENCORE NMR spectrometer. Reprinted with permission from ref 40. Copyright 2008 Elsevier.

included PCB schematics and source code for FPGA programming. Several examples of multipulse experiments and solid-state applications based on the OPENCORE NMR system was demonstrated.⁴⁰

It is worth noting that, apart from the emergence of highly integrated user-programmable logic ICs, the other major factor that contributed to significant improvement of NMR electronics was the development of modern analogue chips capable of signal generation, mixing, and filtering. A remarkable example of the former was the development of digital quadrature detection (DQD) that for today almost completely replaced old-fashioned quadrature detection with dual channel phase-sensitive detectors (PSD). The main drawbacks of the common PSD were the need for two analog-to-digital converter (ADC) channels to acquire real and imaginary parts of the signal and the requirement to maintain very precisely the 90° phase shift and similar gain between the two channels. Phase mismatch led to the appearance of quadrature image peaks, while different gain between channels resulted in O1 spikes. The simple and elegant way to overcome these problems was demonstrated by Gengying and co-workers.⁹⁴ The main idea was to leave only one ADC channel and perform the quadrature detection routine on digital data after frequency down conversion and signal sampling. The digital filtration will remove possible quadrature images from the signal obtained. The DQD was implemented with an AD7008 DDS chip (Analogue Devices) that was capable of rapid phase switching, which was required for the proposed scheme. The only limit was the maximal spectrum width for the experiment that was determined by the speed of DDS chip. Nowadays, the use of DQD has become routine practice for experiments with spectral widths up to several hundreds of kilohertz.

Several studies dedicated to building separate spectrometer modules such as RF generation modules, amplifiers, and receivers have also been reported. A design of an RF source similar to that of the OPENCORE NMR project was reported by Weimin and Liang.⁹⁵ They used a single chip DDS generator driven by an external FPGA controller. The application of the developed synthesizer for low-field MRI was successfully demonstrated. Another example of DDS-based frequency generation for NMR spectroscopy was demonstrated by Gengying and co-workers.⁹⁶ They utilized two AD9854 ICs for two-channel RF generation and a CPLD XC9572 chip from Xilinx as a controller. The system was directly coupled to the PC via an industry standard architecture (ISA) bus. The device

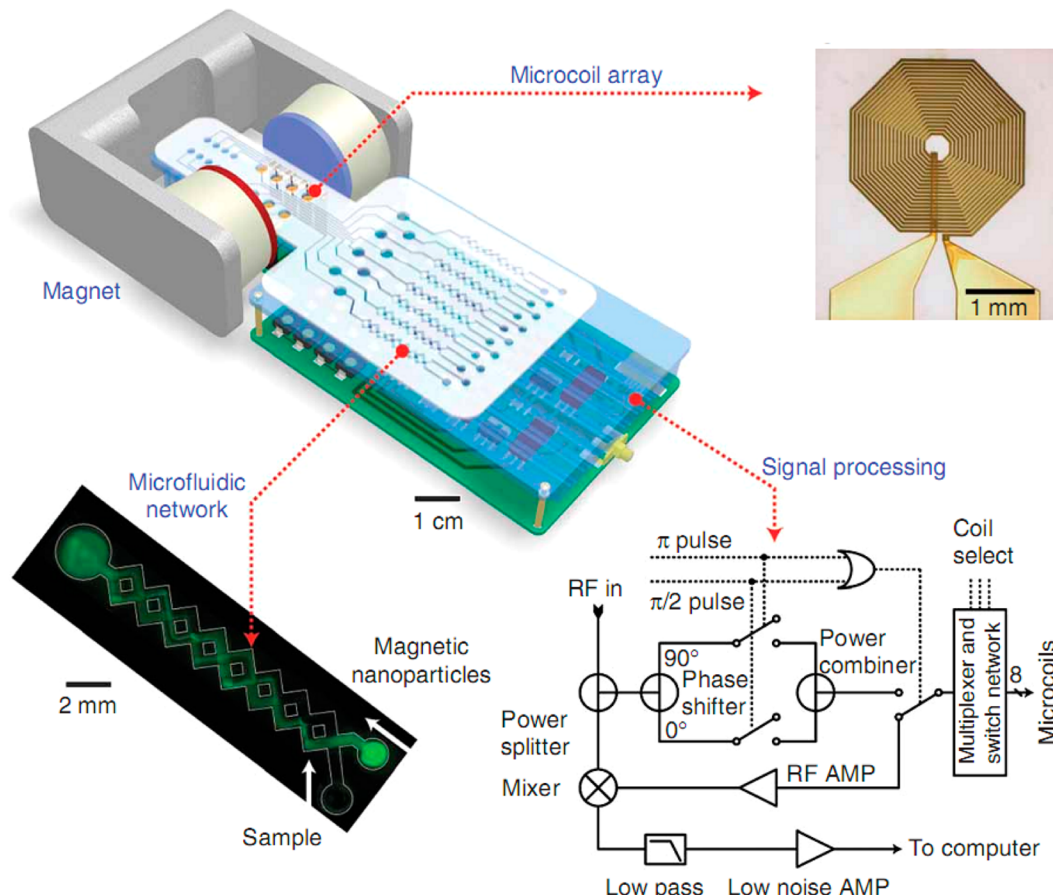


Figure 14. A portable diagnostic magnetic resonance system for biomedical applications. Reprinted with permission from ref 41. Copyright 2008 Nature Publishing Group.

developed was able to generate radiofrequency from DC to 135 MHz on both channels independently.

Several studies aimed at developing different spectrometer components (preamplifier, RF amplifiers) and gains in key NMR parameters such as S/N ratio were reported. Although no complete miniature NMR spectrometer has been described, these studies give guidelines to solve challenging problems in the field of NMR miniaturization. One of those problems is the improvement of the connection of the NMR probe to the preamplifier stage, because the amplitude of NMR signal entering the preamplifier is very low and the contribution of thermal noise in this step is significant. One of the possible solutions is to couple the electrical signal coming out of the coil to an optical transmission line, which is insensitive to external electromagnetic perturbations and has a very low intrinsic noise figure. It has been shown⁹⁷ that this design can be successfully employed in modern MRI applications resulting in an overall noise figure less than 1 dB. An advantage of this technique is a reduction of the number of cable connections between the probe and main console, which is especially important for high-level MRI gradient systems.

Another approach to avoid resistive losses during signal transfer from the detection coil to the preamplifier was reported by Cherifi and co-workers.⁹⁸ The incorporation of the preamplifier circuit and the detection coil on the single CMOS chip allowed a 14 dB improvement in the S/N ratio as compared to the assembly without preamplifier.

One of the most bulky modules of any NMR system is the RF amplifier, because high excitation powers are needed for

pulse NMR. High-power RF generation means components that can bear high currents and consequently require massive setups for adequate cooling. At present, the size of RF amplifiers is still one of the most limiting factors on the way toward decreasing the size of the whole RF assembly. A novel approach to overcome this difficulty was proposed by Blümich and co-workers.⁹⁹ Exploitation of carefully designed phase-encoded pulse sequences for excitation allowed one to decrease the excitation power by 3 orders of magnitude. The presented excitation scheme was reported to have uniform power distribution in time/frequency domains and broad excitation bandwidth.

Considering that one needs to get the best S/N ratio possible, the question of adequate tuning/matching (T/M) is of high importance. It is well-known from physics that improper T/M between circuit sections results in the reflection of RF irradiation at the point of mismatch and formation of standing waves, which leads to signal loss and overload of the RF amplifier output stage. However, the issue appears to be more tricky in the case of NMR, because recent studies show that T/M conditions for transmit and receive lines may significantly differ.¹⁰⁰ The problem arises from different construction of transmit and receive RF paths, resulting in apparently different resonance frequencies. It was shown that the order of this difference can be several hundreds of kilohertz. During the routine tuning procedure, the sweep generator provides the signal through the transmit circuit, which results in the wobble curve optimized for the transmit path. Desvaux and co-workers presented a new tuning method based on

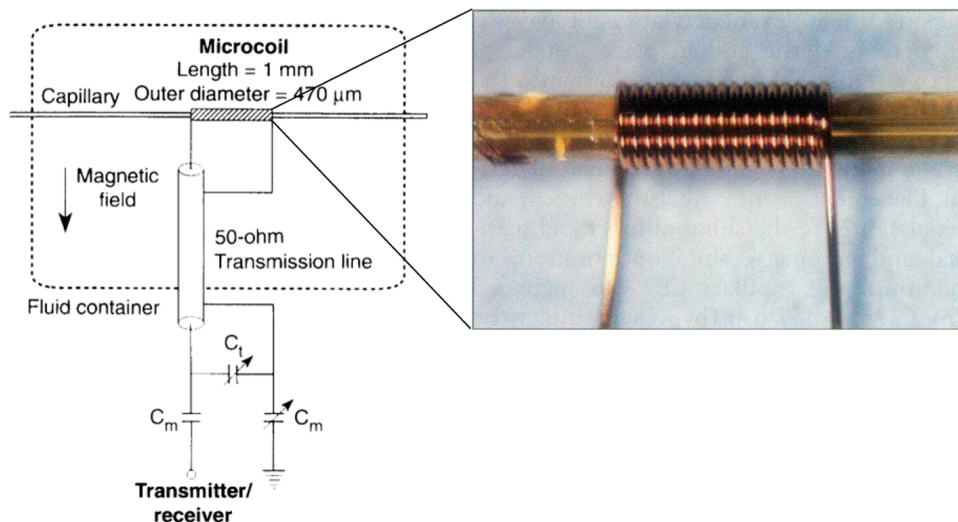


Figure 15. The photograph of a microcoil and schematic connection to an NMR spectrometer. Reprinted with permission from ref 109. Copyright 1995 AAAS.

observation of the spin-noise response, which leads to optimization of the RF parameters of the receive circuit.¹⁰⁰ Subsequent studies¹⁰¹ showed the signal-to-noise enhancement after optimized spin-noise tuning can reach up to 22%.

Weissleder and co-workers presented a compact diagnostic magnetic resonance (DMR) platform.⁴¹ The system consisted of a small magnet, a chip with a microcoil array, small printed circuit board with amplifying electronics, and a micro fluidic network (Figure 14). For several test samples, the developed system demonstrated outstanding sensitivity (aggregation limit down to 15 fmol) that was similar to or better than the detection limit for conventional biochemical ELISA test. Another significant benefit of the DMR platform was the relatively low cost due to use of routine micro fabrication techniques for components machining and assembly. The authors suggested the possibility of mass production of DMR sensors in the form of disposable units. Another example of fabrication of microcoil array receivers was recently demonstrated by Ogawa et al.¹⁰² The system constructed was aimed at water transport studies in the membranes of modern fuel cells.

2.3. Probes and Microcoil Systems Development

The use of microcoil capillary assemblies instead of regular NMR tubes allows one to concentrate a mass-limited sample in a very small volume, thus dramatically enhancing the probe sensitivity.¹⁰³ This may be crucial in the case of trace analysis when the ultimate mass sensitivity is needed.¹⁰⁴ These facts govern the improvement of NMR systems to analyze mass-limited samples of natural and biological compounds. Excellent reviews on the topics of liquid-state and solid-state NMR have been published.^{33,105–107} Another major advantage of microcoil probes is that they can be incorporated into online continuous flow analysis systems, which are discussed in detail in the next section of this review.

Besides the analysis of small amounts of substances, the key application of microcoils is their use in portable NMR scanners. Because of the tiny size of the coil, the requirements for the spatial B_0 field homogeneity are significantly lower. This allows compact and relatively cheap magnet systems to be used in portable magnetic resonance instruments. It was shown that for inhomogeneous magnetic fields (100 ppm/cm at 250 MHz ^1H frequency), the line width increases approximately as a square

root of the total sample volume.¹⁰⁸ As compared to a regular-size solenoid coil, the line width obtained with an 8 nL microcoil decreased from 1700 to about 500 Hz with the signal-to-noise ratio decreasing from 26 to 16. This is still insufficient resolution for most liquid-state NMR experiments, but the authors suggest further improvement by introducing a first-order shim system.

One of the first successful applications of microcoil probes to the analysis of nanoliter-volume samples was demonstrated by Sweedler and co-workers.¹⁰⁹ Their solenoid microcoil is shown in Figure 15. The coil was 1 mm long with a total sample volume of 5 nL. The coil was glued to the capillary with a cyanoacrylate glue. The Fluorinert FC-43 was used as a surrounding medium to reduce field disturbances due to magnetic susceptibility issues.

Previous attempts to design such a microcoil cell were reported to suffer from severe B_0 field inhomogeneities caused by introducing the microcoil close to the sample area. However, due to a better filling factor as compared to 5 mm tubes, the minimum limits of detection (LODs) were about 1 ng with an acquisition time less than 1 min.¹¹⁰ The minimum line width achieved for ^1H spectra was reported to be about 11 Hz at 300 MHz working frequency for the regular size magnet assembly. The inhomogeneity problem was overcome by filling the area around the microcoil with an inert liquid with its magnetic susceptibility matched for that of the microcoil. This allowed the acquisition of high-resolution 1D and 2D NMR spectra from 10 to 30 ng of material. In their further studies, the authors showed the application of microcoil NMR incorporated into an online LC–NMR system to perform peptide mixture separation and analysis.¹¹¹ Incorporation of the switching valve into the flow line allowed more detailed stopped-flow NMR studies of the compounds of interest.¹¹² An excellent review summarizing the studies above with detailed descriptions of various coil geometries and applications has been published.³² The recent findings in this area introduced new materials for microcoil fabrication which may lead to appearance of micropores with superior RF characteristics.¹¹³

The usual problem of microcoil setups was the inefficient transmit to receive (T/R) switching. A classical NMR preamplifier unit contained a T/R switch built as a pair of crossed diodes. This type of T/R switch was triggered

automatically by the RF pulse itself; as soon as high voltage is present, the diode semiconductor junction is forward biased, thus switching to transmit mode. However, relatively low voltage applied to microcoil is often comparable to forward voltage drop on the diode itself leading to loss of signal due to improper switching. Pennington and co-workers were the first to propose the use of actively switched duplexer that solves this problem.¹¹⁴ The developed T/R switch on the basis of active triggered PIN-diodes demonstrated insertion loss as small as 0.6–0.8 dB, while keeping T/R isolation well above 32 dB. Nowadays, PIN-based hotswitches are regular parts of modern NMR spectrometers.

Several studies were dedicated to solid-state microcoil applications. In this case, a major challenge is to combine microcoil technology with fast magic angle spinning (MAS). The most convenient solution of this problem was demonstrated by Sakellariou and co-workers.^{115,116} Their approach relies on the use of a microcoil insert for a standard MAS rotor, which becomes inductively coupled to the RF network of the MAS probe. The whole conception relies on a well-known RF transformer principle.¹¹⁷ The arrangement was called MACS (magic-angle coil spinning). This solution did not require modification neither of the MAS unit nor of the sample insert/eject hardware.

An interesting setup was demonstrated by Kentgens and co-workers.¹¹⁸ The use of classical solenoid coil wrapped around the fused silica capillary with the sample gave excellent sensitivity with spinning speeds up to 25 kHz. The inner volume of the capillary holding the sample was about 65–88 nL. Good quality solid-state ¹H spectra were obtained with modified eDUMBO¹¹⁹ sequence.

The rotating coil approach was extended by Korvink and co-workers.¹²⁰ The improved setup allowed higher spinning rates and resulted in a sensitivity of 230 $\mu\text{mol}/\sqrt{\text{Hz}}$. In ongoing studies, it was demonstrated that the same approach can be readily applied to regular liquid-state NMR investigations.¹²¹ The specially fabricated microchip contained a self-resonant microcoil, which became inductively coupled to the probe network upon insertion of the chip into the NMR probe. The best limit of detection was found to be 0.95 nmol.

Later, it was shown that for double resonance a combination of MAS and MACS coils can be used to detect two different nuclei.¹²² It was shown that despite spatial RF field variations introduced by the microcoil, reasonably good matching conditions for cross-polarization experiments can be achieved. Furthermore it was demonstrated that for samples exhibiting narrow ¹H resonances indirect detection schemes can be employed to boost sensitivity. An example of a ¹H–¹³C HMQC spectrum of 0.3 mmol ¹³C enriched glucose solution is presented in Figure 16. According to the pulse calibration data, the presence of the microcoil on the rotor surface did not significantly disturb the response of the other channel.

A step toward a compact portable system based on a microcoil probe and a permanent magnet was reported by McDowell and co-workers.¹²³ The probehead had a conventional solenoid/capillary design with the sample delivered to a capillary with a syringe. An important feature of the presented setup was the introduction of a tuning/matching circuit onto the microcoil chip. Series of coils were fabricated for sample volumes from 1 to 80 nL (Table 2).

The utilization of an auxiliary inductor in the tuning circuit allowed one to minimize the overall size of the probe schematics and improve the performance of low-inductive

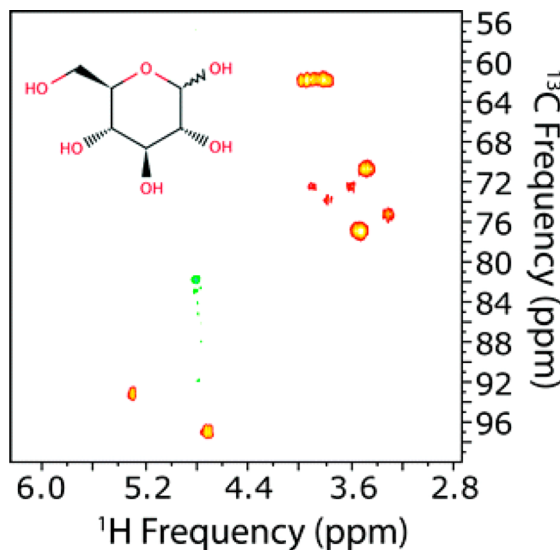


Figure 16. Example of a ¹H–¹³C HMQC spectrum of ¹³C-labeled glucose (340 nL of 0.3 mmol solution) obtained with a MACS/MAS double resonance setup. Reprinted with permission from ref 122. Copyright 2011 Royal Society of Chemistry.

small-size microcoils at low frequencies. It was shown that the main source of S/N ratio degradation is resistive loss due to relatively long wires connecting the microcoil to the rest of the circuit;¹²³ however, the closer alignment of the tuning/matching circuit to the microcoil could result in unacceptable magnetic field distortions. In an ongoing study,¹²⁴ the authors showed an application of the system for the detection of change in water relaxation properties in the presence of ferromagnetic nanoparticles.¹²⁵

Considering the design of the microcoil apparatus, the most widely used arrangement^{108,109,112,126} consists simply of a thin insulated copper wire wrapped around a glass or quartz capillary tube. The whole assembly is then mounted in the magnetic center of the NMR magnet using a modified probehead with a microcoil insert. A variant of this technique suggests the use of specially prepared polymer nanofibers instead of glass capillaries.¹²⁷ The classical variant of a solenoid resonator generates an RF field coaxial with the solenoid axis, which requires sample insertion between the loops in the conventional NMR design.¹²⁸ The development of photolithography and micromachining techniques allows planar microcoils with the B_1 field directed perpendicular to the coil surface to be fabricated.¹²⁹ The conception of planar coils is based on the well-known principle of the loop-gap resonator.¹³⁰ This approach yields smaller size microcoil receivers with more dense packing, which is of high importance for modern lab-on-a-chip applications.¹³¹ One of the first examples of a planar microcoil design was demonstrated by Massin and co-workers.¹³² Their microcoil probes had volumes ranging from 30 to 470 nL, which gave S/N ratios for ¹H varying from 60 to 15 on a 300 MHz instrument. Detailed calculations of the probe geometry and magnetic field simulations allowed one to create a general model to predict the S/N ratio and the spectral resolution depending on the microcoil design. Despite the sensitivity approaching that for solenoid microcoils, the fabricated probes demonstrated poor spectral resolution (line width $\gg 1$ Hz, Figure 18). The authors attribute this fact to the poor sample shape, as suggested by magnetic field calculations.

Table 2. Electrical and Mechanical Data for the Microcoils Shown in Figure 17^a

capillary o.d./i.d. (μm)	turns	length (μm)	calcd inductance (μH)	sample diameter (μm)	sample volume (nL)	obsd S/N ratio ($\pm 10\%$)	line width (Hz)
170/100	4	148	3	100	1.2	10.3	1.5
250/150	5	185	7	150	3.3	46	1.5
330/200	6	222	13	200	7.0	76	2.8
550/400	17.5	648	120	400	81	540	5

^aReprinted with permission from ref 123. Copyright 2007 Elsevier.

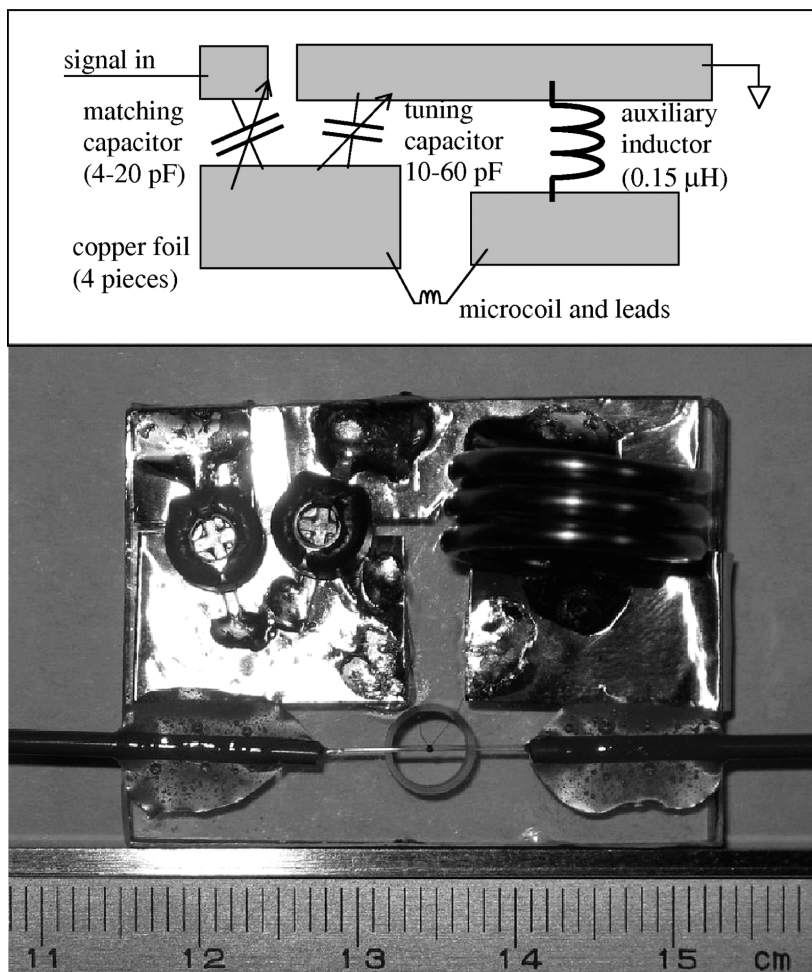


Figure 17. Microcoil probe schematics (top) and photograph (bottom). The microcoil is visible in the middle of the hole in an acrylic pad. Reprinted with permission from ref 123. Copyright 2007 Elsevier.

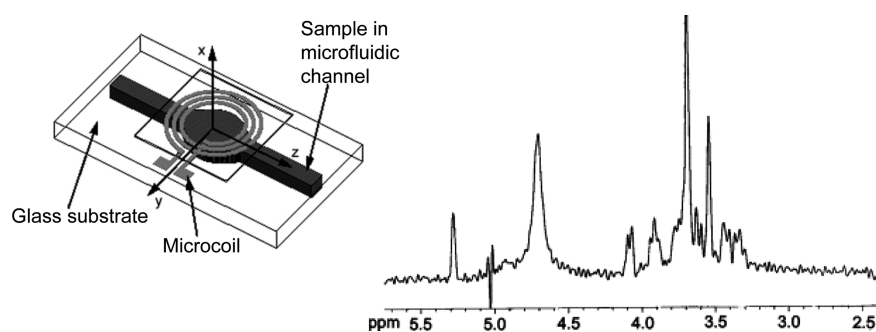


Figure 18. Microcoil probe scheme and associated ^1H NMR spectrum at 300 MHz. The spectrum was obtained from 160 μg of sucrose in 470 nL of D_2O with 16 scans. Reprinted with permission from ref 132. Copyright 2003 Elsevier.

The possible solution to improve field homogeneity is to generate commonly used 3D microcoils (Helmholtz or solenoid-type) with lithographic methods. This results in

much better homogeneity; however, because lithography generates only 2D structures, this is a challenging task involving multiple plating/masking/etching steps to achieve the desired

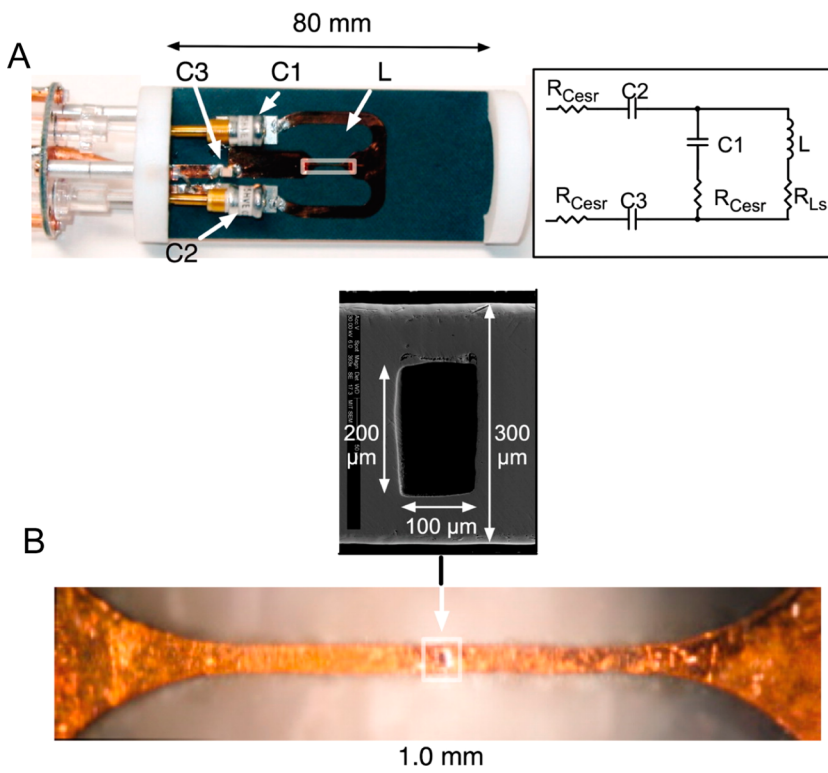


Figure 19. Microslot probes: (A) microslot probe and equivalent schematic; (B) the microslot under magnification. Reprinted with permission from ref 136. Copyright 2007 National Academy of Sciences.

geometry. An example of such a multistep microcoil fabrication process was demonstrated by Besse and co-workers.¹³³ The technique allowed one to produce solenoid, planar, and Helmholtz-type coils in the micrometer-size range. A comparison of different coil types indeed showed the advantage of 3D structures against planar geometries in terms of both S/N ratio and spectral resolution.

Since micro strip RF components emerged in the 1970s, they have largely displaced traditional lumped components especially in the field of RF antennas.¹³⁴ One particular case of micro strip resonators often utilized in NMR studies is the micro slot design. In this case, the sample is placed into the cavity of a micro strip resonator (e.g., Figure 19). Recently, several studies demonstrated the use of micro slot or micro strip receive coils for NMR instruments. The main advantages of the micro strip waveguide detectors are almost absolutely uniform RF magnetic fields and minimal magnetic disturbance introduced into the whole system.

One of the first examples of a micro strip-based probe design for MRI was demonstrated by Chen and co-workers.¹³⁵ Their surface coil had the dimensions of 9 cm × 9 cm and showed a penetration depth of about 8 cm. It was shown that results similar to those from commercially available surface coils could be obtained using the novel resonator design.¹³⁵

An application of micro slot-based resonators to conventional NMR was demonstrated by Maguire and co-workers.¹³⁶ It was emphasized that due to their ease of fabrication and compact size, micro slot detectors can be fabricated in arrays for combinatorial measurements. A photograph of the probe and micro slot is presented in Figure 19. The probe circuit was manufactured on a planar substrate. The sample-holding taper in the micro slot (200 μm × 100 μm) was impedance matched with the surrounding stripline.

This simple and easy way to fabricate a resonator showed unprecedented sensitivity gain, being able to produce spectra from as little as 1.6 nmol of ribonuclease-A comparable in quality to those acquired with a conventional 5 mm NMR probe (5.5 μmol load) even for 2D experiments. The spectra are presented in Figures 20 and 21.

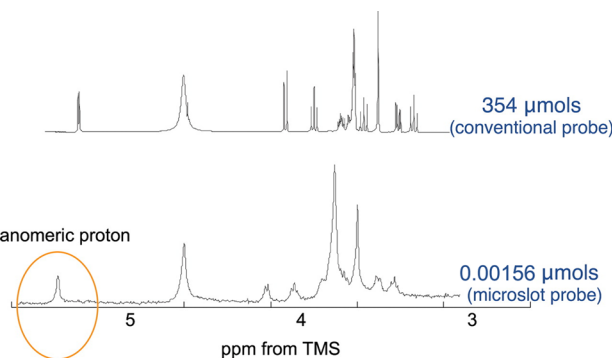


Figure 20. NMR spectra from sucrose dissolved in H₂O acquired with a conventional probe (top) and with a microslot probe (bottom). Reprinted with permission from ref 136. Copyright 2007 National Academy of Sciences.

Extensive theoretical and experimental studies in the area of stripline resonators were conducted by Kentgens and co-workers.^{137,138} The optimized design of a microstrip-based NMR flow probe was presented by Bart and co-workers.¹³⁹ FWHM for the ¹H spectrum of ethanol was 0.7 Hz. The authors demonstrated the application of their probe to study reaction kinetics and its potential for biochemical applications.

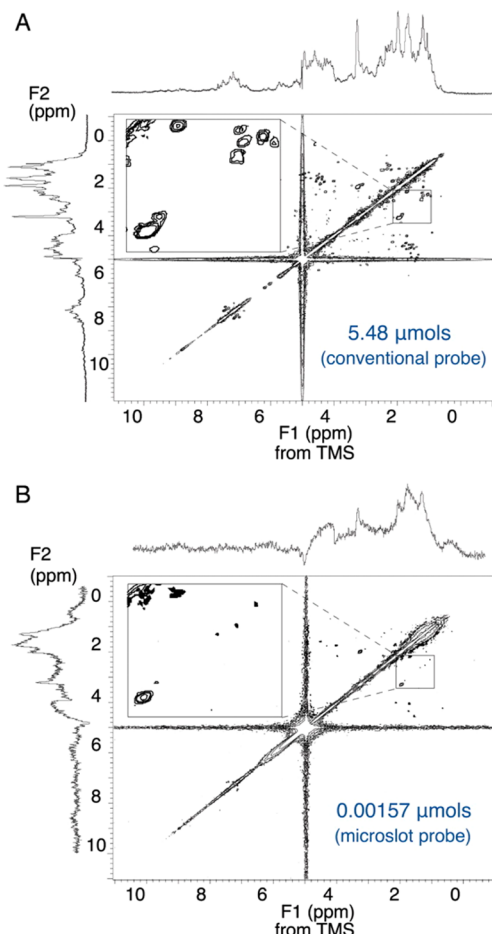


Figure 21. Magnitude COSY spectra of ribonuclease-A measured with a conventional (A) and with a microslot (B) probe. The microslot probe allowed one to analyze 3500 times smaller amounts of sample; however, the acquisition time was increased by a factor of 2. Reprinted with permission from ref 136. Copyright 2007 National Academy of Sciences.

A summary of modern NMR applications to study mass-limited samples was published.¹⁴⁰

An interesting solution to the inhomogeneity problem was demonstrated by Leidich and co-workers.¹⁴¹ A special arrangement of copper windings and silicone layers allowed one to compensate the inhomogeneity arising from the different magnetic susceptibilities of the materials used. The line width achieved with this setup was about 1–3 Hz for the ¹H spectra. The layer-wise construction of the probe allowed adding a second channel simply by adding another coil module on top of the whole assembly. This was one of the first concepts of multiple-channel microcoil setups. The setup represented one of the few examples of dual-channel microcoil probes (Figure 22).

Stacked planar micro coils were recently designed as a multilayer assembly for a single-side application in the NMR-MOUSE system.¹⁴² The coil with the outer dimension of 4 mm × 4 mm was able to measure signal with the same S/N ratio for a sample volume about 5 times smaller as compared to the state-of-the-art 14 mm × 16 mm coil. Designed stacked coils were adapted to a homogeneous slice of about 200 μm in height and uniform gradient depth of about 20 T/m.

An example of a double-tuned microcoil probe was reported by Walton and co-workers.¹⁴³ The system constructed by

microlithography included two coils, a Helmholtz pair for the low-frequency X-channel, and a loop-gap resonator for the ¹H channel. The probe demonstrated good performance in the X-channel on ³¹P and ¹³C. Beyond that, a direct ¹³C–¹³C COSY spectrum of a labeled acetic acid was acquired in only 1.2 h from a 1.4 μL sample. However, the spectral resolution on the ¹H channel was not good enough; a line width of 18 Hz was obtained due to magnetic field nonuniformity near the surface of the coil.

Peck and co-workers reported the first example of a commercially available capillary probe with a dual microcoil cell.¹⁴⁴ The two equivalent microcoil flow cells were arranged in a stack demonstrating a S/N ratio of 50–55 for ¹H. Simultaneous shimming allowed one to adjust field homogeneity for both microcoils resulting in line widths of about 10 Hz. Various regimes of dual microcoil operation, such as sequential, simultaneous, and mixed modes, were tested. The question of much interest in multiresonance setups is the electrical crosstalk between channels. The measured isolation between the microcoil units in the setup reported was 30–35 dB. It was demonstrated that, by using the system presented, multiple 1D and 2D NMR experiments can be run at both channels simultaneously.

Stevens and co-workers showed that commercially available microcoil probes can be successfully embedded into structural genomics pipelines to assist in screening for protein homologues.¹⁴⁵ Scaling down the amount of proteins needed for reliable NMR analysis facilitates the production of small samples, thus increasing the overall matching speed.

The application of commercially available 1 mm microprobes for complete 3D protein structure determination was demonstrated by Montelione and co-workers.¹⁴⁶ They managed to perform a complete resonance assignment for 72 μg (1.4 millimols) of a 8.7 kDa protein. The sample under study was the 68-residue *Methanoscarcina mazei* TRAM protein. To facilitate spectra acquisition, the authors cloned, expressed, and purified uniformly ¹³C, ¹⁵N-enriched TRAM protein. The assigned ¹H–¹⁵N HSQC spectrum and the corresponding 3D structure are presented in Figure 23. The accuracy of the data obtained with the microcoil probe was comparable to that of data obtained with a conventional probe. The RMS deviation between coordinates of the backbone structures between data sets was 0.73 Å. Naturally, the decrease in sample mass required more experimental time, that is, 19 days as compared to 9.5 days for the conventional probe, but the mass gain was ca. 20-fold. The authors propose this approach to be feasible for proteins with concentrations >1.2 nM and molecular weight less than 15 kDa.

Another example of a microcoil NMR application toward characterization of mass-limited samples was recently presented by Horst, Wütrich, and co-workers.¹⁴⁷ Extensive diffusion studies allowed the authors to analyze the behavior of micelle incorporated proteins in solution.

A challenging problem in the application of microcoil NMR to mass- and volume-restricted samples consists of the magnetic separation of the microcoil from the tuning network and the connecting wires. Because of the tiny size of the coil itself, the wires and the tuning circuit are often very close to the sample, so that the free induction decay (FID) signal is induced not only in the microcoil but also in the surrounding conductors, which leads to a decrease in the detected signal intensity. A possible solution to this problem was presented by Haase and co-workers.¹⁴⁸ They combined a receiving microcoil

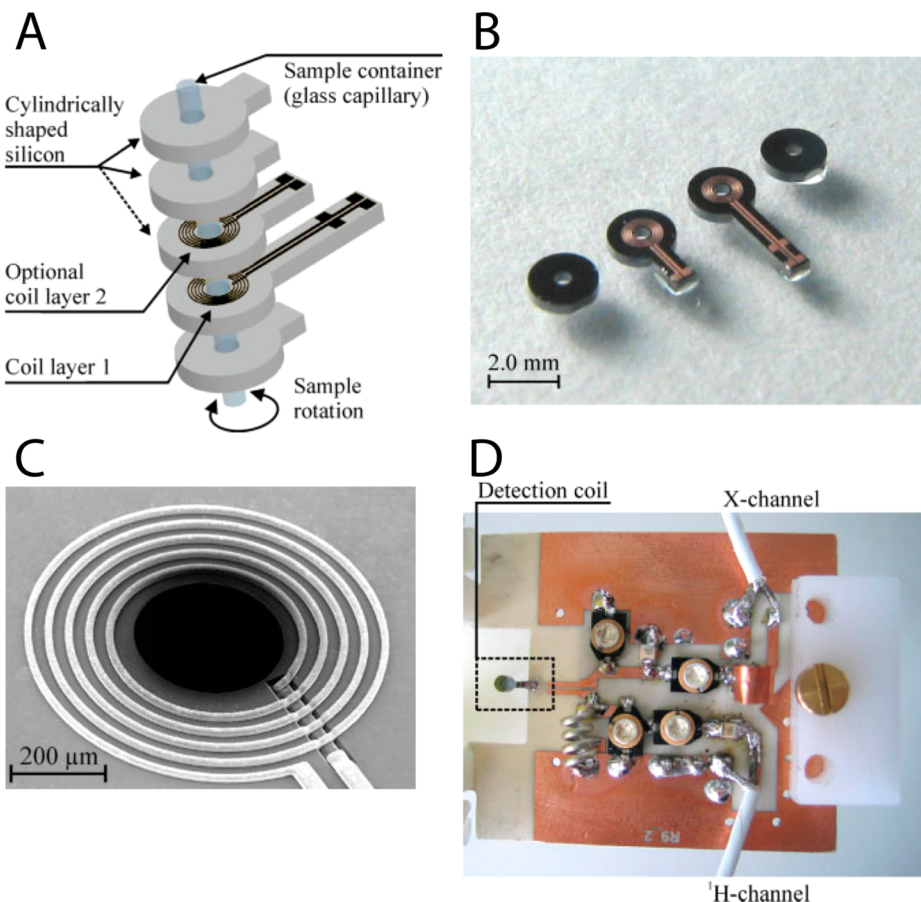


Figure 22. Multichannel microcoils assembly: (A) schematic representation of a multichannel microcoil; (B) photograph of the coil layers; (C) SEM photograph of the coil conductors; and (D) complete $^1\text{H}/\text{X}$ resonator with the coil. Reprinted with permission from ref 141. Copyright 2009 Wiley-VCH.

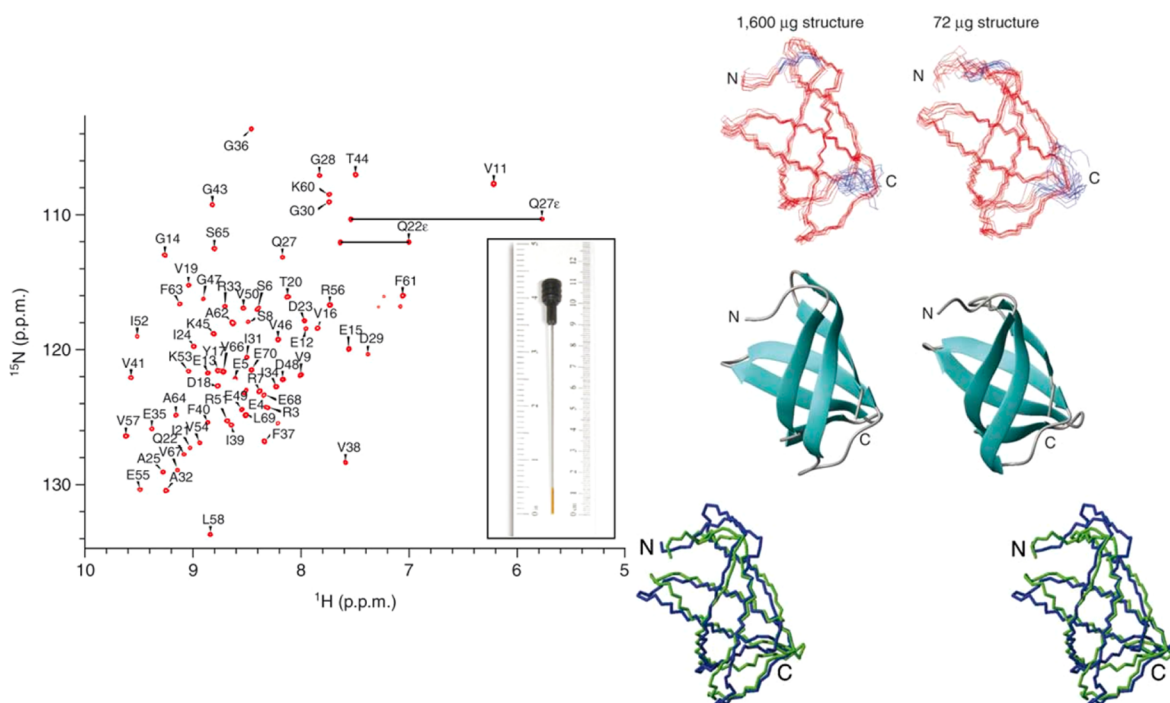


Figure 23. Assigned $^1\text{H}-^{15}\text{N}$ HSQC spectrum and the corresponding 3D structure of the ^{13}C , ^{15}N enriched 68-residue TRAM protein. 3D structures are given to compare the data obtained from the conventional (left) and the microcoil (right) probes. Reprinted with permission from ref 146. Copyright 2007 Nature Publishing Group.

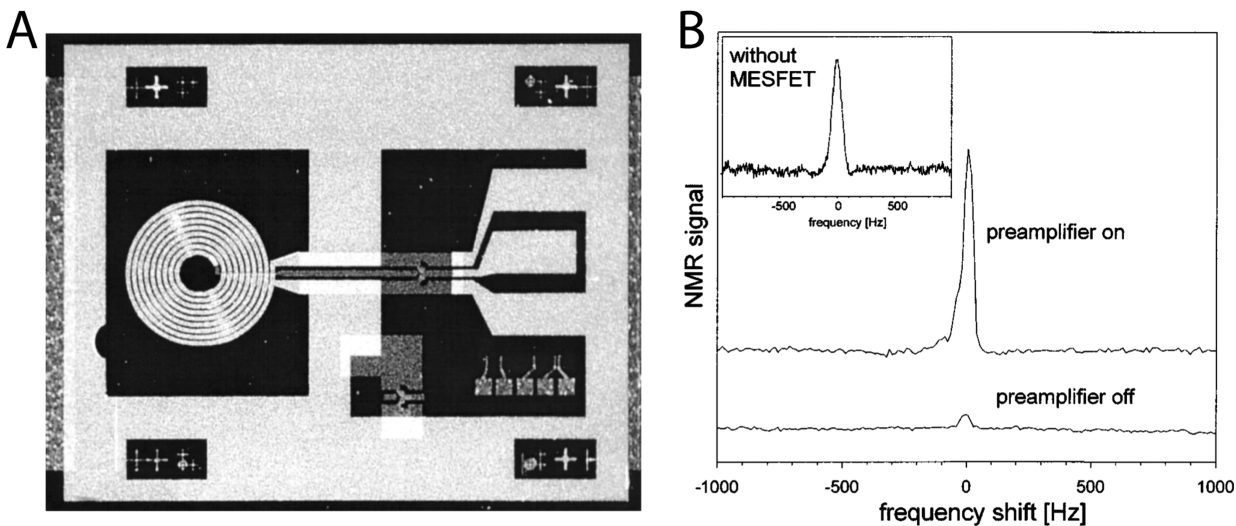


Figure 24. The photo (A) and the effect on the spectral intensity (B) of the integrated MESFET preamplifier. Reprinted with permission from ref 148. Copyright 2003 American Institute of Physics.

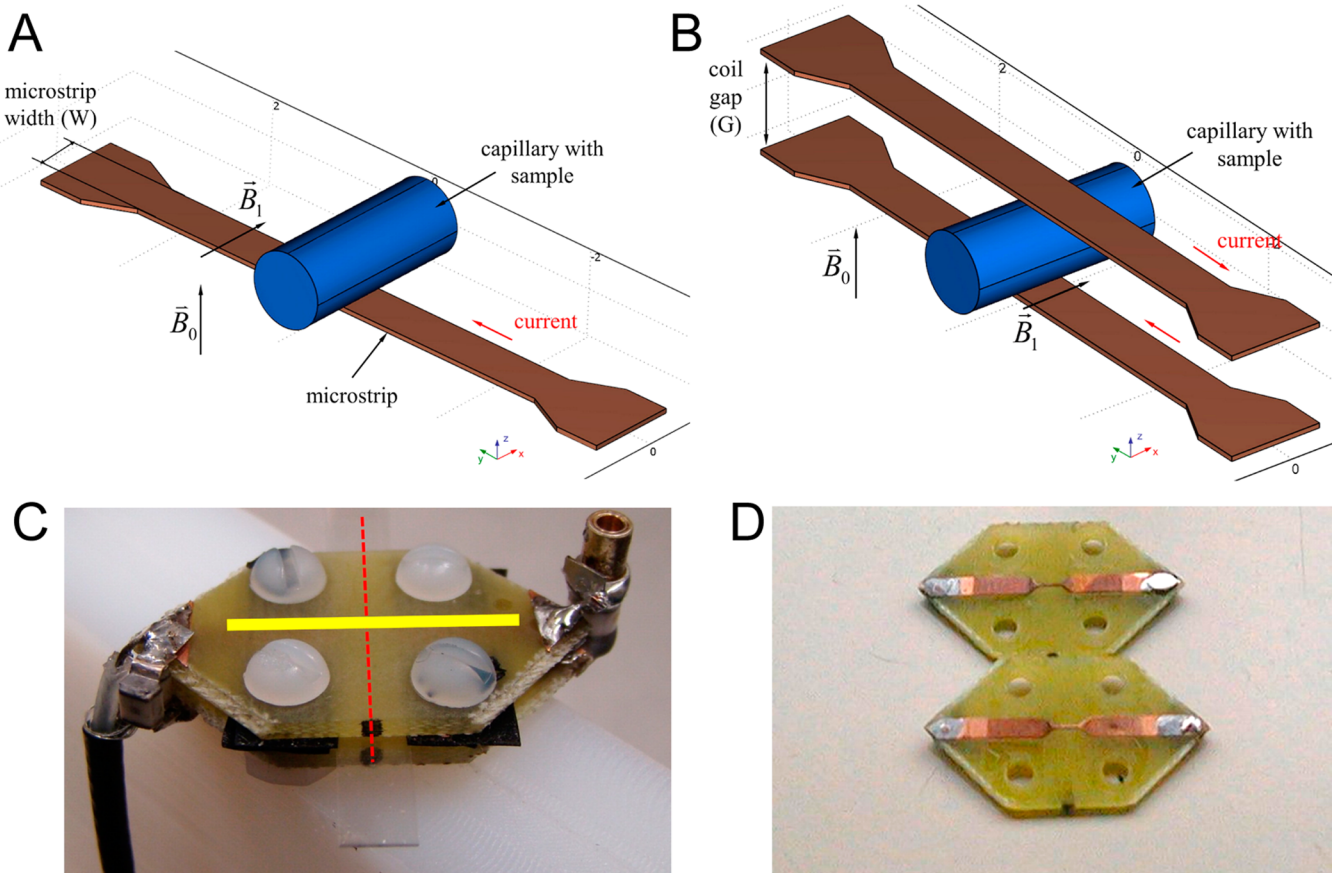


Figure 25. Microstrip RF resonator for imaging: (A) model of single microstrip resonator; (B) model of double microstrip resonator; (C) photograph of double microstrip resonator in assembled state; and (D) disassembled microstrip setup. Reprinted with permission from ref 156. Copyright 2012 Elsevier.

directly with an amplifying transistor. The microchip was prepared using UV lithography and wet etching for semiconductor component fabrication. A lift-off process combined with electron-beam photolithography was used to make the microcoil (Figure 24A). The NMR chip was tuned for 500 MHz proton NMR frequency. Tests showed about a 10-fold

increase in the S/N ratio due to the integrated MESFET preamplifier (Figure 24B).

Another example of highly integrated microcoil probe was described by Boero and co-workers.¹⁴⁹ The probe aimed at magnetic resonance magnetometry consisted of a planar spiral coil, an RF preamplifier, a mixer, and an audio frequency (AF) amplifier on a single 10 mm² CMOS chip. The probe

demonstrated better spatial resolution and a wider measuring range than the probes available on the market.

In general, it should be noted that microcoil strategies improve the balance between sensitivity and spectral resolution. Various coil geometries demonstrate superiority of one parameter but loss in another. The most simple solenoid coil setup exhibits the best sensitivity due to close proximity of the coil to the sample and thus a very high filling factor. However, close interfacing of materials with different magnetic susceptibilities results in strong B_0 field gradients and bad line shape. Planar microcoils allow the most compact and versatile NMR setups to be built, but their spatial field uniformity is even worse than that of solenoid coils. Moving the sample away from the surface of the planar microcoil increases field homogeneity but simultaneously decreases the sensitivity. Helmholtz coils seem to be a good compromise, but it should be taken into account that a complex coil geometry requires sophisticated fabrication techniques. In addition to that, the relatively low filling factor of Helmholtz coils limits their use in receiving assemblies.

An emerging field is the application of microcoil NMR techniques to magnetic resonance microimaging (also called magnetic resonance microscopy, MRM).^{150,151} The best S/N ratio is of crucial importance for MRI techniques because increasing the resolution in an MR image means decreasing the size of the voxel, which in turn leads to fewer nuclear spins in each voxel and lower image quality. Therefore, implementing microcoils to MRI systems¹⁵² would allow one not only to decrease the size of the setup but also to gain high-contrast micro images of small objects and even living cells. One of the key steps on this way is the construction of a triaxial gradient system needed for spatial and phase encoding as in conventional MRI. This is not a trivial task considering the fact that high power gradients are needed to minimize the acquisition time to avoid diffusion artifacts. An example of implementing such a gradient system was demonstrated by Pennington and co-workers.¹⁵³ The system consisted of a triaxial gradient PCB and a solenoid microcoil. The gradient system was available to provide B_0 gradients of more than 1500 G/cm. The uniformity of gradients was measured to be within 5% over a volume of 600 μm^3 . The gradient switching time was about 10 μs , which is enough for a field-of-view (FOV) of several hundred micrometers. Relatively low inductance and resistivity of the gradient system developed allowed for gradient ramping, which is needed for many complex MRI schemes.

Another example of high-resolution phase-encoding constant-time imaging using microcoils was reported by Barbic and co-workers.¹⁵⁴ A custom 3D gradient system capable of delivering gradients up to 6500 G/cm was built around a commercially available microcoil unit. Images of a glass fiber with 3.0 μm resolution were acquired with the presented setup.

Fan and co-workers constructed a compact on-chip MRI system using the MEMS technique. The circuit included the resonance coil, T/R switches, LNA, and the power amplifier. Images of live onion cells with a spatial resolution 6 $\mu\text{m} \times 6 \mu\text{m}$ in a 120 μm slice were obtained with the setup.¹⁵⁵

Jasiński and co-workers recently demonstrated the potential of a microstrip-based resonator applied to quantitative MRI techniques.¹⁵⁶ Quantitative MRI (such as T_1 - or T_2 -weighted imaging) demands high B_1 field homogeneity inside the region of interest. The prototypes and photographs of the resonator are presented in Figure 25. The position of the double

microstrip assembly is indicated by a yellow line in Figure 25C. The intended sample position is marked with a dotted red line.

The microstrip resonator provided homogeneous RF field in the 500 $\mu\text{m} \times 500 \mu\text{m} \times 300 \mu\text{m}$ region of interest. The best spatial resolution achieved was 16 μm . High B_1 field homogeneity across the microstrip (maximum deviation <5%) allowed the quantification of NMR data from transverse regions of the sample (Figure 26).

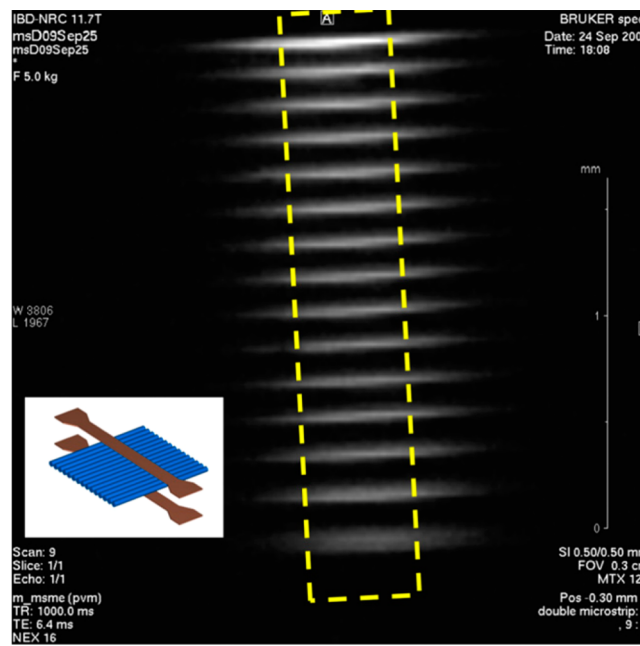


Figure 26. MRI of a multicapillary phantom acquired with microstrip resonator. Each of the 15 capillaries has an i.d. of 160 μm and an o.d. of 200 μm . Reprinted with permission from ref 156. Copyright 2012 Elsevier.

To demonstrate the potential of microstrip coils in MRI applications, the authors obtained an image of an asparagus slice soaked in CuSO₄-doped water (Figure 27). The image was obtained using a MSME spin-echo imaging method with a FOV of 0.3 cm and an image resolution of 24 $\mu\text{m} \times 24 \mu\text{m} \times 300 \mu\text{m}$.

A prototype of a portable system for MRI characterization of flow processes was presented by Sahebjavaher and co-workers.¹⁵⁷ The system is based on a custom designed 0.6 T permanent magnet. A microcoil probe was made from a polyethylene capillary and AWG 36 copper wire. The 3D gradient system was fabricated using a coating/etching process on printed-circuit boards (Figure 28). Custom-built electronics were used to interface with the RF coil/gradient system and digitize the output signal. The setup demonstrated moderate performance for static imaging as a resolution of 40 μm was achieved. An example of a phantom image is presented in Figure 29. The phantom consisted of a water-filled 250 μm capillary placed into a 1.67 mm water-filled capillary. A regular spin-echo experiment (echo time 5 ms, repetition time 51 ms, 64 averages, 9 min acquisition time) was employed for imaging. The slice thickness was 3 mm. The black ring in the picture corresponds to the 40 μm wall of the inner capillary. For flow imaging, flow velocities ranging from 5 to 50 mm/s were reliably measured.

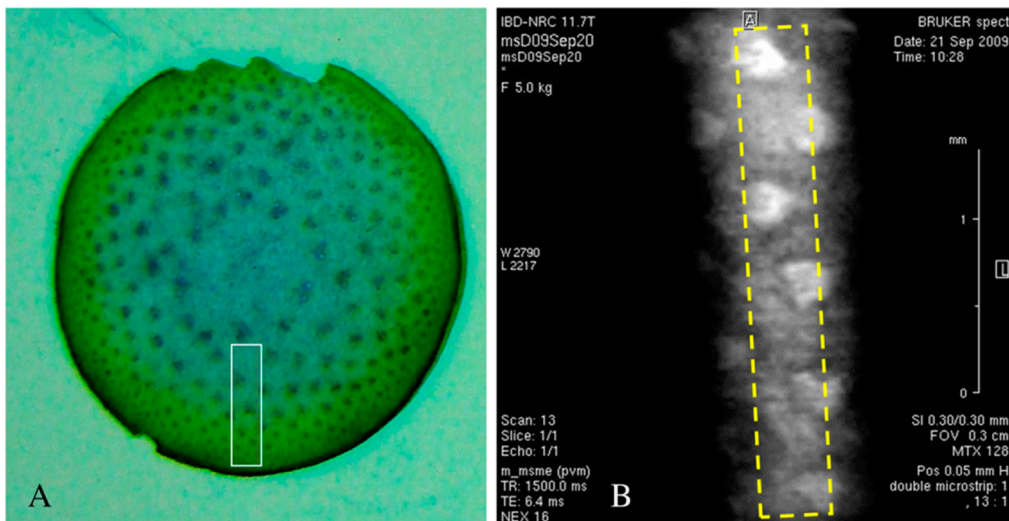


Figure 27. Microphotograph (A) and MR image (B) of an asparagus slice acquired with a microstrip resonator. Reprinted with permission from ref 156. Copyright 2012 Elsevier.

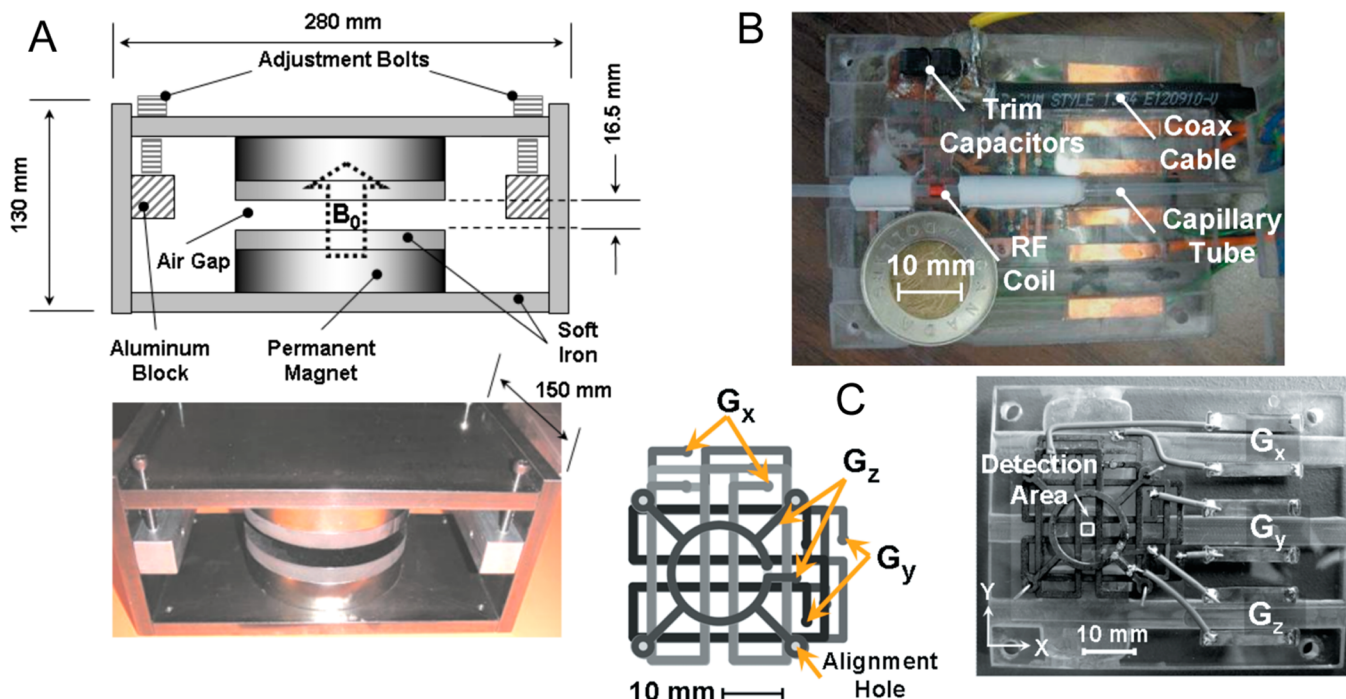


Figure 28. Portable MRI system: (A) drawing and photo of the magnet assembly; (B) photograph of the microcoil probe; and (C) scheme and photograph of the custom-built triaxial gradient system before application of the epoxy cover. Reprinted with permission from ref 157. Copyright 2010 American Institute of Physics.

Another approach for the producing solenoid microcoils for MRI was reported by the group of Korvink.¹⁵⁸ The coil support was prepared using conventional photoresist etching techniques, and the coil itself was wound using an automated microelectromechanical system (MEMS) wire bonder.¹⁵⁹ The authors emphasize the high speed (approximately 200 ms for a coil) and excellent reproducibility compared to winding by hand. The parameters such as the number of turns and the pitch of the coil could be easily varied. The photograph and the equivalent electric scheme of the microcoil are presented in Figure 30A. The coil was wound in 5 turns on a glass base and bonded onto a PCB. The inner diameter of the coil was 700 μm , and the outer diameter was 1 mm. The measured

resistance and inductance of the coil were found to be 2.05 Ω and 38 nH, respectively.

An excellent example of multiple-coil array for MRI detection was recently presented by Keil and Wald.¹⁶⁰ Thorough simulations were made to investigate the optimal number of coils and their locations accounting for coil superposition effects. The resulting array consisted of 64 coils covering the whole head surface (Figure 31). Each coil contained individual tuning/matching circuitry and was connected to individual preamplifier boards. Tuning and matching were the most time-consuming procedures as strong coupling with neighbor coils was observed. The system demonstrated excellent performance with in-plane isotropic resolution 0.47 mm and 0.9 mm slice

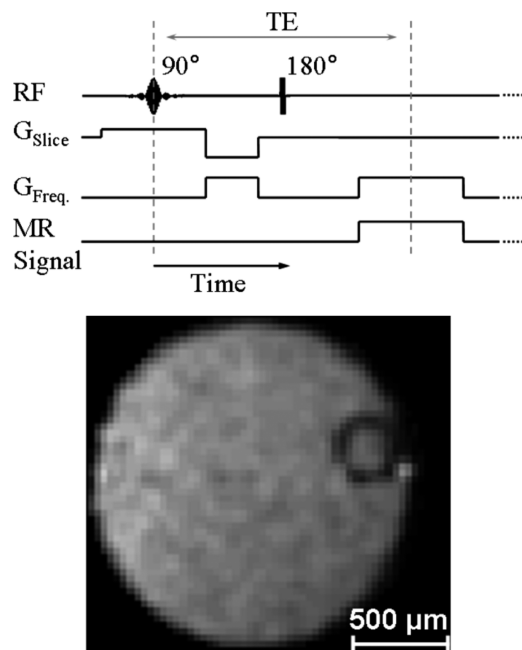


Figure 29. Imaging sequence for acquisition of the image (top) and reconstructed image of the phantom. Reprinted with permission from ref 157. Copyright 2010 American Institute of Physics.

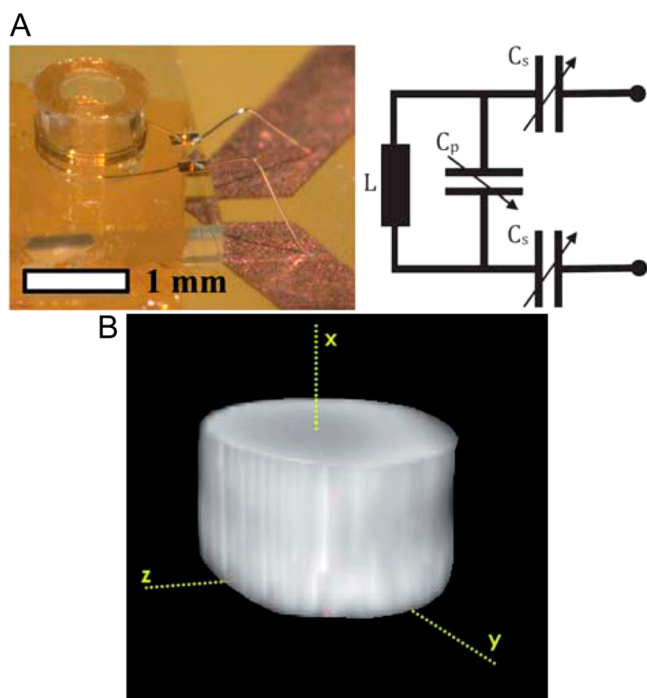


Figure 30. MEMS-manufactured microcoil: (A) the photograph of the assembly and its equivalent electric circuit; (B) MR image obtained from a test phantom sample. Reprinted with permission from ref 158. Copyright 2010 Royal Society of Chemistry.

thickness. With the exception of resolution enhancement, the authors demonstrated application of the coil array detection to decrease total acquisition times via parallel slice imaging. The acceleration factor (keeping reasonably high resolution) was found to be up to 10–16 times depending on the MRI method employed.

An interesting application of microcoil NMR techniques to clinical MRI was demonstrated by Pruessman and co-workers.¹⁶¹ The authors used a microcoil-based NMR probe as an auxiliary sensor to measure RF field inhomogeneities during the MRI scan. The microprobe consisted of a glass capillary filled with H₂O/CuSO₄ wrapped with a thin copper wire. The reconstructed EPI image with the field corrections from the auxiliary probe applied is depicted in Figure 32. By accounting for the measured field distortions, enhanced images could be reconstructed.¹⁶²

Catheter coils are another example where the size of critical hardware components needs to be reduced. Originally designed to visualize a catheter tip in a magnetic resonance image during surgery interventions, micro coils were placed inside the catheter with dimensions in the range 1–5 mm. The position of the catheter can be identified in the image from the magnetic field distortions created by a weak current through the catheter coil. The same coil can be employed to record the local NMR signal from the spins in the surrounding tissue for a relaxation and diffusion analysis or even to record a local image with high sensitivity. Various coils such as loop coils,¹⁶³ solenoid coils,¹⁶⁴ and inductively coupled RF coils¹⁶⁵ have been reported with different geometries depending on the study to be conducted and the region of the body under inspection. A complete and detailed review of this topic can be found elsewhere.¹⁶⁶

2.4. New Designs and Alternative Detection Methods

Other areas of intensive research for improving NMR sensitivity include development and application of various noninductive detectors to obtain NMR signal from the sample. One of those is magnetic resonance force microscopy (MRFM),¹⁶⁷ which is based on the interaction of nuclear spins with precise magnetic cantilevers as in atomic force microscopy. A prototype of an MRFM-based NMR spectrometer was proposed by Madsen.¹⁶⁸ Their setup relied on conversion of the NMR signal to mechanical resonance, which was detected by a fiber-optic interferometer. The main advantages of the proposed setup were very high sensitivity as compared to traditional inductive detectors and easy scaling down to micrometer sizes. Further research in this area, including the design of magnetic lenses¹⁶⁹ and laser-detected MRI,¹⁷⁰ can seriously improve the characteristics achieved. Mamin and co-workers reported MRFM-based imaging operating in the nanoscale regime.¹⁷¹ Their setup utilized specially prepared thin film magnetic tips with a CoFe active layer. The authors demonstrated ¹⁹F imaging with 100 nm spatial resolution. This corresponds to active detection volume of less than 650 zL, which means roughly 1200 nuclear spins were observed.

To push the resolution limits further down to subnanoscale mode, the design of new high-sensitive nanomagnetic tips capable of delivering strong gradient currents is important. Several reports to satisfy the goal were presented. Utilizing the nitrogen-vacant (NV) center in diamond as MRFM detector combined with extremely sensitive optical readout, the detection volume of 4.3 nm³ was achieved.^{172,173} An application of NV-detection to conventional NMR was also demonstrated.^{173,174}

A well-known example of noninductive NMR sensors is a SQUID (superconducting quantum interference device).¹⁷⁵ The basic principle underlying the operation of a SQUID is the Josephson effect, which consists of the appearance of a voltage bias across a junction in a superconducting loop in the presence

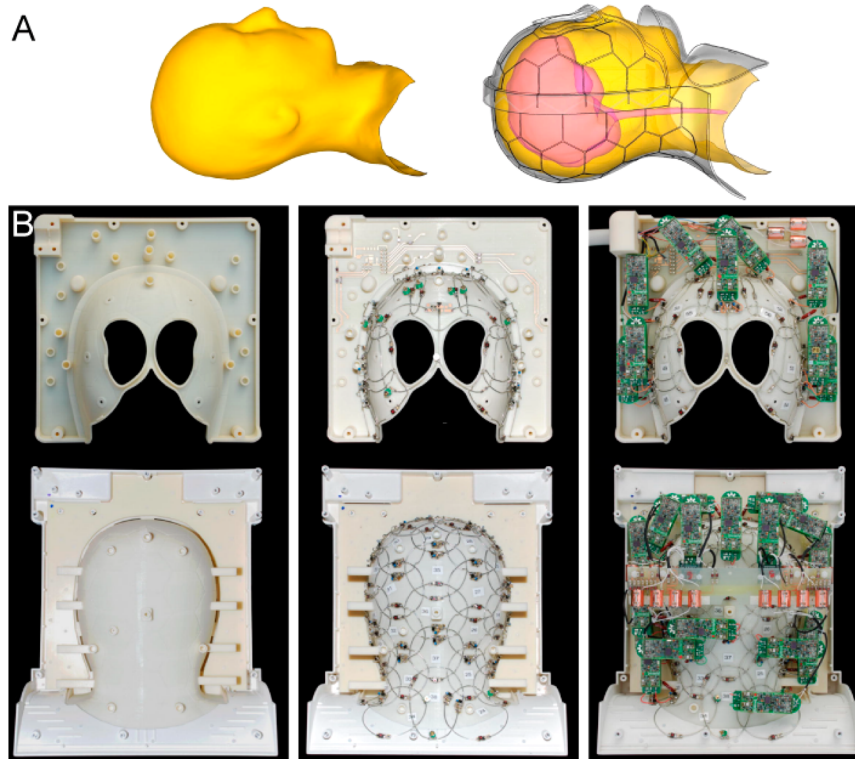


Figure 31. Design and construction of 64-coil array for brain MRI studies: (A) modeling the position of the coil holding helmet on the patient head; and (B) assembling the coils. Reprinted with permission from ref 160. Copyright 2013 Elsevier.

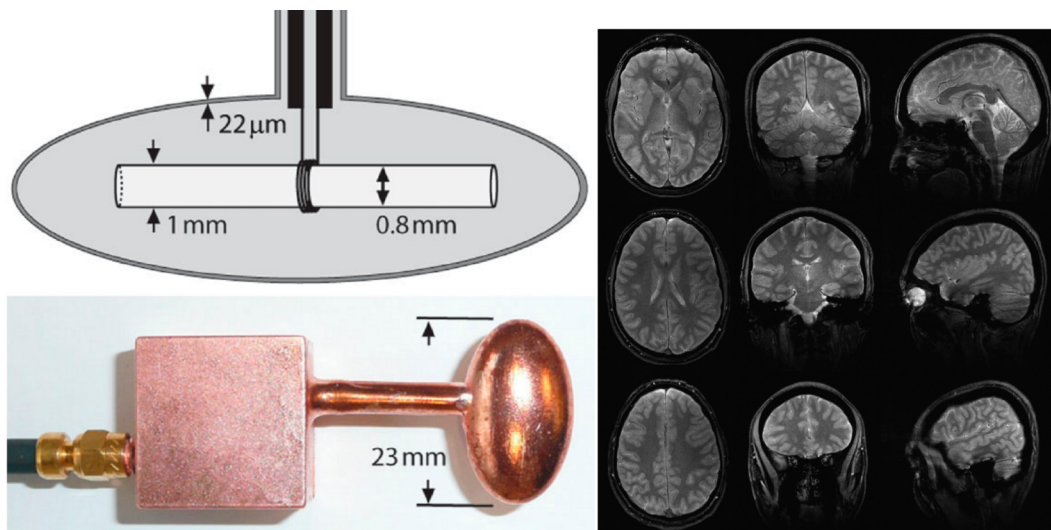


Figure 32. Field monitoring sensor and reconstructed MR image with corrections applied. Reprinted with permission from ref 161. Copyright 2009 Wiley-VCH.

of an external magnetic flux. The major problem in the use of SQUID detectors is the fairly weak output signal, which is often overwhelmed by the thermal noise in the preamplifier stage. The possible solution of the problem was suggested by Casey and co-workers.¹⁷⁶ They used a double-stage SQUID setup with the first stage operating at 1.2 K temperature. The utilization of the SQUID-based transformer allowed one to amplify the signal above the noise level.

Even considering the weak output signals, SQUID-based detection is indispensable in the cases when ultimate sensitivity is needed. An example of such is low-field NMR and MRI.¹⁷⁷ Imaging in low magnetic fields (<1 T) can overcome several

restrictions inherent to conventional techniques, high cost and big size of MRI machines.

An example of SQUID detector miniaturization was presented by Granata and co-workers.¹⁷⁸ The developed nano-SQUID had the dimension of 80 nm × 100 nm, which resulted in the possibility to conduct very precise measurement of local magnetic fields. However, the dramatic loss in sensitivity prohibited the application of the detector developed in measurement of nuclei polarization. The further research on MRI miniaturization and elaboration mostly relies on exploitation of other detection schemes.^{173,179}

The main contradiction that lies in the fundamentals of NMR inductive detection is that the requirements are opposite to those of the coil for excitation of the sample and detecting the FID. To uniformly excite the spins in the region of interest, a large coil at a distance away from the sample is required. Moving the coil from the sample increases the uniformity of the excitation because local magnetic field inhomogeneities are greater near the coil surface. The magnetic field strength is not an issue in this case because one can achieve any desired flip angle for the spins of interest simply by increasing the pulse current in the coil. However, for detection of the FID, the requirements considerably differ. The main goal now is to get the maximum amplitude of the response signal in the detection coil. This requires the use of detection coils with the maximum filling factor, which means the coil has to be as close as possible to the sample. Commercially available probeheads often use optimized coil geometries (saddle or Helmholtz coils), which operate at a compromise between the uniformity of excitation and the sensitivity of detection.

A principally different, straightforward approach of improving NMR instrumentation is to separate the polarization and detection steps.¹⁸⁰ Pioneering investigations in this area on hyperpolarized ¹²⁹Xe conducted by Pines and co-workers led to the invention of remote detection.¹⁸¹ They demonstrated that employing different coils for polarization and detection results in about a 150-fold increase in the S/N ratio. The commercially available imaging probe was modified, utilizing the original imaging coil only for the polarization step (Figures 33 and

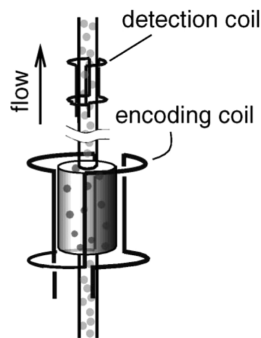


Figure 33. Separation of encoding and detection steps in a remote detection setup. Reprinted with permission from ref 182. Copyright 2006 Elsevier.

34).¹⁸² For detection, they fabricated a micro solenoid coil made from 130 μm copper wire. It was essential to locate the detection coil as close as possible to the encoding coil to minimize signal losses due to relaxation during sample flow from the excitation to the detection region. The position of the detection coil with respect to the external magnetic field was not crucial; however, the authors believe that the placement of the detection coil in the region of maximum B_0 homogeneity is advantageous to minimize signal losses from inhomogeneous line broadening during multiecho acquisitions.

The additional benefit of remote detection is the availability of conducting time-of-flight (TOF) imaging studies.^{183,184} In recent studies, it was demonstrated that time-of-flight imaging by remote detection is a useful tool for studying gas propagation in porous media. In Figure 35, microchip TOF imaging is demonstrated by example of a ¹²⁹Xe gas flow through a 50 μm etched channel in a microchip. The results show a nonuniform velocity distribution across the flow region,

which indicates that mixing due to transverse diffusion is slow enough to proceed over the time scale of gas flow. These data demonstrated the ability of noninvasive flow studies and transport studies in porous materials using prepolarized ¹²⁹Xe as a spin label.

Another example of magnetometer-based NMR detector was demonstrated by Pines and co-workers.¹⁸⁵ They managed to build a setup that was operating at zero applied magnetic field (spin-exchange relaxation free or SERF regime),¹⁸⁶ where inductive detection is not applicable. The combination of remote detection with noninductive detection schemes gave rise to a unique hybrid setup. The best sensitivity achieved for protons was about 120 pmol for 1 s acquisition time with the room-temperature anisotropic magnetoresistive sensor for remote detection. The high sensitivity of magnetoresistive sensors combined with small physical dimensions has a huge potential for portable NMR-on-a-chip applications.

Apart from sensitivity, another problem of microfluidic NMR imaging arose from application of conventional Fourier techniques: the shorter the observation time, the poorer is the resolution. This limits the speeds of flow that can be studied by MRI. An elegant solution to the problem was initially suggested by Harel and Pines.^{187,188} They suggested the use of a "time slicing" scheme, which under constant flow velocity conditions allows one to obtain flow images with 2 ms time resolution. A further improvement of this setup introduced sparse sampling,¹⁸⁹ which allows one to increase the speed of sampling by a factor of up to $\sim 10^6$. An interesting application of remote detected MRI to column chromatography detection was demonstrated by Bajaj and co-workers.¹⁹⁰ The separation of encoding and detection steps made it easier to incorporate the NMR setup into a flow LC system.

2.5. Perspectives of Hardware Miniaturization

Although the examples presented in this section have shown the first step of NMR miniaturization in all three disciplines of NMR, that is, in imaging, spectroscopy, and relaxation studies, further miniaturization may change the game of how NMR is used. Today, it is the trained scientist expert who applies NMR to solve analytical tasks in medicine, chemistry, and engineering. Tomorrow, smartphone size analyzers containing NMR modules can become a standard personal care item in every household, or a common instrument in the laboratory. To arrive at cell-phone size analyzers, the volume of the NMR magnet must be reduced by at least another order of magnitude. In this procedure, controlling the homogeneity of the system will become challenging. This will require exploring new shimming technologies, or even interaction with scientists of other areas, such as material science, to improve the quality and performance of hard magnetic materials, to reach or better approximate the extreme demands imposed by NMR.

To reduce the energy consumption and tending to the situation of stand alone magnets, it is also necessary to address the problem of the temperature dependence of the magnetic fields generated by permanent magnet arrays. The main factors influencing the field drift of permanent magnets are (a) the strong temperature dependence of the remnant magnetization of hard magnetic materials and (b) the thermal expansion coefficient of the materials commonly used to build the magnet housing. The combination of these effects can lead to a field drift in the range of 300–1000 ppm for a change of just 1 °C in the temperature of the sensor. This eliminates the possibility of signal averaging to improve sensitivity, or executing any

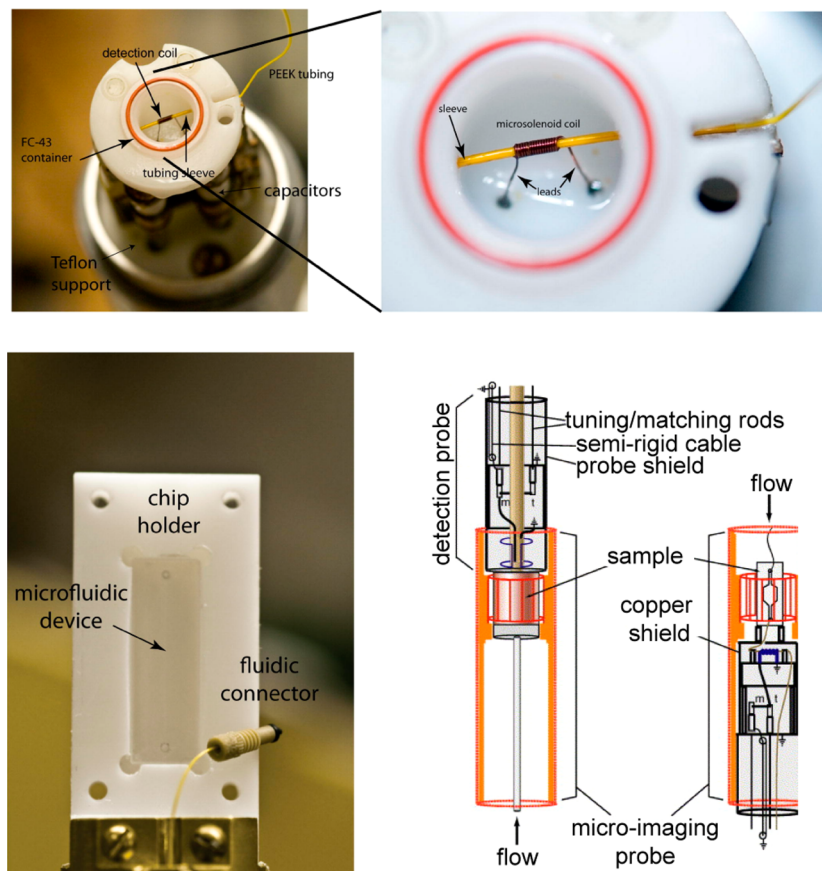


Figure 34. Modification of commercial imaging probe for remote detection. Reprinted with permission from ref 182. Copyright 2006 Elsevier.

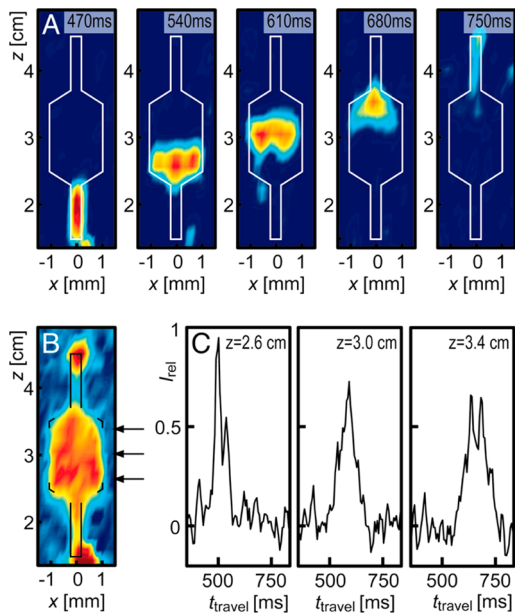


Figure 35. Time-of-flight imaging of ^{129}Xe flow through a microchip. Reprinted with permission from ref 183. Copyright 2005 National Academy of Sciences.

spectroscopy experiment requiring more than one shot. Actually, the problem is solved by actively controlling the temperature of the magnet at a value different from room temperature and covering the magnet with an insulating layer to minimize heat transport between the magnet and the

environment. To overcome this problem, a passive method has been proposed that combines magnetic materials with different thermal coefficients such as NdFeB and SmCo.⁸⁷ The condition to be fulfilled requires that the ratio of the fields generated by each unit matches the ratio of their effective thermal coefficients defined as the combination of both the reversible temperature coefficient of the remnant magnetization and the thermal expansion of the magnet array. The concept was experimentally demonstrated¹⁹¹ with a modified Halbach array similar to that shown in Figure 3, obtaining a negligible frequency drift with changing temperature. The final magnet represented a cylinder 8 cm long with inner and outer radius of 1 and 2.5 cm, respectively, and a magnetic field strength of 0.25 T. The implementation of this concept for different magnet geometries would help to reduce power consumption and thus to simplify the sensor.

The study of samples with broad resonances resulting from any anisotropic interactions like residual dipolar or chemical shift interactions, and local magnetic field gradients arising from variations in the bulk magnetic susceptibility of the samples, is at the moment largely excluded in the use of portable devices. Conventionally, these problems are solved by rotating the sample around an axis that is at the magic angle with respect to the magnetic field direction.¹⁹² The design of specialized probes to achieve this goal could be implemented on small magnets with certain advantages mainly in terms of good accessibility.¹⁹³ Another advantage observed in small sensors is that for cases in which the sample might be damaged due to centrifugal forces, instead of spinning the sample it would be possible to spin the magnet while the sample remains at rest. The concept has

recently been presented¹⁹⁴ and demonstrated experimentally.¹⁹⁵

Highly sensitive radio frequency coils are being developed in multilayer technology for compact NMR with permanent magnets combined with microfluidic sample preparation technology. There are only a few examples of small magnets assembled with microcoils,¹²³ and even less studies involving also small spectrometers.⁴¹ New applications emerging from the combination of these three hardware pieces have already found some practical applications and are expected to rapidly develop in the near future.

It should be noticed that further increase in sensitivity using conventional electronics can be achieved with the use of cryoprobe technology. The original idea relies on the decrease of thermal noise in the probe circuitry via cooling it to cryogenic temperatures.¹⁹⁶ Modern setups offer either liquid nitrogen or cold gaseous helium cooling systems incorporating both the probe itself and the preamplifier assembly.¹⁹⁷ The overall gain in terms of S/N ratio may be 3–5 times.¹⁹⁸ This technique is widely used in biomolecular NMR,¹⁹⁹ metabolomics,²⁰⁰ MRI,²⁰¹ and other areas. However, detailed discussion of this topic falls out of the scope of this review.

No less important in terms of improving the S/N ratio of miniature NMR is its combination with hyperpolarization techniques. Parahydrogen-induced polarization appears to be a particularly promising approach, because the polarization transfer efficiency benefits from low field,²⁰² and because the polarization transfer step can be made chemically selective depending on the choice of the transfer catalyst, so that otherwise crowded spectra of complex mixtures like bodyfluids may be simplified. Another hyperpolarization technique suitable for miniaturization is ¹²⁹Xe NMR spectroscopy, where the chemical shift of hyperpolarized xenon trapped in cages loosely bound to marker molecules functions as biosensor.²⁰³ The hardware package would then constitute the combination of a miniature NMR spectrometer, a miniature hyperpolarization stage, and microfluidic components for sample handling.

3. PROPERTIES AND APPLICATIONS OF MINIATURIZED NMR

3.1. Flow Systems and LC–NMR

An attractive aim is to combine different analytical methods into a unified high-throughput workflow. Such hyphenated techniques allow more rapid and complete characterization of samples by resolving the data provided by one technique in terms of the data provided by the other. One well-known example of a hyphenated technique is HPLC–MS, which provides an exact mass determination for each principal component from a mixture.

Regarding the incorporation of NMR spectroscopy into the analysis workflow, the probe needs to be modified to incorporate a flow interface.²⁰⁴ Two principal designs of flow NMR probes exist: continuous flow (or online) and stopped-flow (or offline) probes. In the continuous flow design, a sample solution is withdrawn by a pump through a capillary network and passed to a variety of analyzers, for example, HPLC, NMR, IR, MS, etc. NMR spectra can be recorded at any point in time without interrupting the flow.²⁰⁵ However, continuous flow through the NMR cell causes field disturbances, which degrade the quality of the spectrum. Another issue is a limitation of the measurement time imposed

by time-dependent variations of the sample composition, for example, in the case of chromatographic separation.²⁰⁶ This prohibits the use of long time NMR experiments such as complex 2D sequences. An even more challenging situation arises when NMR is coupled to HPLC with gradient elution. The extensive change in solvent composition in the course of the analysis requires the use of special time-synchronized adaptive schemes for solvent suppression. Several excellent reviews of the construction and application of LC–NMR systems and their applications were given by Albert and co-workers.²⁰⁷ To access systems with volatile components, the GC–NMR method was reported.²⁰⁸

Stopped-flow NMR detection is free from most of the problems described above. Nevertheless, it requires additional flow control units to stop and continue the flow for the NMR analysis. Stopping the flow during HPLC analysis is highly unfavorable because it can spoil the quality of separation. Thus, the common design for stopped-flow systems includes a flow splitter, which directs only the component of interest to the NMR system. This topic is covered in detail in a review by Lindon and co-workers.²⁰⁹

Recently, an application of LC–NMR to analyze natural products was reported by Wilson and co-workers.²¹⁰ They utilized HPLC–MS and HPLC–NMR to separate a mixture of natural steroids and determine their structures. The setup for the HPLC–NMR operated in stopped-flow mode using a commercially available flow probe. Experiments were carried out with WET²¹¹ solvent suppression.

Bringmann and co-workers²¹² coupled NMR with circular dichroism measurements in a stopped-flow system to determine stereostructures for the metabolites from plant extracts. They coupled a 600 MHz spectrometer with an HPLC system via a PEEK capillary. A commercial BPSU-12 module was used as an intermediate storage for the compounds of interest. Operation in the stopped-flow mode allowed one to acquire 2D experiments such as COSY and TOCSY. A review on plant metabolomics studies via NMR spectroscopy was presented by Verpoorte and co-workers²¹³.

Nicholson and co-workers²¹⁴ employed directly coupled HPLC–NMR setup to analyze lipoproteins from human serum. The total analysis time was 90 min with three fractions collected. The system was operated in stopped flow mode with auxiliary UV detector triggering the NMR acquisition. A commercially available flow probe with flow cell volume of 120 μL was used. Each spectrum was collected in 7 min with 128 scans. The ¹H NMR data obtained allowed reliable identification of three major lipoprotein metabolites.

A microscale LC–NMR platform has been described by Kautz and co-workers.²¹⁵ Their setup shows two major innovations, a special flow splitter capable of delivering a small fraction of HPLC eluate to the MS equipment without interrupting the HPLC flow, and a microdroplet NMR system for rapid analysis of sample libraries.

Wolfender and co-workers demonstrated the application of UPLC–MS–NMR measurements to elucidate the structure of plant metabolites.²¹⁶ They used a system based on a commercially available CapNMR capillary probe from Protasis. The workflow is illustrated in Figure 36. After extraction, the crude material was subject to prepurification by UPLC with a 3% slope gradient elution.²¹⁶ The final purification was done in isocratic mode with an A/B = 92/8 system (A, 0.1% formic acid/water; B, 0.1% formic acid/acetonitrile). Fractions were collected in the well plates every 30 s. The NMR measurements

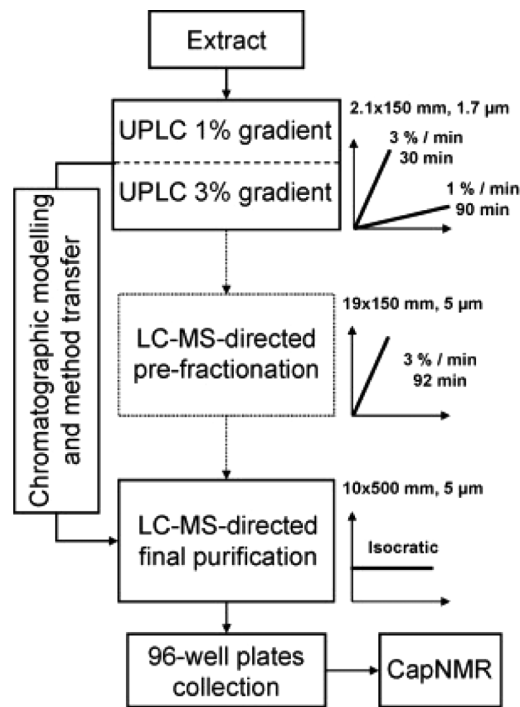


Figure 36. Hyphenated UPLC-MS-NMR setup. Reprinted with permission from ref 216. Copyright 2008 Elsevier.

were done with a system equipped with a 5 μL microflow CapNMR probe.

Example spectra are presented in Figure 37. In the first step, the masses for the peaks of interest were determined with the HPLC-MS setup. The peaks selected on the basis of retention time then were analyzed by NMR spectroscopy. High-resolution 1D and 2D (TOCSY) NMR spectra were obtained from microgram quantities of isolated natural products.

All of the flow NMR examples cited above use dedicated flow NMR hardware, which is often expensive and delicate to handle. An essentially different concept for reaction monitoring involves direct addition of reagents to the NMR via syringe line.²¹⁷ A recent example of such a setup was presented by Morris and co-workers.²¹⁸ The authors designed a special insert for the NMR magnet that incorporates a regular 5 mm NMR tube with a flow interface. A liquid pump continuously passes the solution through the NMR tube returning it back to the reaction vessel. All parts of the system were made either from PEEK or from Teflon, thus allowing fluid transport even for aggressive chemicals. An optical liquid sensor was used to protect the system against leaks. With a stainless steel frit installed on the pipe from the reactor to the pump, even heterogeneous processes (reductive amination of an aldehyde mediated with polymer-supported NaBH₃CN) could safely be monitored. A photo of the flow cell and a drawing of the whole assembly are depicted in Figure 38. The two PEEK capillaries in the photo are the injection and withdrawal lines; the black tube is a connection to the leak sensor.

An application of the flow system to reaction monitoring is shown in Figure 39. The total duration of the experiment was 5 h. Each spectrum was acquired with 4 transients separated by 7 s recycle delay. The resulting signal shape, sensitivity, and resolution were comparable to those from data acquired with a regular 5 mm NMR sample tube.

A similar example of continuous flow NMR application toward reaction monitoring was reported by Albert and co-workers.²¹⁹ The capillary probe with detection volume of 1.5 μL demonstrated excellent line shape characteristics that allowed one to discriminate between two diastereomers being formed in the reaction. The detected chemical shift difference between diastereomeric forms was as small as 0.02 ppm.

An interesting example of the use of flow NMR for rapid screening of large combinatorial chemistry libraries was demonstrated by Keifer and co-workers.²²⁰ Usually screening

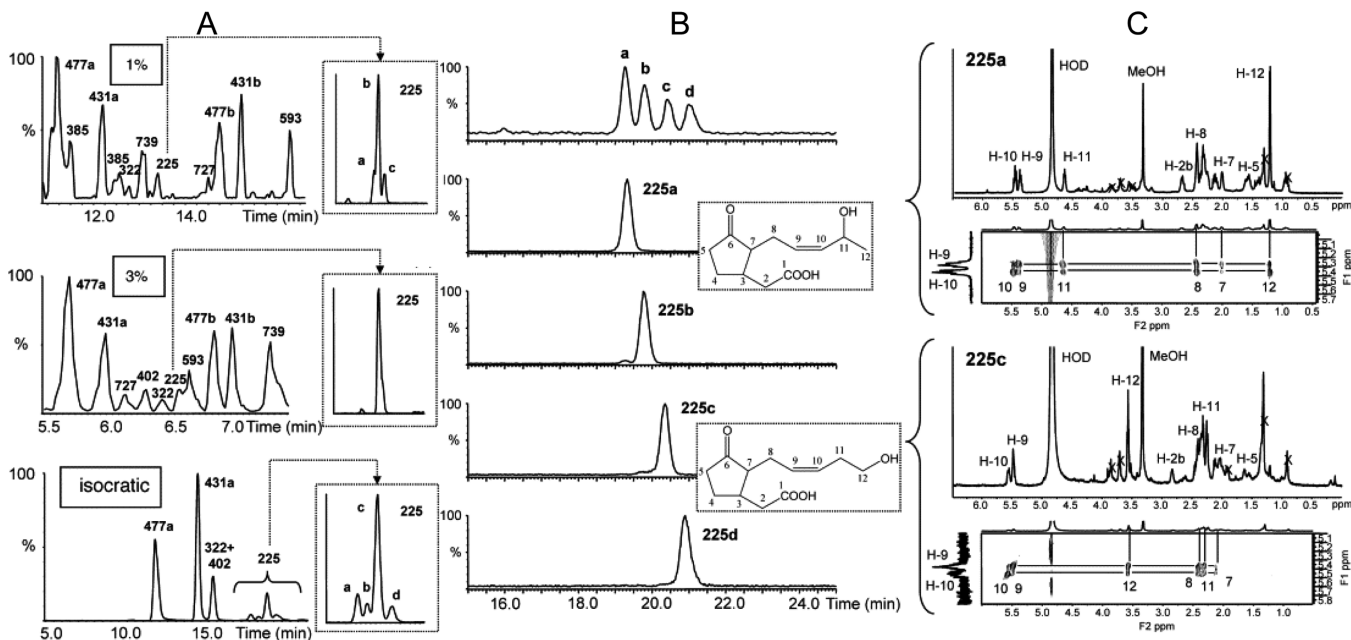


Figure 37. Example spectra from an HPLC-MS-NMR setup: (A) chromatograms obtained under various elution conditions; (B) selected ion chromatograms for isomeric metabolites; and (C) NMR spectra of eluate fractions. Reprinted with permission from ref 216. Copyright 2008 Elsevier.

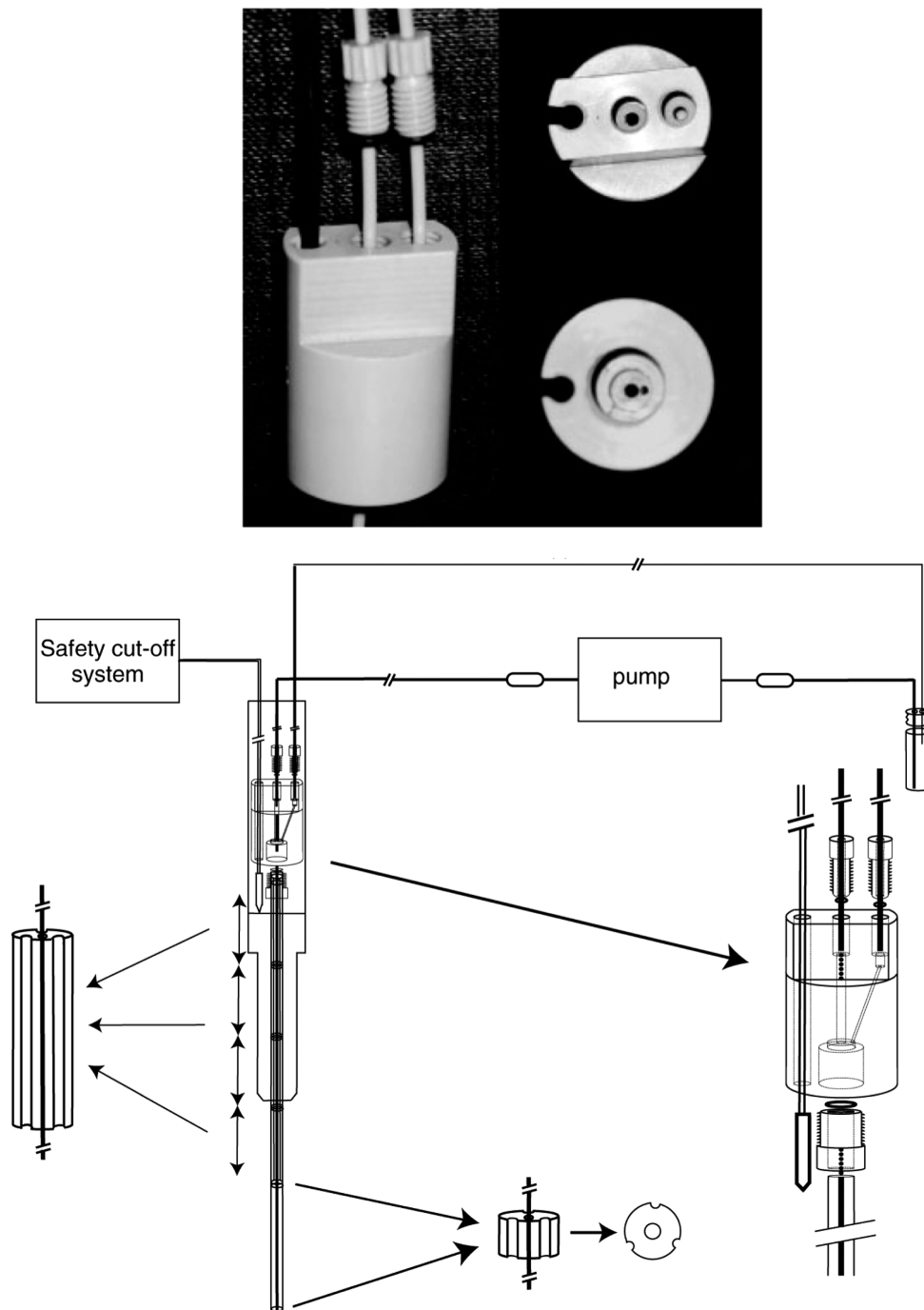


Figure 38. NMR flow apparatus for chemical reactions monitoring. Top: Photo of the in-magnet section of the flow system. Bottom: Drawing of the assembly. Reprinted with permission from ref 218. Copyright 2010 Wiley-VCH.

a large amount of compounds involves manual preparation of samples in ordinary NMR tubes followed by loading the tubes into a robotized auto sampler, which puts the NMR tubes one by one into the NMR instrument. The authors suggest a much simpler auto sampler design, which transfers predissolved samples from a standard multiwell microtiter plate into the inlet of a capillary NMR probe. This allows avoiding the use of sophisticated NMR tube handling apparatuses as well as regular NMR tubes. Dissolving the samples on a microplate is easier and less time-consuming than the traditional technique. After analysis, each sample is returned to its cell on the microplate, and the capillary probe is washed with an appropriate solvent.

Another example of reaction monitoring by flow NMR has been reported by Maiwald and co-workers (Figure 40).²²¹ The process under study was the polymerization of formaldehyde. By suppressing the solvent signal selectively with WET, native reaction solvents could be employed (see the spectrum below). The application of the flow probe (detection volume 120 μL) specially optimized for high pressures allowed the authors to estimate the rate of formaldehyde polymerization reaction in a stainless steel reactor. A comprehensive review on industrial applications of NMR was given by Guthausen and co-workers.²²²

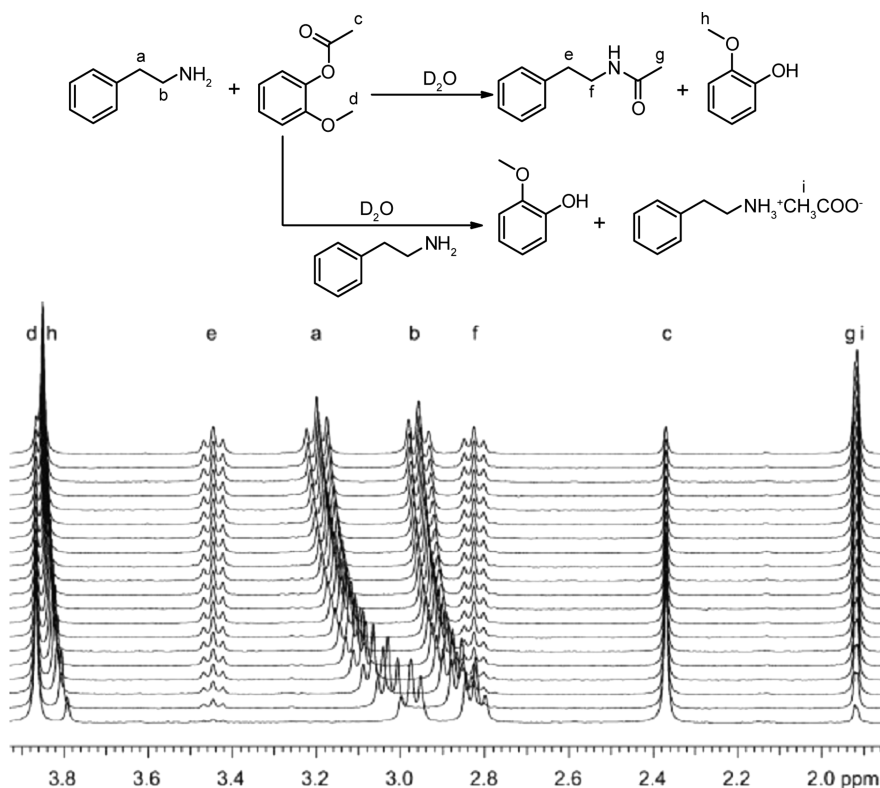


Figure 39. An example of reaction monitoring with the NMR flow apparatus. Reprinted with permission from ref 218. Copyright 2010 Wiley-VCH.

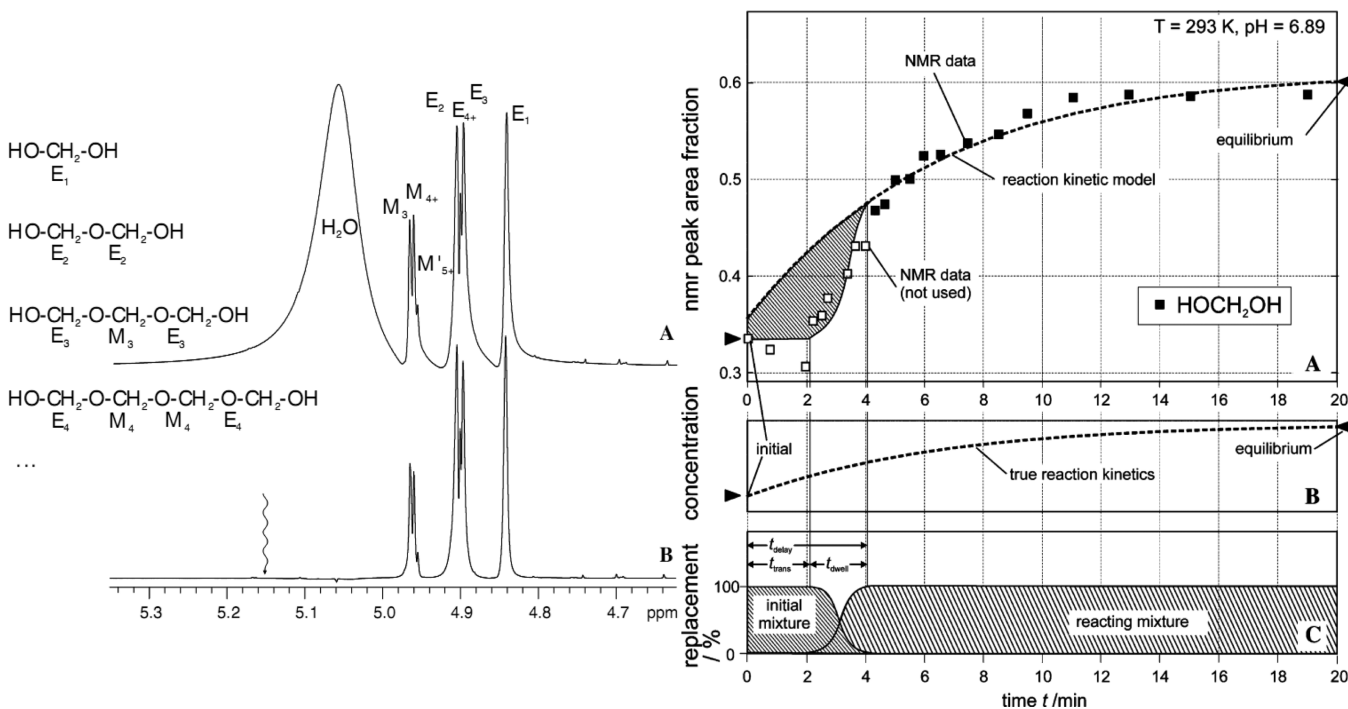


Figure 40. Example of a flow spectrum and kinetic data obtained from the monitoring of the reaction by NMR spectroscopy. Reprinted with permission from ref 221. Copyright 2004 Elsevier.

In the field of high-resolution portable NMR spectroscopy, microcoil probes in compact Halbach array-based permanent magnets are particularly attractive to miniaturization (see previous section of this review). This combination was successfully exploited by Herberg and co-workers to build a prototype of a portable NMR system.⁶³ The authors used a

special 3D laser lithography technique to produce a high-quality solenoid microcoils. Preliminary results demonstrated an S/N ratio of 32 for sample ¹⁹F spectrum. The authors attributed such a low S/N to poor magnet design. To test the coil performance, the coil was installed into a regular probe of a 500 MHz NMR spectrometer. The measured S/N ratio under those

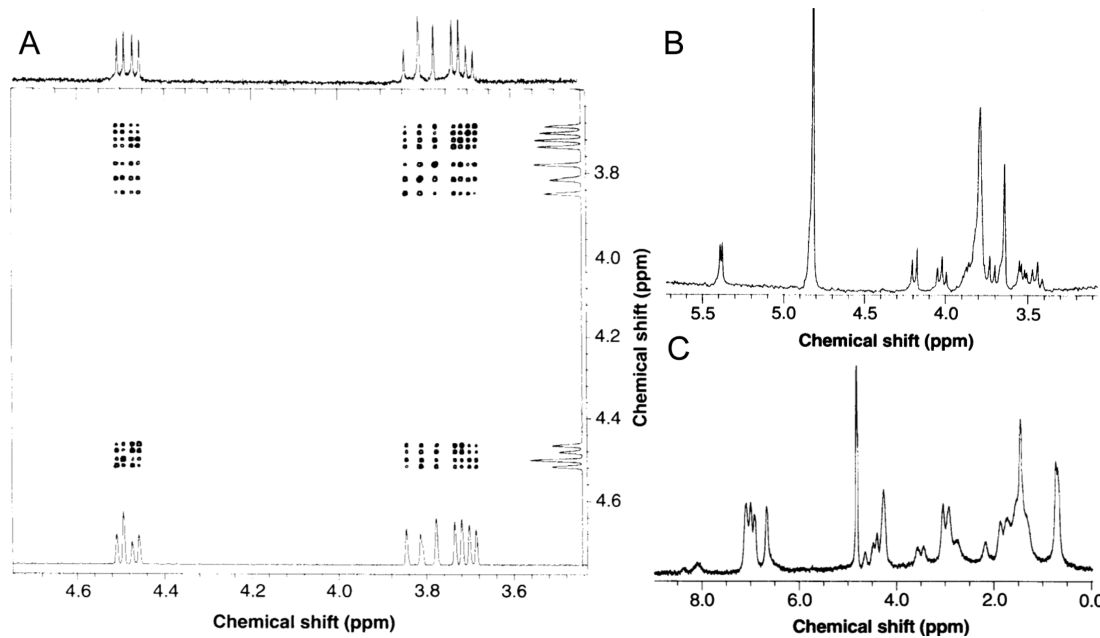


Figure 41. ^1H NMR spectra obtained with a microcoil NMR probe: (A) ^1H COSY spectrum; and (B,C) selected regions of one-dimensional ^1H spectra. Reprinted with permission from ref 109. Copyright 1995 AAAS.

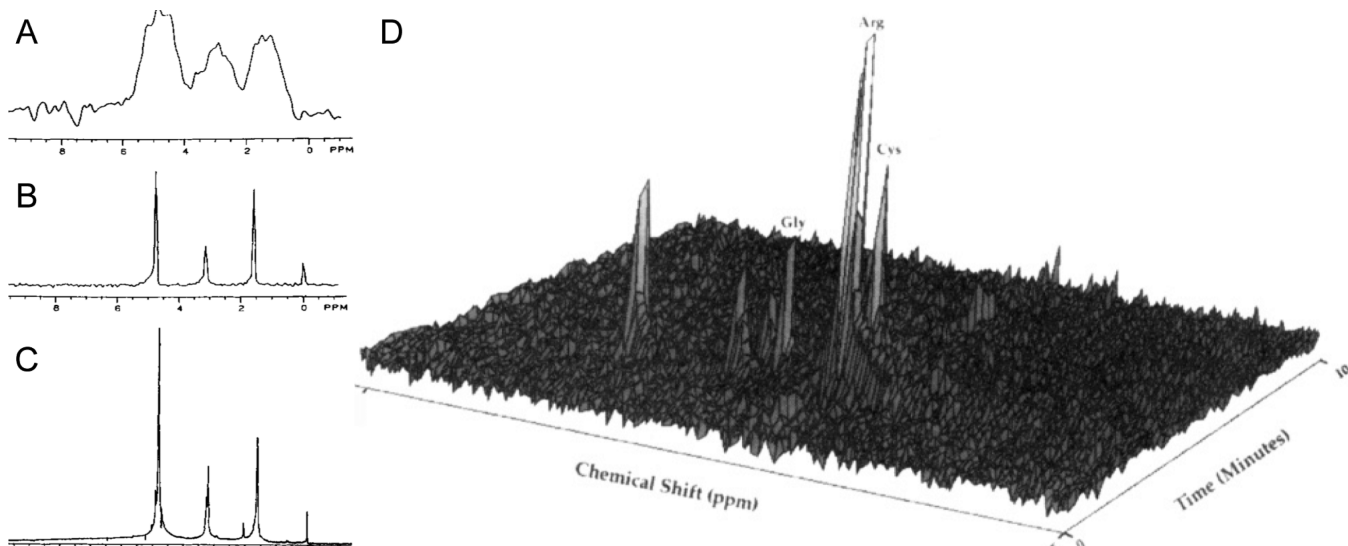


Figure 42. ^1H NMR spectra obtained with microcoils: (A) spectrum of arginine in a $145\ \mu\text{m}$ diameter microcoil; (B) the same in a $350\ \mu\text{m}$ diameter microcoil; (C) reference spectrum acquired with the sample in a $5\ \text{mm}$ NMR tube; and (D) demonstration of online NMR electrophoresis separation for a mixture of amino acids. Reprinted with permission from ref 110. Copyright 2004 American Chemical Society.

conditions was 15.8 for $360\ \mu\text{m}$ coil and 452.4 for $1\ \text{mm}$ coil. The possibilities to build shim coils, gradient coils, and construct a double-resonance probe with the laser lithography techniques were also demonstrated.

3.2. NMR on a Chip and Total Analysis Systems (TAS)

In the early 1990s, it was shown that the use of microcoils for mass-limited samples provides an excellent opportunity to gain complex spectral information from nanomole amounts of samples. This approach is illustrated in Figure 41. A COSY spectrum (Figure 41A) was obtained from $1.0\ \mu\text{g}$ ($4.5\ \text{nmol}$) of 2,3-dibromopropionic acid in $2.2\ \text{h}$ (256 points in the indirect dimension; 16 scans per increment; $0.3\ \text{s}$ repetition time). The spectrum shows well-resolved magnitude peaks from all protons in the system. Figure 41B demonstrates one-dimensional

^1H NMR spectra from a $2.5\ \text{nmol}$ sucrose sample registered with a microcoil. The total acquisition time was $1\ \text{min}$. The relative enhancement as compared to a regular $5\ \text{mm}$ NMR tube was estimated to be 23 200 times. An example of a spectrum from a natural compound is presented in Figure 41C. The sample was prepared from $3\ \mu\text{g}$ ($3.3\ \text{nmol}$) of *Aplysia californica* α -bag cell peptide. The measured limit-of-detection was $112\ \text{ng}$ ($124\ \text{pmol}$).

Another demonstration of the capabilities of microcoil probes was reported by Sweedler and co-workers.¹¹⁰ The set of 1D spectra A–C in Figure 42 demonstrates the dramatic loss of resolution with the decreasing size of the microcoil. However, an optimum compromise between the microcoil dimensions and the associated spectrum quality can often be found (Figure 42B). Figure 42D shows one of the first

examples of using the NMR system as a detector for different analytical routines, in this case, electrophoresis.

The overall approach to miniaturize the NMR instrumentation combined with the rapid development of modern microscale device fabrication methods resulted in the emergence of so-called micro total analysis systems (μ TAS). These are several analytical instruments for materials studies united in an assay on a small-sized chip. All flow manipulations such as mixing, separation, etc., are carried out in a specially designed flow paths on the same chip. Excellent reviews on the subject covering chip fabrication, sample handling and transfer, detection methods, and application of μ TAS for *in vivo* analysis were published by Manz and co-workers.^{223–225}

In the study by Gardeniers and co-workers,²²⁶ a microchip-based flow NMR detector was utilized for the measurement of the imine formation kinetics. The optimal microcoil geometry was calculated with finite element method simulations. A sputtering/etching process was used to fabricate the planar microcoil on a glass chip (Figure 43). The coil resonance frequency was adjusted to 60 MHz for ^1H . The possibility of monitoring reaction kinetics was successfully demonstrated (Figure 44).

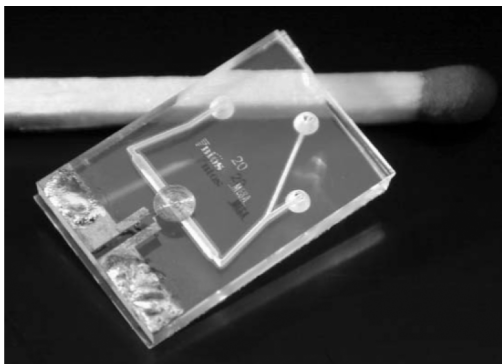


Figure 43. The photograph of a microchip used for monitoring reaction kinetics. Reprinted with permission from ref 226. Copyright 2005 Royal Society of Chemistry.

During fabrication of the microchips, it is always crucial to precisely control the dimensions of the structures built. Ahola and co-workers²²⁷ reported a magnetic resonance flow imaging technique capable of mapping the flow velocity. The microchip is operated in a modified Micro2.5 imaging probe equipped with a self-made rectangular surface coil made of a single winding of 1 mm copper wire (Figure 45A). The spatial resolution achieved allowed microchannels with diameters of 10 μm and less to be characterized. The image of the mixer in the absence of flow (Figure 45B) depicts clearly resolved individual channels. However, the B_0 field homogeneity was compromised by the small structures of the device, which resulted in variations of signal intensity even under static conditions (two identical channels giving different signal intensity are shown in Figure 45B with green arrows). The flow velocity mapping technique could be used not only as a quality control tool during chip fabrication but also as a monitoring instrument during microchip operation.

An improved version of this approach was presented by Pines and co-workers.²²⁸ Extending the remote detection approach (see section 2.4) to time-of-flight imaging, the authors were able to obtain high-resolution TOF images of the flow pattern in the microchip. By using chemical shift

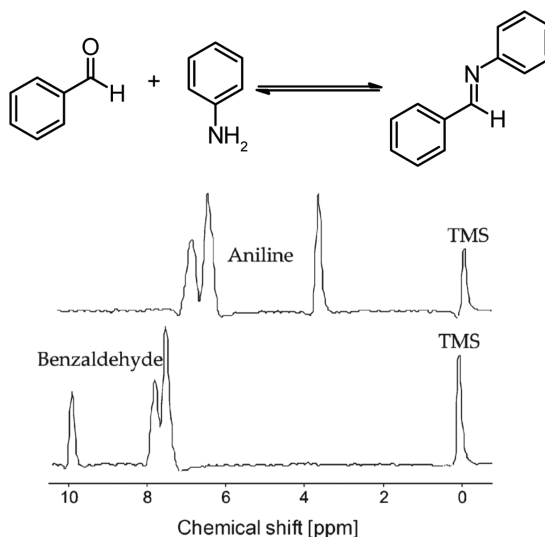


Figure 44. Model reaction for monitoring the reaction kinetics and spectra of individual components obtained with the microchip. Reprinted with permission from ref 226. Copyright 2005 Royal Society of Chemistry.

selection, the mixing of two different components (water and EtOH) could be tracked.

The microchip-based solenoid coil NMR detector reported by Besse²²⁶ was successfully applied later for the study of perfusion of the mammalian cells.²²⁹ To make the analysis more convenient, the microprobes produced imitated ordinary Petri dishes used for cells handling.

Velders and co-workers²³⁰ demonstrated the potential of microchip NMR for studying supramolecular interactions between cyclodextrin and NaPF₆ with ^{19}F NMR spectroscopy. The microchip (Figure 46) was fabricated from borofloat glass with rounded V-shaped channels 450 μm in depth and 500 μm in width under the coil. The active detection volume was about 50 nL. The microcoil consisted of nine copper windings prepared by electroplating (inner diameter 200 μm , interwinding spacing 20 μm). The NMR chip was mounted in a custom-built probe.

The minimally detected quantity was reported to be about 50 pmol of NaPF₆. The quality of the ^{19}F NMR data obtained allowed the authors to precisely measure the association constant and the stoichiometry (Figure 47) of the complex.

In the study by Anders and co-workers,²³¹ eight separate NMR micro receivers, each consisting of a microcoil, a tuning circuit, a low-noise amplifier (LNA), and a 50 Ω buffer, were combined into a single tiny CMOS chip. A common excitation microcoil was placed around the chip. The best reported spin sensitivity was about 4×10^{15} spins/ $\sqrt{\text{Hz}}$. The main drawback of the presented design was the electric crosstalk between adjacent coils. The authors claimed that signal deviations due to crosstalk can be as much as 20% of the overall signal intensity. Thus, additional measures should be taken to avoid this undesirable effect. A follow-up generation of the NMR chip was fabricated using the 0.13 μm CMOS technology. The improved design contained an on-chip feedback loop to compensate for variations during the chip manufacturing process. The architecture of the LNA was also improved to provide full differential output. Including the mixer on the chip resulted in significantly decreased interchannel crosstalk. In later studies, this setup was applied to build an integrated single-channel

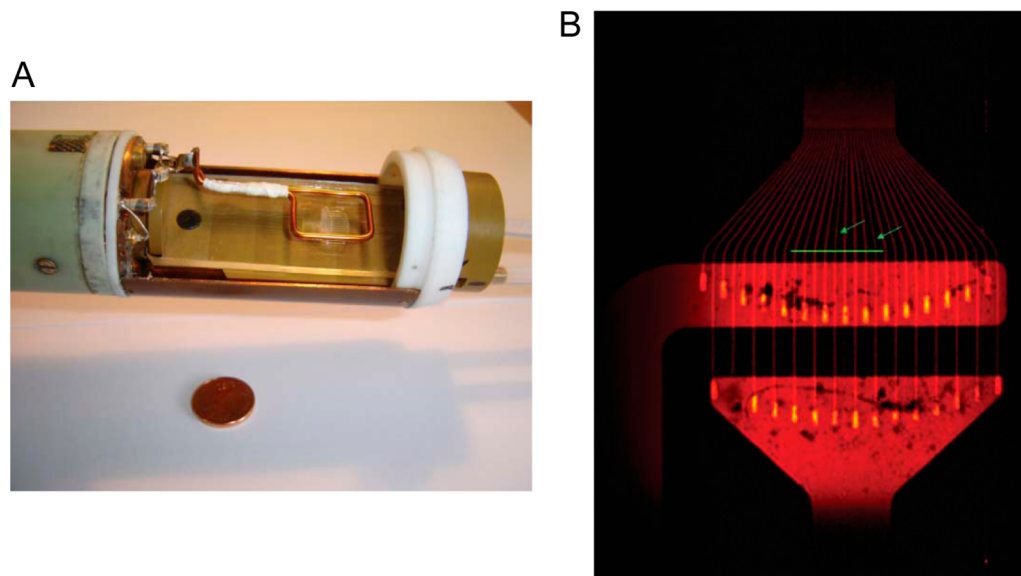


Figure 45. A setup for multichannel flow velocity imaging: (A) microcoil probe used for image acquisition; and (B) image of the micromixer in the stopped flow mode. Reprinted with permission from ref 227. Copyright 2006 Royal Society of Chemistry.

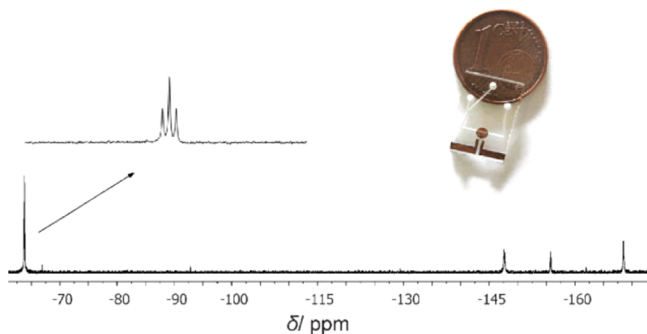


Figure 46. ^{19}F NMR chip and single-scan ^{19}F spectrum of octafluorotoluene. Reprinted with permission from ref 230. Copyright 2008 Wiley-VCH.

detector for MRI.^{232,233} The portable MRI scanner is illustrated in Figure 48.

As the system developed did not include capabilities for the RF pulse shaping required for slice selection, it was not possible to obtain 3D images in reasonable time. However, first 2D cross sections demonstrated good performance. The phantom sample constructed for testing the sensor consisted of a 450 μm outer diameter glass capillary filled with CuSO_4 -doped water and polystyrene beads with a diameter of 75 μm . Because the epoxy cover of the chip did not permit one to directly place the sample on the coil, it was located 250 μm above the chip's surface as illustrated in Figure 48B. The authors estimated the sensitivity loss arising from the 250 μm gap to be a factor of about 6 with respect to direct placement. Images of the phantom are presented in Figure 49. The total acquisition time was 83 h. The circles drawn on the images represent the capillary and bead borders. The isotropic resolution of the 400 $\mu\text{m} \times 400 \mu\text{m} \times 600 \mu\text{m}$ image was found to be 8 μm^3 .

An interesting example of on-chip NMR as an auxiliary analytical tool was presented by Beebe and co-workers.²³⁴ They managed to fabricate a microcoil on the bottom side of a

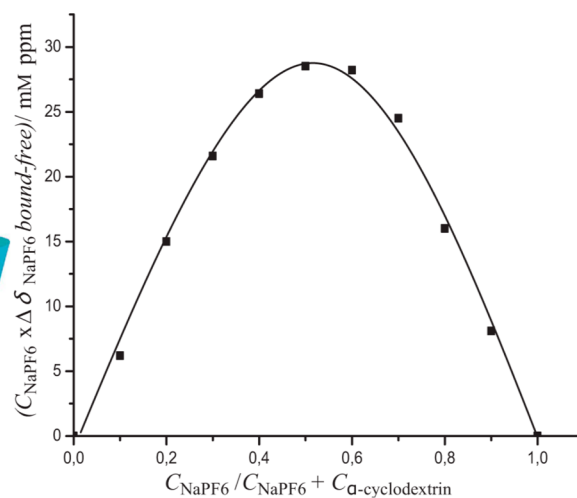
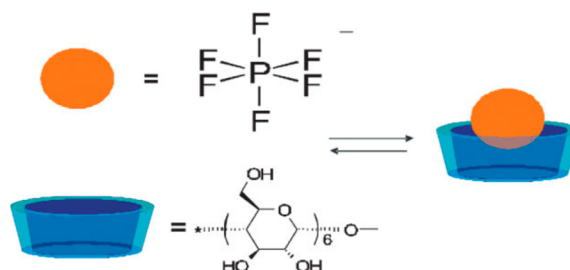


Figure 47. Schematic representation of PF_6^- anion complexation and NMR titration results. Reprinted with permission from ref 230. Copyright 2008 Wiley-VCH.

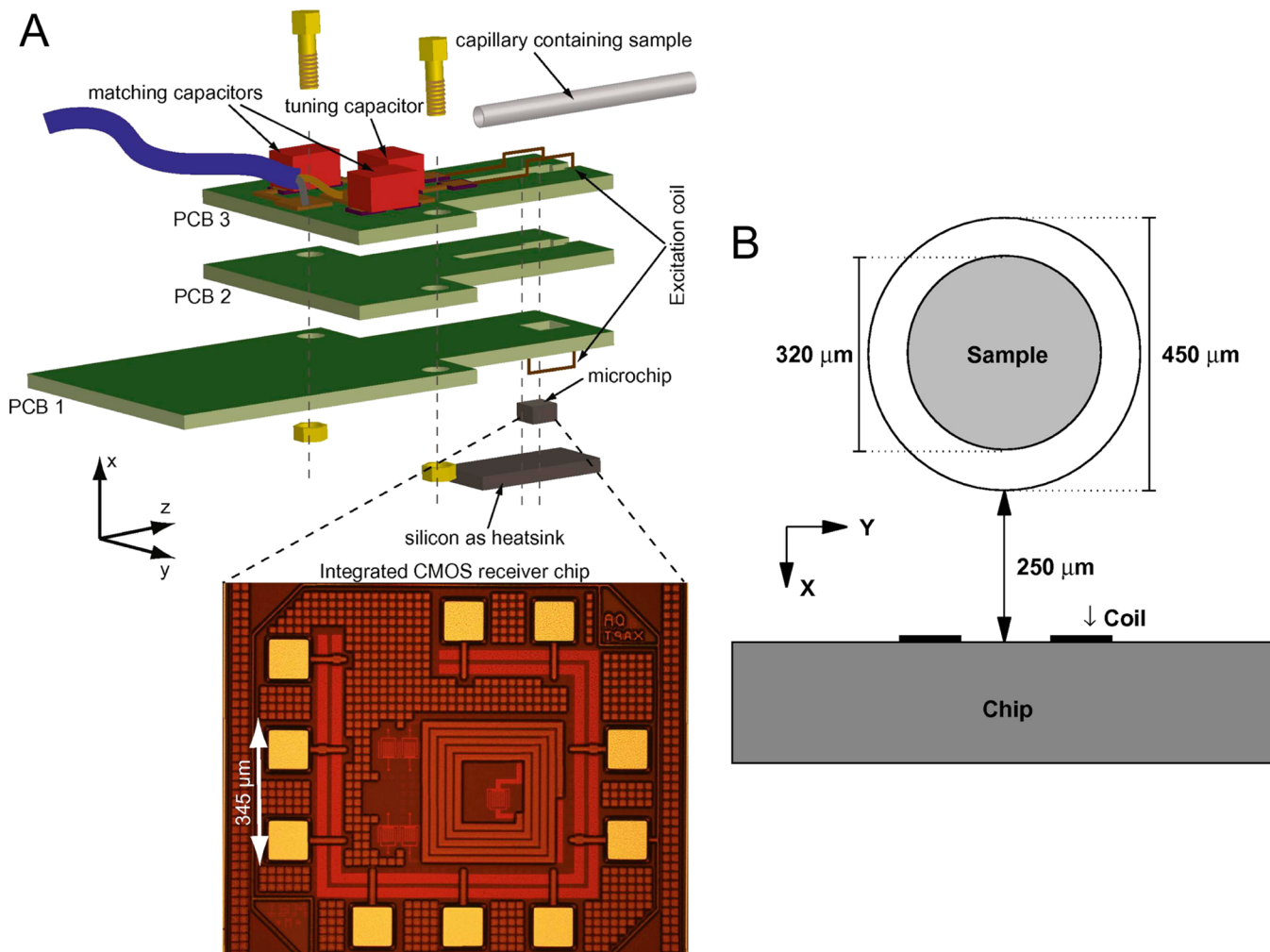


Figure 48. A portable MRI scanner: (A) microprobe assembly for portable MRI studies; and (B) alignment of the sample-containing capillary with the microcoil. Reprinted with permission from ref 233. Copyright 2011 Wiley-VCH.

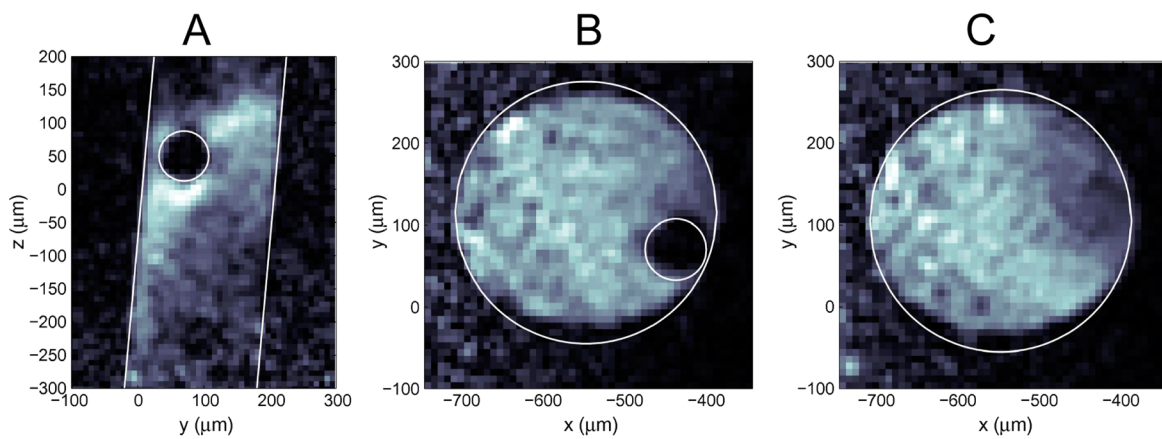


Figure 49. Projections of the MR images for a bead phantom obtained by microprobe MRI. The microcoil is located in the $y-z$ plane at $x = 0$: (A) $Y-Z$ slice; (B) $X-Y$ slice showing the cross-section of the bead; and (C) another $X-Y$ slice without the bead. Reprinted with permission from ref 233. Copyright 2011 Wiley-VCH.

capillary electrophoresis cell so that micro quantities of compound mixtures could successfully be analyzed.

Two novel portable NMR systems built around a modern CMOS NMR sensor were reported by Sun and co-workers.^{235,236} The system contains a complete NMR relaxometer with an integrated transceiver, a portable magnet, and a

microcoil probe on a single frame. The components of both setups are depicted in Figure 50A. The first system consisted of a ping-pong ball sized 0.56 T permanent magnet combined with a high-performance CMOS NMR transceiver. To further decrease the overall size of the system, the authors developed the one-chip NMR assembly (Figure 50B). Both systems

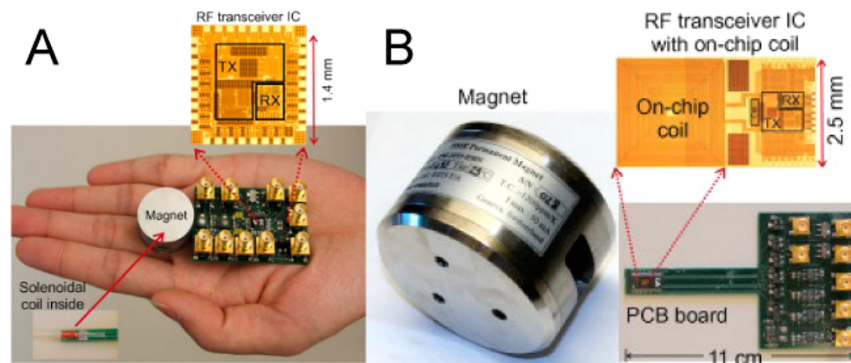


Figure 50. Portable chip-NMR systems: (A) 100 g of palm NMR system; and (B) one-chip NMR system. Reprinted with permission from ref 236. Copyright 2013 Elsevier.

included all of the components needed for conducting NMR measurements including the RF power amplifier. The authors compare their systems with NMR setups published before (Table 3).

Table 3. Comparison of Portable NMR Systems^{236a}

transceiver integration	small magnet	on-chip coil	ref
●rec/trans	●0.07 kg	○	235
●rec/trans	●1.25 kg	●	235
○	●1.25 kg	○	41
○	●2.5 kg	○	77
●rec	○	●	149
●LNA	○	●	231
●LNA	○	○	98
●LNA/PA	○	○	155
●LNA	○	○	150

^aA filled circle denotes implementation of the corresponding feature: rec, receiver; trans, transceiver; LNA, low-noise amplifier; PA, preamplifier.

Unfortunately, no NMR spectra were presented by the authors because the system developed was aimed at detecting biomolecules marked by ferromagnetic nanoparticles via T_2 relaxometry. The principle lying underneath the method is the change of marker relaxation rate due to coordination of target

molecules with ferromagnetic particles. The concept is illustrated in Figure 51. Antibodies bound to ferromagnetic nanoparticles and coordinated with specific target molecules give rise to a strong decrease of the T_2 relaxation time by clustering of ferromagnetic particles. In all cases reported, the change in the T_2 relaxation rate was big enough to firmly determine the target molecules in the solution under analysis. The detection limits for the protocols illustrated in Figure 51 were 17.5 cancer cells/ μ L and one hCG hormone molecule in 12 billion water molecules.²³⁵

Fabrication of an NMR chip enclosed in a standard dual inline package case with the dimensions of a small IC was successfully demonstrated.^{237,238} The NMR chip presented in Figure 52 was able to detect $\sim 10^8$ As atoms. The sample under study consisted of the intrinsic material of the semiconductor junction. It was shown that the device developed is capable of controlling the coherence of nuclear spins on the nanometer level, which makes it a major step toward the development of quantum computing devices and qubit-based memory technologies.

3.3. In Vivo Studies

An intriguing challenge in the field of in vivo NMR studies is the investigation of living cells. The results from such investigations could explain various aspects of the behavior of

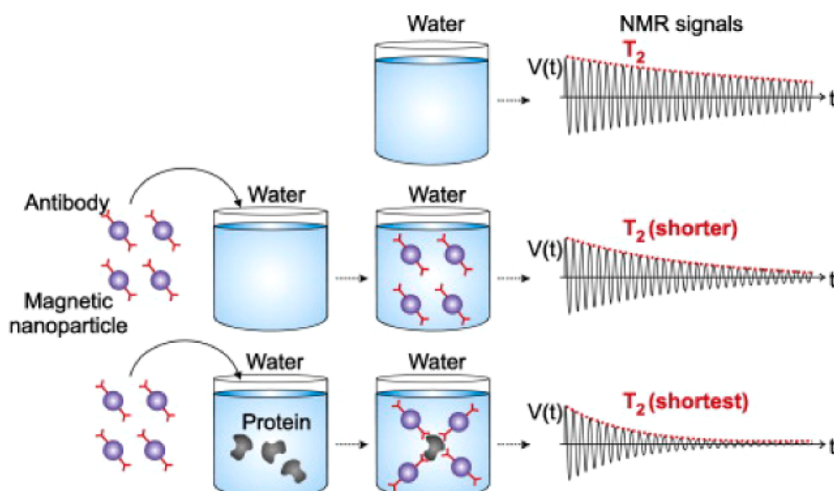


Figure 51. Principle of using magnetic nanoparticles as biomarkers with NMR-assisted detection. Reprinted with permission from ref 236. Copyright 2013 Elsevier.

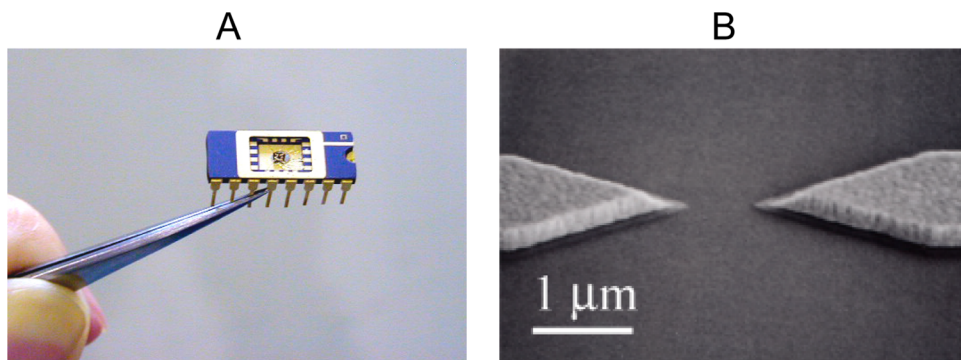


Figure 52. The NMR chip in standard DIP-16 case: (A) the photograph of the chip itself; and (B) SEM image of the sensing semiconductor gap. Reprinted with permission from ref 238. Copyright 2005 Nature Publishing Group.

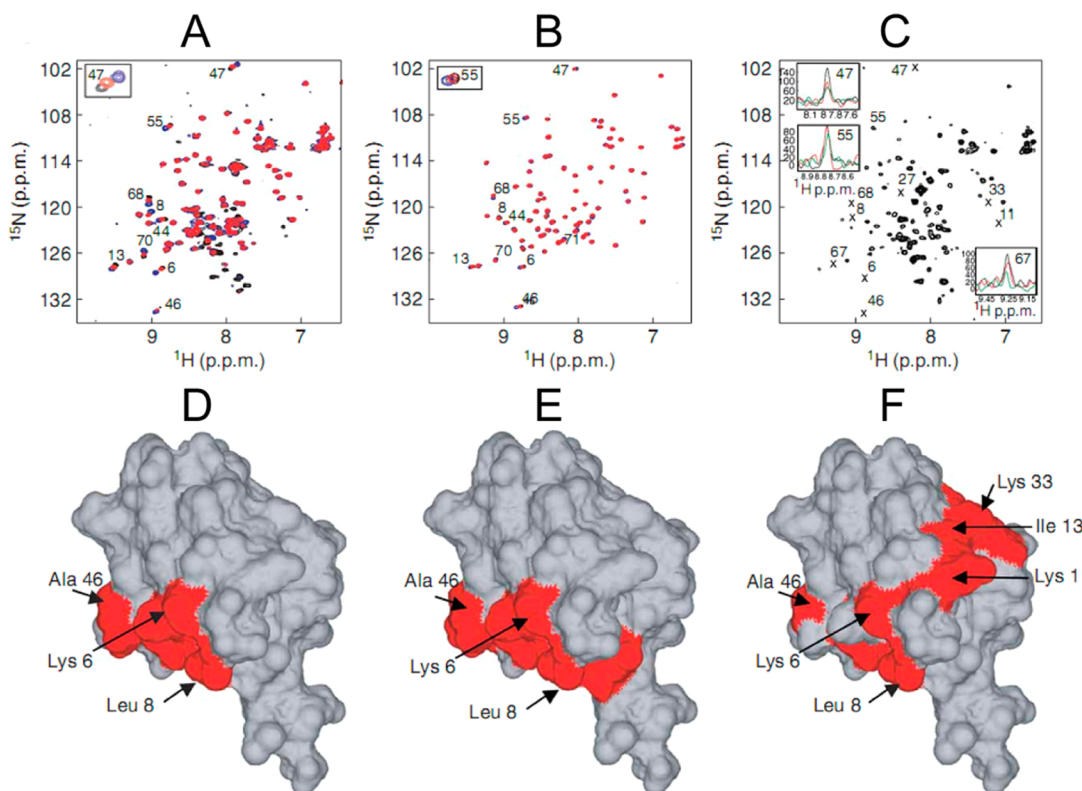


Figure 53. ^1H - ^{15}N HSQC spectra (A–C) and interaction maps (D–F) of ubiquitin–ligand complexes under different overexpression conditions with various proteins. Reprinted with permission from ref 243. Copyright 2006 Nature Publishing Group.

different cell components such as specific proteins and lipids in their natural environments without any external interference.

One of the early reviews on the NMR study of the living cells was published by Ciobanu and co-workers.²³⁹ The authors focused on the mathematical and physical concepts of microscale MRI and also discussed practical issues of achieving the best possible spatial resolution and sensitivity. Another important question to address is the survival of the cells during sample preparation. Being especially temperature and pH-sensitive, living cells require very specific handling and sample preparation procedures.²⁴⁰

Except sample preparation, there are two major issues in these kinds of studies. These are the selectivity in detecting the molecules of interest inside the cell and the high correlation times for the macromolecules, which lead to broad lines in the NMR spectrum. Both problems were solved in 2001 when two

groups independently published protocols for conducting *in-cell* NMR studies.²⁴¹

For the observation of the molecule of interest, a specially designed selective labeling technique was employed. It allowed one to grow cells with a specific protein being isotope enriched in ^{13}C or ^{15}N . TROSY NMR and HR-MAS techniques were used to overcome the issues associated with the long correlation times of the macromolecules.²⁴²

The disadvantage of the method suggested by Serber and Dötsch is the limitation to study only one protein at a time after a time-consuming cell-preparation process. This approach was extended via the STINT (STructural INTeractions) NMR methodology proposed by Shekhtman and co-workers.²⁴³ The use of sequential expression of two or more proteins within a single bacterial cell allowed the authors to study the interaction between two sites of different proteins inside a single cell. Results of this approach are illustrated in Figure 53. After

chemical shift changes were mapped onto the known 3D structure of ubiquitin, the active binding sites for different proteins tested on the ubiquitin surface could be identified.

Another limitation of the original protocol was the small number of cells to which the labeled protein could be delivered. A solution of this problem was suggested by Inomata and co-workers.²⁴⁴ Application of the cell-penetrating peptides allowed one to inject labeled proteins into living human cells. A comprehensive review on modern in-cell NMR spectroscopy methods and applications was presented by Shekhtman and co-workers.²⁴⁵

A complete NMR system aimed at the analysis of biological samples was presented by Weissleder and co-workers.^{41,246} The system design is based on the concept developed previously by the same group of authors (see section 2.4). The Diagnostic Magnetic Resonance platform was shown to be able to detect trace amounts of proteins and pathogenic bacteria in native samples.

Solid-state NMR techniques allow one to study interactions in cells membranes, which cannot be investigated by liquid-state NMR techniques because of the restricted mobility of the membrane-composing proteins.²⁴⁷ A comparison of ¹³C–¹⁵N solid-state correlations with solution data enabled the assignment of the backbones for the peptide of interest.²⁴⁸

Because of their portability and competitive resolution in comparison to clinical whole-body MRI tomographs, mobile MRI equipment may provide valuable information regarding early medical diagnostics, hydration processes, and can be used as a monitoring tool for studying drug delivery. Mobile and inexpensive devices can be installed in doctors' offices to perform routine evaluations and diagnose diseases at an early stage (Figure 54A). To determine skeletal maturity in children, for example, is important when diagnosing endocrinological

diseases or when predicting height for prognostic and therapeutic purposes. The use of MRI in this respect is a relatively novel idea. Terada and co-workers have demonstrated the use of a compact MRI scanner based on permanent magnets for skeletal age assessment.²⁴⁹

The system works at 0.3 T with a homogeneity better than 50 ppm and a footprint of about 1 m². Hand images of children with spatial resolution better than 500 μm were obtained in less than 3 min (Figure 54A). From the dimensions of particular bones determined in MR images (red arrows in Figure 54B), the age of the volunteers can be obtained.

Mobile sensors were also used to study small animals *in vivo*, for example, mice and rats. Kose and co-workers developed a 1 T yokeless permanent magnet with a 9 cm bore, a 3.2 cm in diameter and a 5 cm long solenoid RF coil.²⁵⁰ They recorded images of the whole mouse brain and body with in-plane resolution of about 200 μm and typical slice thicknesses of 1 mm. Besheer and co-workers used a commercial benchtop MRI system to evaluate a contrast agent based on Gd-chelate of hydroxyethyl starch to improve contrast in MR images and determined its residence time in the circulation.²⁵¹ Besides the compactness of these small devices in comparison with clinical MRI systems and the reduction in maintenance cost, there are other advantages to be mentioned. Image contrasts are similar to those obtained at 1.5 T, and there is improved sample accessibility. Additionally, biological isolation, which is required at some occasions for this type of studies, is easier to implement.

Because of their natural open geometry, unilateral devices such as the NMR-MOUSE are suitable tools to study skin tissue of humans because almost any part of the human body can be accessed. Single-sided stray-field devices are less expensive and less intimidating than conventional clinical tomographs. In some cases, they are an attractive alternative to large MRI machines as they provide spatial information in terms of one-dimensional profiles noninvasively and at high resolution.

In vivo depth profiles through human skin, corresponding to different parts of the body, were reported in the past.^{252–255} The most common strategy to record such profiles is by acquiring trains of echoes either by using CPMG sequences ($\pi/2)_0-\tau/2-[(\pi)_{90}-\tau-]_n$, or multisolid echo sequences ($\pi/2)_0-\tau/2-[(\pi/2)_{90}-\tau-]_n$, thereby sampling the effective decay of the signal. In these cases, the complete echo train can be fitted to determine the effective transverse relaxation times $T_{2\text{eff}}$ and the corresponding amplitudes, or, alternatively, different parts of the train can be integrated to obtain relaxation-time-weighted profiles.^{253,255} By varying the pulse separation τ of the sequence, it is also possible to modify the effective signal decay due to diffusion attenuation in the presence of the stray-field gradient, thereby introducing diffusion contrast between different skin layers. Alternatively, spin-echo or stimulated spin-echo experiments have been designed²⁵⁶ to measure self-diffusion coefficients in stray fields, in a way similar to that used with pulsed field gradient (PFG) NMR setups. Combining this information with the imaging capabilities of singled-sided NMR devices, it is possible to spatially resolve diffusion coefficients. Figure 55 shows a depth-diffusion map measured *in vivo* from the skin at the palm of the hand of a volunteer.²⁵⁵ Within the first 200 μm, two distinct diffusion coefficients are clearly distinguished, which collapse into a single value at larger depths. At the surface of the skin (0 mm in the plot), the largest diffusion value is comparable to the

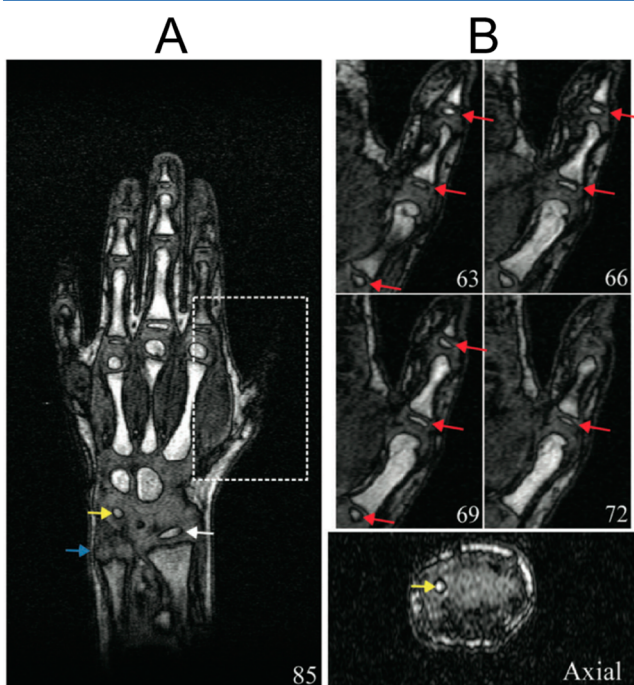


Figure 54. Mobile MRI systems for *in vivo* human studies: (A) typical image of a child's hand recorded with 3D echo MRI in less than 3 min; and (B) different slices corresponding to the highlighted region of (A) in which the bones of interest can be seen. Reprinted with permission from ref 249a. Copyright 2012 Wiley-VCH.

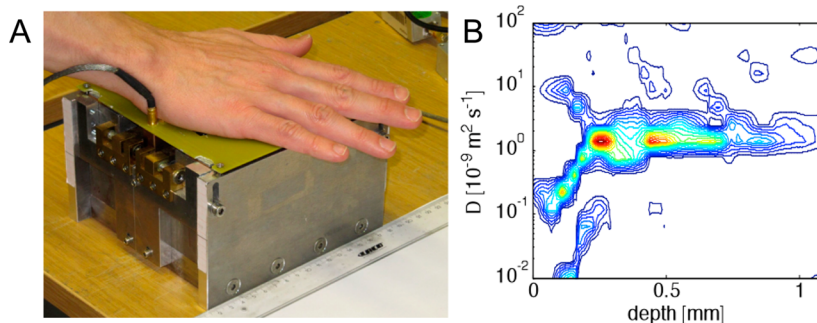


Figure 55. Skin study by singled-sided NMR: (A) single-sided magnet with an extended uniform and reduced gradient of 2 T/m along the depth direction suitable for skin measurements; and (B) depth-diffusion map from the skin at the palm of the hand measured using a single excitation experiment, without the need to reposition the sensor with respect to the hand. Reprinted with permission from ref 255. Copyright 2012 Elsevier.

self-diffusion coefficient of free water at 37 °C; the second one, almost 2 orders of magnitude smaller, is assumed to belong to restricted water, fat, and less movable biological tissue in the cells. Deeper in the skin, the diffusion coefficient is around $10^{-9} \text{ m}^2 \text{ s}^{-1}$ with a monomodal distribution.

Recently, dynamical studies such as measurements of skin hydration experiments have also been reported.^{253,254} The influence of vehicles for moisture delivery into the skin was studied by measurements of average relaxation times and self-diffusion coefficients as a function of depth.²⁵⁴

Given the simplicity of handling mobile, single-sided NMR sensors and the fact that the generated magnetic field can be oriented parallel to the surface of the magnet, the angle dependence of NMR parameters in systems presenting order anisotropy such as cartilage²⁵⁷ and tendon^{258,259} can be measured. In vivo studies of relaxation rates in the Achilles tendon (Figure 56A), which are difficult to conduct by

consisting of 1 mm cross section through the finger were acquired in 9 min with 1 mm in plane resolution. Images with different T_2 contrast values were calculated from the original data.²⁶¹

3.4. Industrial Applications

Different areas such as material testing, industrial quality control, and art conservation, to mention a few, can considerably benefit from in situ implementations of NMR or MRI. For such cases, the mobility of the whole NMR system rather than good spectral resolution and sensitivity has prime priority. In the present section, some examples are outlined to demonstrate the potential of mobile MR systems and give a general overview of the state of the art of the applicability of the technique. For a detailed explanation, we encourage to check the different literature sources provided in the corresponding sections, as well as recently published works where further examples can be found.^{262,263}

3.4.1. Rubber and Polymer Materials. Elastomers find multiple uses in society, for example, as rubber seals, adhesives, tires, impact absorbers, surgery devices, tubings, etc. They can be stretched to multiples of their initial length without suffering permanent deformations. Moreover, they easily undergo deformation, making them moldable into any desired shape. Elastomers consist of amorphous polymers above their glass transition temperature in which the mechanical properties are controlled by chemical cross-links between the macromolecular chains of rubber molecules. Because cross-linking affects the mobility of the polymer chains, transverse relaxation times map the cross-link density. T_2 also provides information about aging processes and strain in rubber. Nondestructive measurements of the cross-link density have been reported using different compact NMR devices and correlated with mechanical measurements.^{264–268} The cross-link density of rubber samples has been determined at different depths, with the profile NMR-MOUSE revealing significant differences when the curing process is done at constant or variable temperature.²⁶⁸

Single-sided imaging has also been employed to non-destructively determine defects in fiber-reinforced rubber tubes (Figure 57A). Figure 57B shows a slice-selective image of the rubber tube with a defect located at the inner rubber layer, which was placed over the single-sided tomograph. The black spots following the rubber contour are the textile fibers, and the hole in the rubber wall is located toward the center of the rubber portion. To reduce the imaging time from about 1 h to the limit of a few minutes, the strength of the external gradient should be reduced so that a thicker slice can be selected. By reducing the gradient by a factor 2, images of the

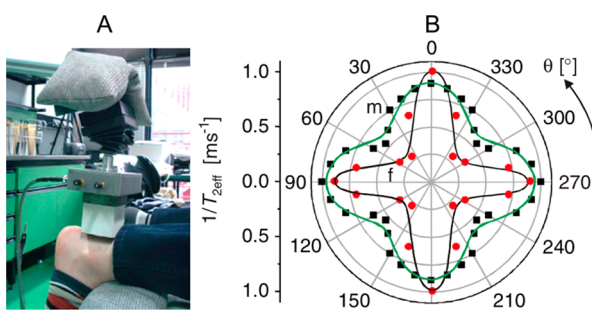


Figure 56. Orientation dependence of NMR parameters studied by mobile NMR: (A) NMR-MOUSE measuring the human Achilles tendon of a volunteer; and (B) angle dependence of the effective relaxation time $T_{2\text{eff}}$ measured at a depth of 5 mm using a CPMG sequence. Reprinted with permission from ref 27. Copyright 2008 Elsevier.

conventional medical MRI as the patient is difficult to reorient perpendicular to the magnet axis, were reported using the NMR-MOUSE.²⁵⁸ Figure 56B shows the effective transverse relaxation rate as a function of the angle subtended by the field direction and the main collagen fiber directions of the tendon. Because of the high order in tendon, the magic angle effect is observed as the tensorial spin interactions for fibers are reduced when oriented at the magic angle.²⁶⁰

Two-dimensional MR images through different parts of a human finger joint were recorded *in vivo* using a singled-sided tomograph. By acquiring complete CPMG echo trains, images

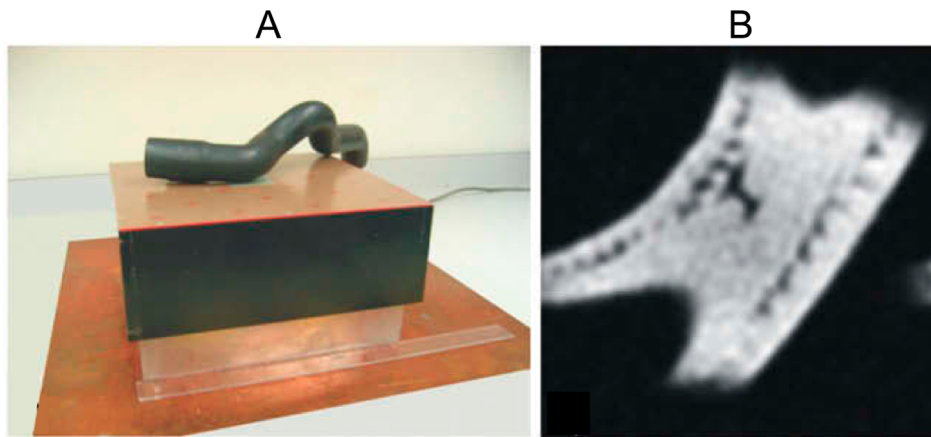


Figure 57. Defect analysis by single-sided NMR: (A) a fiber-reinforced rubber tube placed over the magnet; and (B) slice-selective image of the inner part of the tube showing the region where a defect (hole) is located. The slice thickness is 0.6 mm, and the in-plane resolution is 0.8×0.8 mm. Reprinted with permission from ref 273. Copyright 2005 Elsevier.

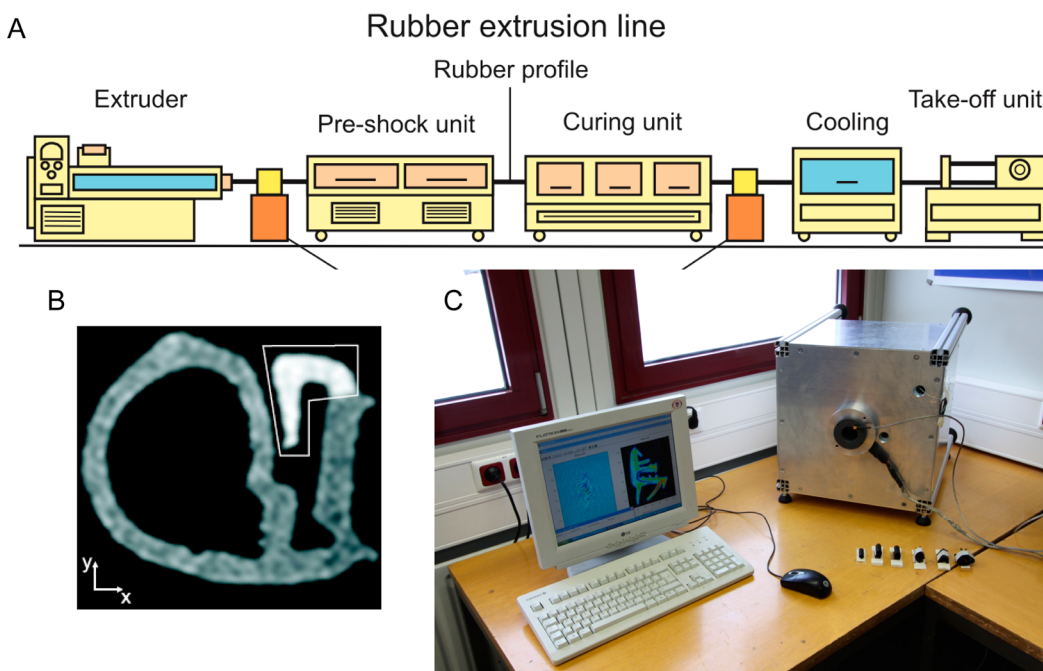


Figure 58. Benchtop MRI for rubber quality control: (A) Typical extrusion line, where the orange squares show the potential locations of the benchtop MRI sensor. (B) Slice-selective 2D NMR image of a rubber fitting measured with a mobile Halbach magnet. Because of short relaxation times ($T_1 = 20$ ms and $T_2 = 2.7$ ms), the MRI methodology implemented was a spin–echo sequence with the shortest echo time possible (800 μ s). The nominal spatial resolution is 0.4×0.4 mm (pixel size). Reprinted with permission from ref 272. Copyright 2010 Elsevier. (C) The whole setup view.

same quality could be obtained in about 15 min. On the other hand, the sensor can be used in the vicinity of steel, as some distortions of the measuring field can be tolerated.²⁶⁹

Another example for the use of mobile MR tools in industry is the study of polymer extrudates. In the extrusion process, raw materials such as uncured rubber or polymer melts are mixed and transported in the extruder through a die that defines the shape of the final product (Figure 58A). The interplay between different production and sample parameters, such as speed of the strudger screw, temperature distribution, sample viscosity, and shear forces at which it is subjected, or the onset of instabilities/defects can influence the efficiency of the process altering the product quality. For quality control of rubber products, off-line techniques such as random sampling and

manual inspection or in-line methods relying on optical means are typically used. Nevertheless, NMR offers certain advantages over these methodologies due to the nondestructive nature of the measurement, the accessibility of molecular information, and the possibility to assess nontransparent samples that is usually the case for polymers. These characteristics have promoted the use of different mobile NMR sensor for the study of extrudates. A single-sided NMR sensor has been used to measure relaxation rates of polymer melts directly at the output of the extruder at temperatures up to about 200 °C.²⁷⁰ Another example where relaxation measurements of polymer melt extrudates have been performed in-line and combined with mechanical instabilities measurements in the die due to pressure fluctuation has recently been reported.²⁷¹ A Halbach

magnet generating a field strength of about 0.5 T was used to measure the extrudate at different positions relative to the die for different polymer melts and extruder speeds. By combining the information obtained at molecular level through NMR relaxation rates with macroscopic mechanical or optical measurements, it is expected to identify the sources of defects or instabilities to optimize the production process. The spatial information obtained through MRI can also be used to monitor the production process of rubber fittings in-line, which are employed in multiple applications, for example as thermal insulators and seals in diverse areas including the building, aircraft, and car industries. The contrast in MRI images (Figure 58B) can provide information about filler distribution, specific gravity, shore hardness, and cross-link density. Moreover, it is possible to obtain geometrical information from cross-sectional images not only from the outer but also from the inner contours, which are hidden for most of the techniques in use today for in-line control. For this purpose, images with modest spatial resolution can be executed with benchtop systems in very short acquisition times of the order of a few seconds to 1 min (Figure 58C). The performance obtained has proved to be enough to implement edge-detection algorithms to reconstruct the geometry of the sample with accuracy better than the nominal resolution and below technical specifications.²⁷²

Plastics or solid polymers represent another important type of synthetic materials of high commercial importance with a wide variety of industrial and domestic applications. They often are resistant to deformations, have high impact resistance, and can be optically transparent. Several objects, which originally were produced from metals, are now replaced from plastic material. The NMR study of rigid polymer materials is more demanding than that of soft polymer materials, because the characteristic relaxation times are much shorter, in some cases being even shorter than the dead time of the sensor, which is of the order of some tens of microseconds. Nevertheless, several nondestructive studies have been reported.^{77,269,273,274}

In particular, pipes made from polyethylene are one of the most common polymer products. Polyethylene consists of crystalline domains, where polymer chains are ordered and less mobile, and of amorphous domains, where the chains are disordered. The difference in the morphological composition is reflected in the NMR signal in terms of an effective relaxation decay with at least two different characteristic relaxation times, one associated with each phase. This fact renders NMR relaxometry a suitable nondestructive tool for studying the effects that different factors such as temperature, pressure, or chemical aging have on the morphology of PE pipes aiming to estimate the residual lifetime of a pipe in service.²⁷⁴

The example in Figure 59A shows a lateral scan across a welding line joining two polyethylene sheets. The signal amplitude has been calculated by partial integration of the CPMG decay at each position and corresponds to a relaxation-weighted spin-density amplitude. The contrast shows results from the differences in relaxation times. It can be used to assess the state and the quality of the welding line. Using the same procedure, the state of annealing and the heterogeneity of the morphology can be identified laterally, and the gradient of crystallinity across the pipe wall can be determined.^{274–276}

The strong stray-field gradient of single-sided devices can be used to determine self-diffusion coefficients D quickly and easily.²⁵⁶ The diffusion of liquids taken up by the pipe material can provide useful information to assess the state of aging.²⁷⁷ Figure 59B shows self-diffusion coefficients of *n*-hexane that has

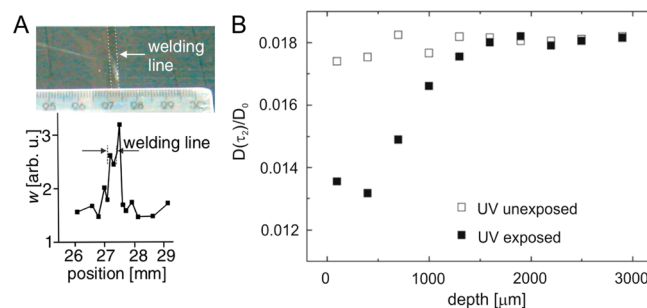


Figure 59. Nondestructive testing of polymer materials by single-sided NMR: (A) Welding line of two planar plastic sheets (top). Relaxation-weighted spin density w at different positions in a lateral trace across the welding line (bottom). The origin of the bottom axis is arbitrary. Reprinted with permission from ref 276. Copyright 2005 Institute of Physics, Polish Academy of Science. (B) Diffusion profiles of *n*-hexane in polyethylene pipes revealing the effects of UV-aging across the pipe wall. D_0 is the value corresponding to the bulk diffusion coefficient, and $T_2 = 70$ ms is the diffusion encoding time of a steady gradient stimulated spin echo sequence. Reprinted with permission from ref 277. Copyright 2012 Wiley-VCH.

penetrated into the wall for a new polymer pipe and for pipes exposed to UV-light. In the unexposed regions, the value of the diffusion coefficient is almost constant across the pipe wall. In the exposed regions, D is reduced close to the outer pipe surface, and its value grows with increasing depth to that of the new material. This curve shows that the UV-light cannot effectively degrade the interior of the polymer. An aged layer about 1 mm thick can be identified from the plot, in which the polymer chains are less mobile than in the other parts of the material.

3.4.2. Concrete and Building Materials. Mobile NMR sensors can also determine moisture content and diffusivity in buildings and monuments. Playing a key role in the lifetime of such structures, the investigation of moisture can help in identifying proper restoration strategies, or infer material properties to water storage and transport, which can be used to predict functional properties of building structures under various conditions. Considerable detail can also be learned from NMR measurements about pore and chemical structure and processes of hardening in cement-based materials, which is of relevant economic interest.²⁷⁸ Unilateral NMR sensors, such as different versions of the NMR-MOUSE,^{279,280} and the surface GARField²⁸¹ magnet were demonstrated to be suitable for *in situ* measurements. Hand-held²⁸² magnets and even miniature sensors, which were embedded in the concrete structure,²⁸³ have been used to monitor the hydration and drying processes.²⁸⁴ Different parameters measured in concrete samples such as relaxation times,²⁸⁵ signal amplitudes,^{78c} diffusion coefficients,²⁷⁹ and two-dimensional relaxation correlation maps²⁸⁶ can be combined with the characteristic spatial localization of single-sided devices to provide valuable information about the water uptake, migration, and drying dynamics.²⁸⁵

Figure 60A shows a small unilateral sensor consisting of a NdFeB disk magnet generating a field strength of about 0.25 T and a surface RF coil, which is etched on a printed circuit board and tuned to the ^1H Larmor frequency with small, fixed-value capacitors.²⁸⁷ Magnet and coil are encased in a waterproof epoxy resin whose dimensions are 30 mm in diameter and 12 mm in height (Figure 60B). Typical decays of Portland cement recorded with a CPMG sequences are depicted in Figure 60C.

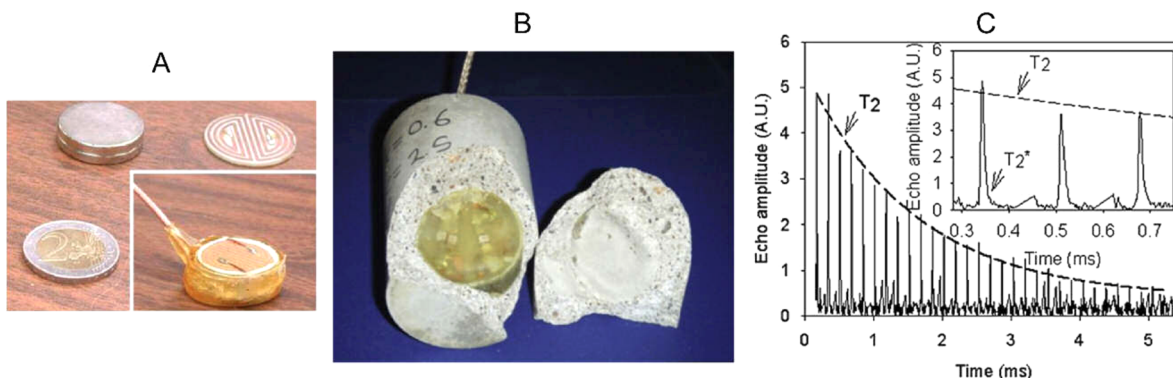


Figure 60. Study of concrete aging with an embedded NMR sensor: (A) magnet and RF coil composing a miniature stray-field sensor; (B) sensor embedded in a Portland cement cylinder of 40 mm diameter; and (C) typical CPMG echo train decay measured in Portland cement in 30 min. Reprinted with permission from ref 283. Copyright 2009 Elsevier.

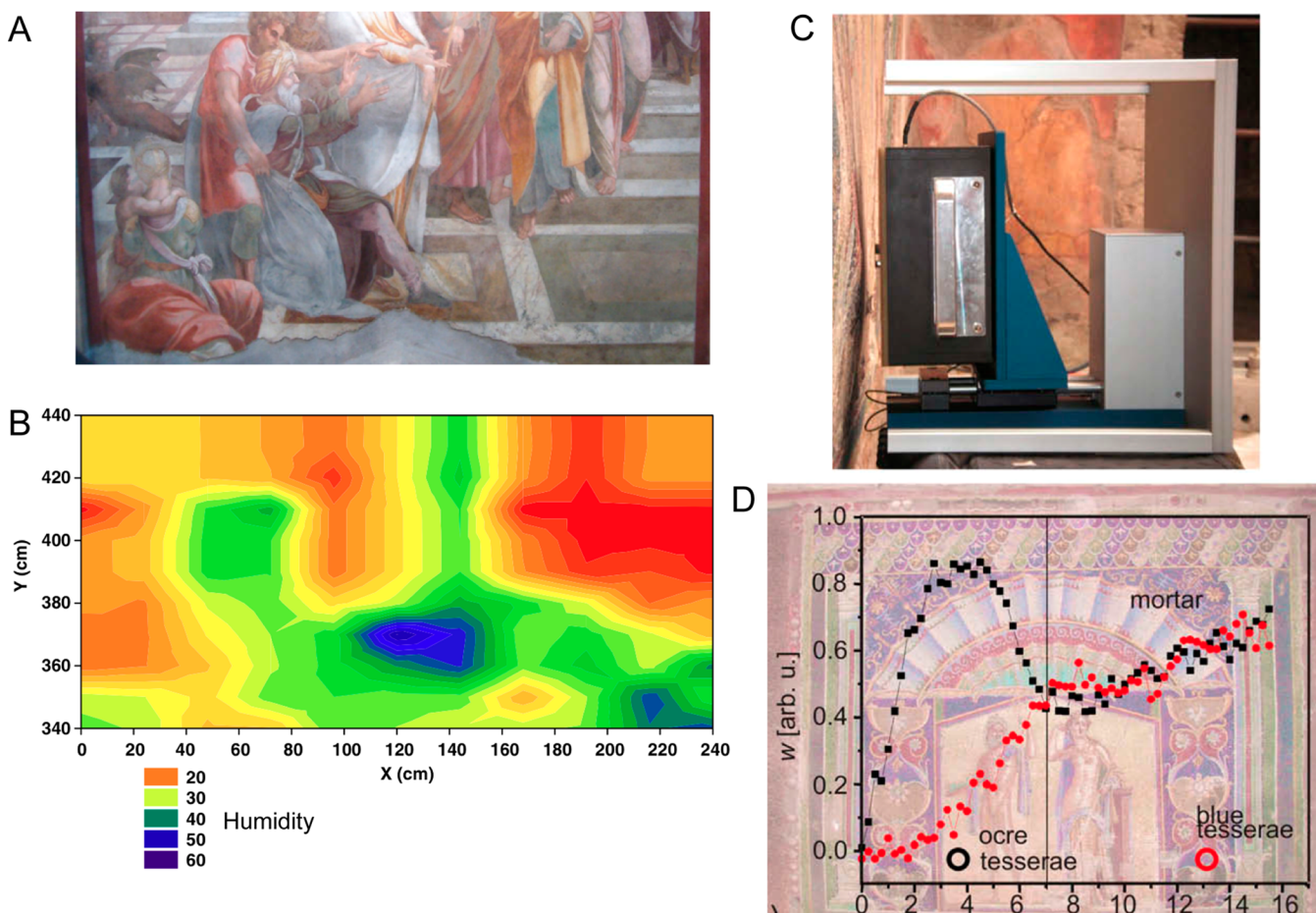


Figure 61. Noninvasive singled-sided NMR measurements of painted walls: (A) Fresco by Pellegrino degli Aretusi in the Cappella Serra of the church of Nostra Signora del Sacro Cuore in Rome. (B) Moisture distribution in the fresco in (A). Reprinted with permission from ref 290. Copyright 2007 Elsevier. (C) Picture of the profile NMR-MOUSE while measuring the proton content in the mosaic of Neptune and Amphitrite in Herculaneum; (D) Relaxation-weighted proton spin density *w* measured on the mentioned mosaic as a function of depth (in mm). Measurements over different colored regions (ochre and blue spots) show differences close to the surface. Reprinted with permission from ref 289. Copyright 2010 American Chemical Society.

More recently, the same concept was used with an improved magnet design,²⁸³ which provides higher S/N ratio, and the correlation between NMR relaxation rates and mechanical compressive strength has been demonstrated.

3.4.3. Cultural Heritage. When studying cultural heritage objects, the use of noninvasive techniques is mandatory. Mobile NMR devices, in particular singled-sided NMR sensors,

represent an attractive tool that has found many applications for this purpose over the last 10 years. Studies on stones, wall paintings, wood, paper, master easel paintings, and mummies have been reported and reviewed.^{288,289}

Different singled-sided sensors were used to study the state of wall paintings. Moisture content in the wall is a critical factor that impacts the moisture transport and with it the transport of

salts to the surface. It can be easily and nondestructively assessed by simple NMR measurements. Proietti and co-workers performed extended surface scans on the fresco by Pellegrino degli Aretusi in the Cappella Serra of the church of Nostra Signora del Sacro Cuore in Rome (Figure 61A).²⁹⁰ From the amplitude of the NMR signal of a Hahn echo, detected at 1 mm below the fresco surface, they obtained moisture maps of regions of the order of 1–2 m² (Figure 61B). Additionally, *T*₂ distributions were measured and found to be sensitive to the wall paintings porosity and to the presence of salt outcroppings. This information can be used for restorers to determine or evaluate the state of the painting and proper restoration strategies.

Another example is the use of the profile-NMR MOUSE in measuring one-dimensional depth profiles up to 25 mm into a wall with the magnet mounted on a mechanical sled, which adjusts the relative position between the wall and the magnet (Figure 61C). Depth profiles were measured to investigate the moisture content of the world famous mosaic of Neptune and Amphitrite in Herculaneum (Figure 61D).²⁸⁹ Measurements over two different positions were performed. The measurement of the porous blue tesserae suggests that at this location the proton content is low, unlike the proton content in the porous ochre tesserae. Further NMR evidence suggests that the fresco has been treated with wax, which has been taken up by the porous ochre tesserae. For regions deeper in the wall, the values recorded from both spots coincide and correspond to the moisture content of the mortar bed.

Mummies and bones represent another type of object that has been studied by single-sided NMR like other objects that are not allowed to leave a museum or need to be maintained under specific conditions to avoid degradation.²⁹¹ An interesting example is a 5300 year-old glacier mummy in the Archeological Museum of Bozen (Figure 62A), which needs to

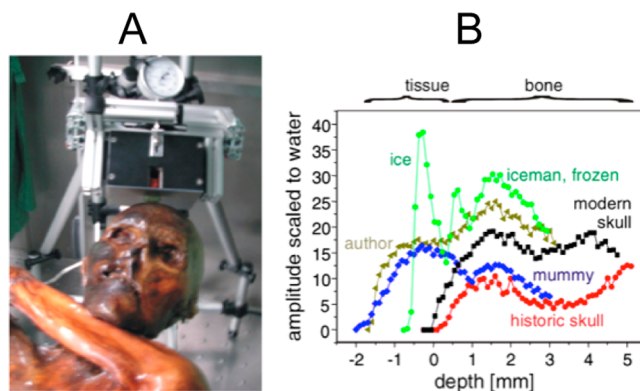


Figure 62. Bones measurements by single-sided NMR: (A) profile NMR-MOUSE placed on top of the ice man head to measure a forehead profile; and (B) depth profiles over different mummies, skulls, and living people showing intensity difference as a function of depth and sample. Reprinted with permission from ref 291. Copyright 2007 Elsevier.

be kept frozen at a few degrees below 0 °C. The NMR information obtained from the biological tissue of such samples can give insight into the state of conservation. Depth profiles can discriminate between textile material and biological tissue in wrapped mummies from Egypt and a surface ice layer, cutis, and skull bone for the glacier mummy up to a depth of 5 mm. The information obtained from depth profiles through different

foreheads of mummies, skulls, and living people evidences that also organic bone densities can be determined (Figure 62B).

3.4.4. Plant Phenotyping. The use of NMR and MRI has proven to be effective for quantifying functional and structural characteristics of plants, which resulted in a better understanding of the plant–environment interaction. These studies are targeted toward specific traits to optimize resource use efficiency of plants. This concerns present and future plant research objectives to ensure the stability of yield at the regional and global scale.²⁹²

Various portable MRI sensors have been reported in recent times for field or greenhouse studies of plants.⁶⁶ Kose and co-workers reported a portable scanner based on a C-shaped permanent magnet generating 0.2 T provided with a mechanical lift used to study Japanese pears during the growth process.²⁹³ Longitudinal and transverse relaxation times were obtained as well as apparent diffusion coefficients throughout the growth process. High-quality images were also reported. Jones and co-workers designed a portable sensor to fit around a living tree, without exceeding reasonable weight to allow portability.²⁹⁴ The resultant magnet called “tree hugger”, is a modified C-shaped magnet, which can fit trees up to 200 mm diameter. The magnet generates a field of 0.025 T and is provided with gradient coils, which allow recording MR images. Measurements over long periods of time were reported. Windt and co-workers used the NMR-CUFF (Figure 5) for imaging intact plants and measuring water (xylem) flow.

Even simple NMR-signal amplitude measurement can provide useful information because they provide a unique way to measure growth noninvasively and to assess dynamic changes in the plant water status.²⁹⁵ A small C-shaped permanent magnet of NdFeB was used (Figure 63A) to monitor the growth process of a 1-week-old bean pod that remained inside the magnet for 2 weeks under controlled ambient conditions.²⁹² The water content in the bean pod was constantly monitored during day and night (Figure 63B). The NMR data revealed that the amount of water inside the plant increases constantly during the first week and starts decreasing toward the end of the second week. Interesting to notice is that for the behavior of the pod responses at the day–night–day transition periods, some of them can be seen enlarged in Figure 63 below the plot covering the complete observation period. The bean-pod water-content curve shows significant changes during the day–night cycle for the whole 2-week period. The growth rate during the night is always larger than that during the day. Toward the end of the second week, the pod began losing water during the day and exhibited zero growth rate during the night period. This behavior was explained as an apoplastic connection of the pod to the rest of the plant throughout the whole growth period, thus, instantly experiencing the same changes in water potential as the vegetative part of the plant.

3.4.5. Pharmaceutical Industry. During the past few years, the pharmaceutical industry starts exploiting the use of benchtop NMR and MRI scanners, mainly for *in vitro* studies of drug delivery, led by the advantages in costs as compared to conventional superconducting equipment with similar performance for that purpose. Characterization of emulsions and lipid ingredients, and measurements of adsorption characteristics, have been reported using NMR.²⁹⁶ Magnetic resonance images following the hydration and swelling of hydroxypropyl methylcellulose-based monolayer and double-layer tablets (Figure 64A) were shown. Studies of drug release mechanism

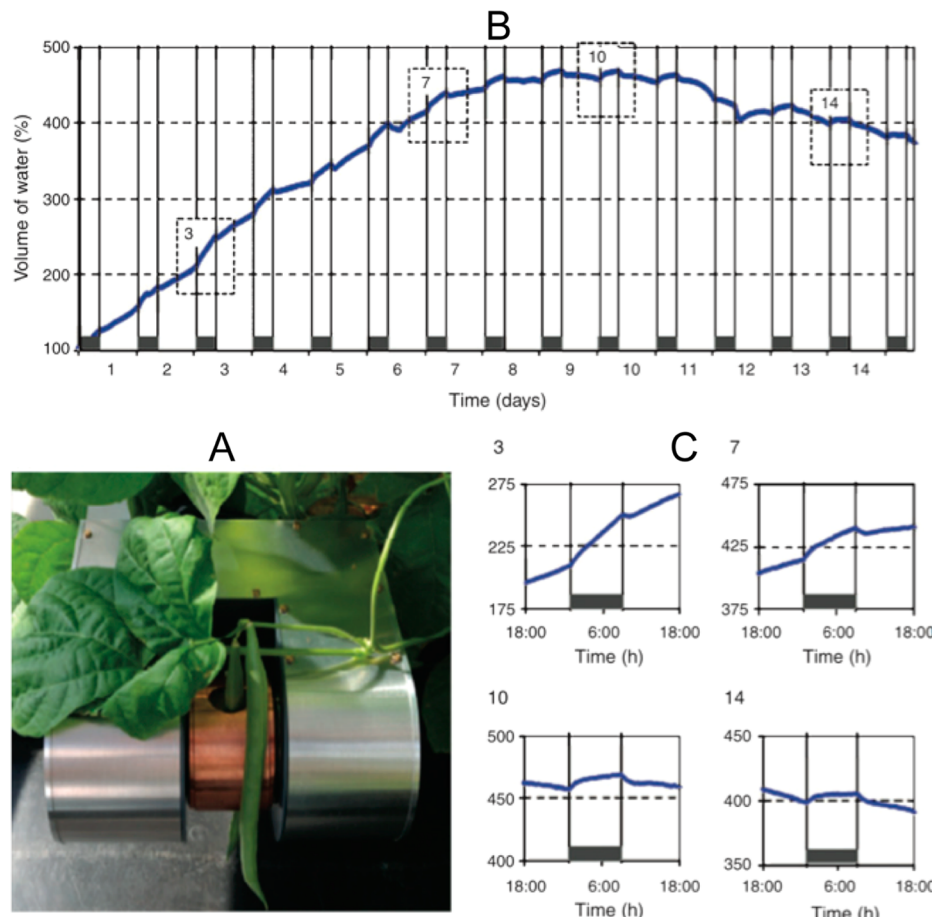


Figure 63. Plant study with a portable NMR apparatus: (A) C-shaped NMR sensor and RF probe containing a bean pod; (B) growth of the bean pod during a 2-week period (the dark-gray bars indicate the night periods); and (C) 4 day–night–day transition periods are enlarged from the original plot at the bottom-right of the figure. Reprinted with permission from ref 292. Copyright 2011 CSIRO Publishing.

from push–pull osmotic systems by mobile MRI have shown that the tablet composition plays a key role in the swelling and hydration processes.²⁹⁷ Figure 64B shows the kinetics of the hydration process measured with a benchtop MRI system. At the beginning, the intensity of both layers increases to reach a constant level at around 4 h. The thickness of the push layer then starts increasing correlated with a decrease in the thickness of the drug layer. After 16 h, only the hydrated push layer remains inside the tablet. This study indicates that the hydration of both the drug and the push layers needs to be properly balanced to efficiently deliver the drug.

Another example is the use of a mobile magnet and RF probe (Figure 65A) to measure in-line the weight of liquid and powdery pharmaceutical products, which are contained in vials.²⁹⁸ For the case of powdery products, 150 closed vials per minute should be measured, imposing a challenging requirement on the system. Moreover, to properly determine the weight via the NMR signal, no interference between neighbor vials is desired, neither signal coming from external sources than the product, such as the vial stopper. For this purpose, the RF probe (Figure 65B) consisted of a ring into which the vial is placed, designed in such a way that the B_1 field is effective at the sample place, being negligible at the cap and neighboring places.²⁹⁹ By acquiring a train of solid echoes, measurement accuracies of the order of 1% were obtained (Figure 65C).

3.4.6. Food Industry. One of the areas in which the use of compact NMR has been exploited for several years is the food

industry. The interest relies on the fact that NMR-based sensors can provide information regarding composition and structure simultaneously, which is an advantage over other measurement techniques such as IR, X-ray, or optical methods. The diversity of contrast in soft matter that can be exploited with NMR is applied to resolve tissues of similar density but different molecular structure, morphology, and even molecular mobility. Moreover, these properties can be measured from regions inside the products in a nondestructive way and at high throughput rates. Different studies have been reported involving one- and two-dimensional relaxometry and diffusometry NMR experiments and MRI aimed at the analysis of oil/moisture content in different systems such as fruits, seeds, cheeses; solid-fat/moisture content in dairy and bakery products; droplet size distributions of emulsions; internal disorder in fruits and vegetables; studies of freezing phenomena; water migration; etc. The literature covering this area is vast including books^{300–303} and reviews.^{304–307}

An example of the use of MRI in this context is the detection of seeds in citrus fruits, such as oranges, to separate seedless from seed-containing fruits. Figure 66B–D shows typical slice-selective MR images of orange fruits recorded using different fast pulse sequences to optimize the contrast between pulp and seeds. The sequences used were: fast spin echo, turbo fast low-angle shot, and gradient recalled echo. The images were recorded in a horizontal bore 1 T magnet with a 60 cm × 60

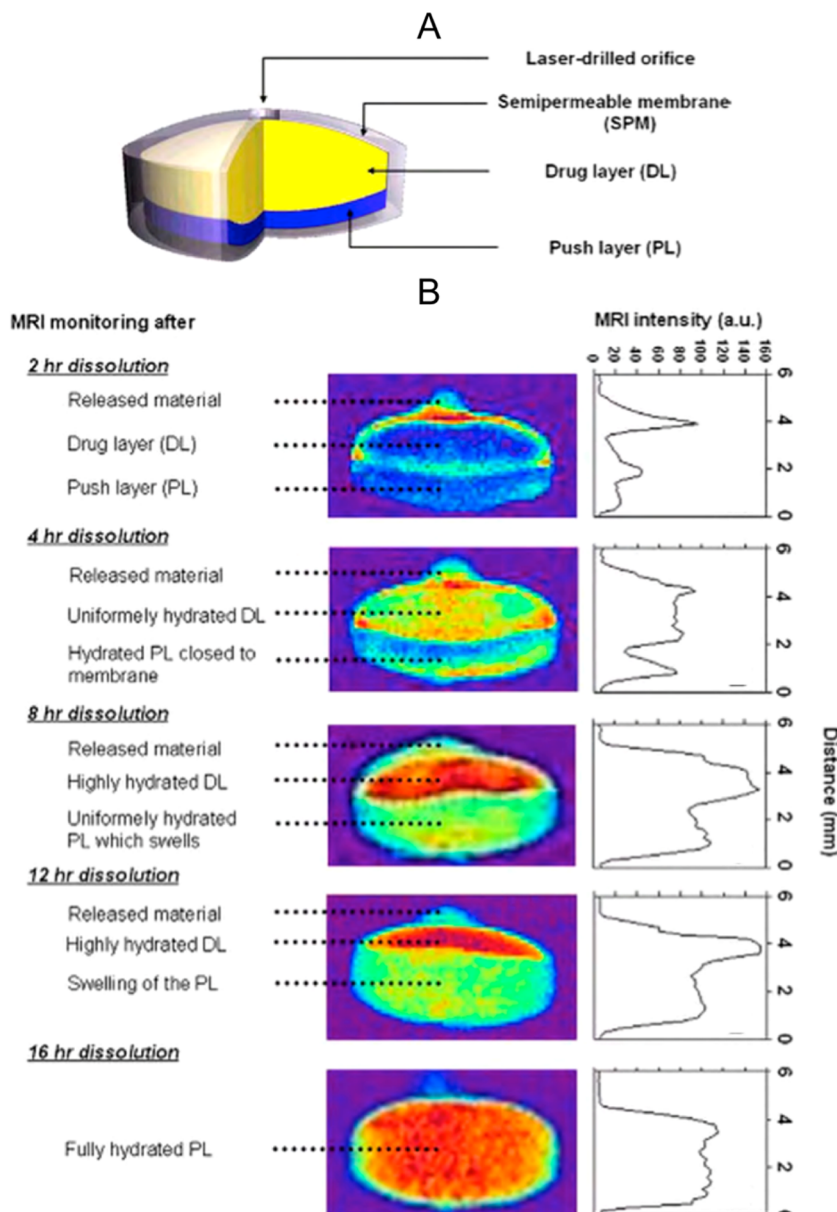


Figure 64. MRI study of tablet hydration process using a benchtop system: (A) drawing of the structure of a typical bilayer tablet core; and (B) hydration kinetics of a commercial formulation tablet measured using T_1 -weighted MR images and amplitude profiles corresponding to the center of the image. Reprinted with permission from ref 297. Copyright 2009 Elsevier.

cm footprint (Figure 66A) and a bore of 6 cm in diameter. The in-plane image resolution is 0.57 mm \times 0.57 mm.

Time-domain NMR has been used in the food industry for about 40 years. Bench-top NMR devices have been used to distinguish different components of a given sample by their different relaxation times and molecular self-diffusion coefficients, which can be assessed by NMR with the aid of pulsed-field gradients. A common characteristic of these measurements is that they do not require high homogeneity of the magnetic field.

A typical example is the determination of solid/fat content in dairy products such as margarine. For this purpose, the NMR signal is acquired after a simple 90° pulse. The FID of the mixture of solid and liquid fats consists of a fast decaying component associated with the solid part of the sample, which lasts for some tens of microseconds. From there, the signal is entirely determined by the liquid fat present in the sample,

which may last on the order of several 10 to 100 ms. For this experiment, it is mandatory to have a system with a short dead time to properly sample the solid component. By extrapolating the curve to time zero with the help of a calibration procedure from reference samples, the total spin density of the sample is obtained. Neglecting the decay of the liquid fat component during some tens of microseconds, a duration that is much shorter than the lifetime of the liquid fat signal, it is possible to determine the percentage of solid and fat in the product with high accuracy. Important to consider in these experiments is the temperature of the sample, which needs to be equilibrated prior to the experiment, because the solid:liquid fat ratio is very sensitive to temperature changes.

The measurement of droplet-size distributions is routinely determined by PFG-NMR in food emulsions. These consist of either water-in-oil (W/O) or oil-in-water (O/W) emulsions where the first compound denotes the disperse and the second

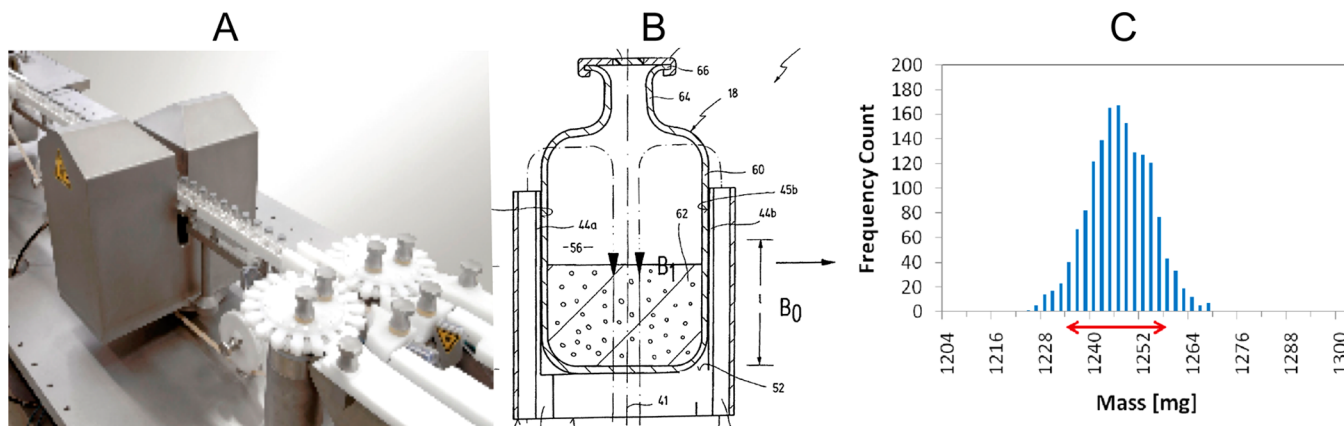


Figure 65. Noncontact weighing machine: (A) in-line NMR measurement of a powdery drug; (B) drawing of the vial placed inside the resonator; and (C) frequency distribution of mass measured by NMR. Reprinted with permission from ref 298a.

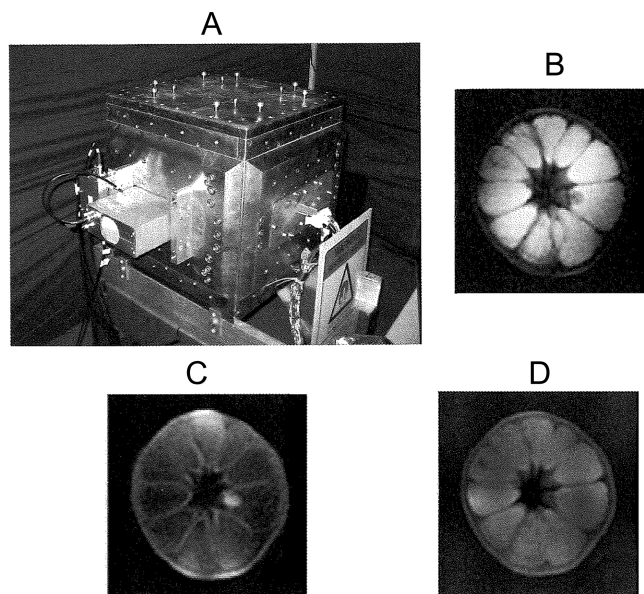


Figure 66. Seed detection in citrus fruits: (A) mobile MR system suitable for fruit inspection; and (B–D) typical 1.6 cm slice-selective images of an orange fruit acquired with a Fast Spin Echo, Turbo FLASH, and Gradient Recalled Echo sequences, respectively. Reprinted with permission from ref 304. Copyright 2009 Wiley-VCH.

compound the continuous phase. The droplet-size distribution is used to analyze emulsion stability, the rheological properties, and the microbial stability.^{304,305} Size distribution measurements are based on the restricted diffusion of the liquid inside the droplets (Figure 67),³⁰⁸ which can be obtained by pulsed field-gradient experiments,^{309,310} and predicted analytically by theoretical models.^{310–312} To suppress the signal from the continuous phase, time-domain filtering techniques based on differences in longitudinal relaxation times T_1 or diffusion coefficients of both phases are normally used for W/O or O/W systems, respectively.³⁰⁴ In this way, droplet size distributions can be determined for droplet diameters in the range of 1–10 μm .

By combining a compact NMR magnet (Figure 68A) with an RF microcoil (Figure 68B), sufficient spectral resolution could recently be obtained to discriminate the chemical shifts of the oil and water phase peaks in the NMR spectrum.³¹³ By resolving the NMR spectrum with pulsed-field gradients

according to the distribution of diffusion coefficients, the droplet size of different types of emulsions has been determined and compared to the distributions obtained by optical microscopy and by PFG-NMR using diffusion filtering (Figure 68C).

3.4.7. Process Analysis and Control. The use of in-line sensors for monitoring and controlling production lines is popular in many industries. Compact NMR systems with chemical shift resolution are an attractive option to install in production lines to provide feedback control based on a chemical shift analysis in real time to adjust parameters or to save time and resources by early optimizing the processes. During the last years, several examples of ^1H NMR spectroscopy have been reported using compact sensors. For example, a 1 T magnet was used to study the oxygenated additive contents, such as methyl *tert*-butyl ether (MTBE) in gasoline.³¹⁴ For this purpose, the blended mixture was circulated through the magnet, while the additive concentration was varied. Figure 69A shows spectra obtained after averaging 12 transients from which the detection limit can be determined to be on the order of 1% v/v additive concentration.

Spectra of biodiesel obtained from different feedstock have also been recorded with a compact desktop NMR spectrometer (Figure 69).³¹⁵ The samples were measured with a 1 T magnet similar to that shown in Figure 3, but with far higher resolution and sensitivity. Percentages of unsaturated fatty acid methyl esters (FAME) could be determined for each of the samples, from which information about biodiesel properties can be obtained such as density, viscosity, and combustion values. Biodiesel–petrodiesel mixtures were also measured (Figure 69B).

Nordon and co-workers have monitored the homogeneous esterification reaction of crotonic acid and 2-butanol in toluene in-line using a simple sampling loop connecting the magnet and the 5 L reactor.³¹⁶ A 0.7 T magnet was used with a flow cell having a prepolarization volume located before the detection volume. The mixture was pumped at a flow rate of 8 mL min⁻¹. The reaction progress was monitored by following the increase and the decrease of the CH signal integrals of butyl crotonate (5 ppm) and 2-butanol (3.5 ppm), respectively. Figure 70A shows spectra acquired at different times, with 16 transients averaged for each spectrum. By integrating the areas under the signals mentioned and normalizing them with respect to the toluene methyl signal area, it was possible to determine the

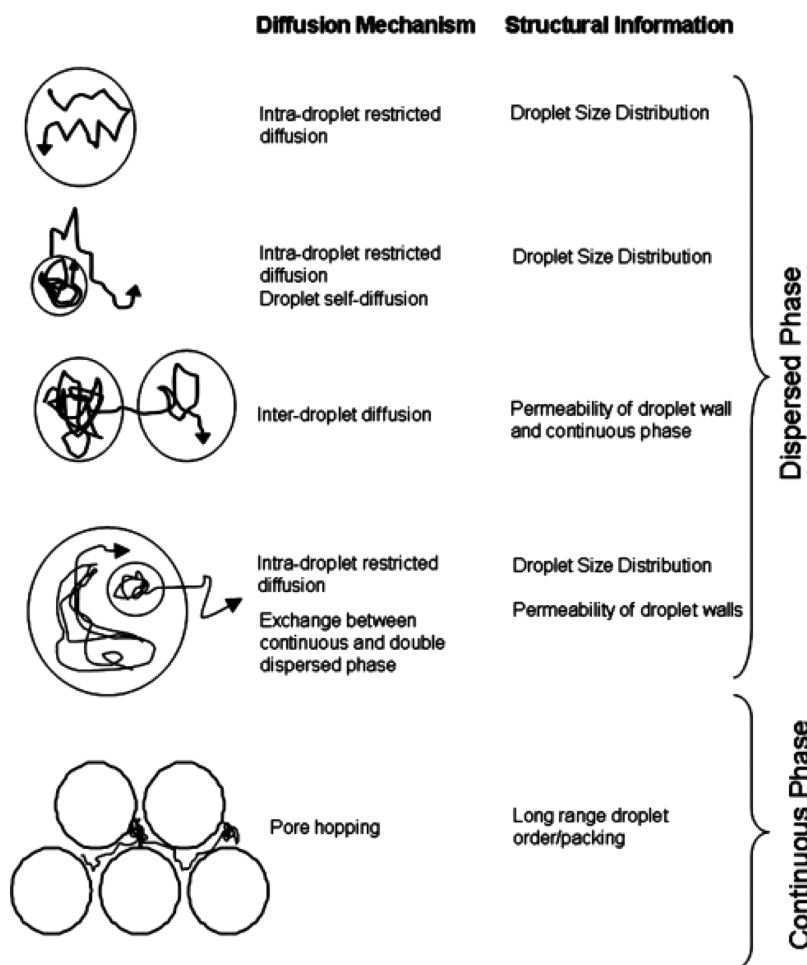


Figure 67. Diffusion mechanisms and structural information obtained by PFG-NMR measurements in emulsions. Reprinted with permission from ref 308. Copyright 2009 Elsevier.

concentration changes during 250 min approximately (Figure 70B).

For many applications involving toxic or aggressive compounds, it is necessary to conduct the reactions in a controlled and safe environment, for example, under a fume-hood. To analyze the reactions in real time, long feeding tubes then would be required to connect the reactor and the NMR spectrometer located outside the fume hood introducing undesired delays. This obstacle can be overcome by using compact NMR spectrometers that can be installed directly under the fume hood.

A palm-sized magnet array has been placed into the fume hood of a chemistry lab to measure a hazardous chemical reaction in real time (Figure 71).³¹⁷ The trimerization of propionaldehyde catalyzed by indium trichloride, which due to its toxicity requires it to be run in a safe environment, was continuously monitored in real time by ¹H NMR spectroscopy. With a peristaltic pump, the reactant liquid was circulated from the reactor through the magnet back again to the reactor in a closed loop. The experiment demonstrated that NMR spectroscopy can be made available to the chemist for direct *in situ* measurements, opening the door to the design of setups where the NMR probes can be integrated into the reaction process at specific points of interest.

Another example in which NMR spectroscopy is helpful during the course of the reaction is in polymer synthesis as the

product quality depends on the reaction conditions. This is true in particular for an emulsion polymerization. Vargas and co-workers used a 0.5 T magnet to monitor the emulsion polymerization of butyl acrylate in real time.³¹⁸ Aided by a flow setup connecting the batch reactor with the magnet, they recorded spectra (Figure 72A,B) during the reaction with a temporal resolution of about one-half a minute. The progress of the reaction was followed by monitoring the olefinic peak corresponding to the monomers of butyl acrylate (6.5 ppm), and the aliphatic signal (2.1 ppm) characteristic of poly(butyl acrylate). A decrease of the olefinic signal was observed due to the concentration decrease of the monomers during the polymerization (Figure 72C). This was correlated with an increase of the area under the signal at 2.1 ppm, which also shows an increase in line width due to a reduction in mobility from the growing chains (Figure 72C). By analyzing the NMR spectra in terms of a kinetic model of the emulsion polymerization, the reaction rate was determined.

Reactions involving polymer materials have also been studied in real time by NMR relaxometry and imaging. *In situ* NMR studies of the curing process in polyurethanes³¹⁹ and polyester resins³²⁰ have been presented recently and compared to NIR measurements. Network structure developments during the cross-linking photopolymerization in polyethylene have been monitored online using fast reactions to determine the limits of temporal resolution of the NMR technique.³²¹ One-dimen-

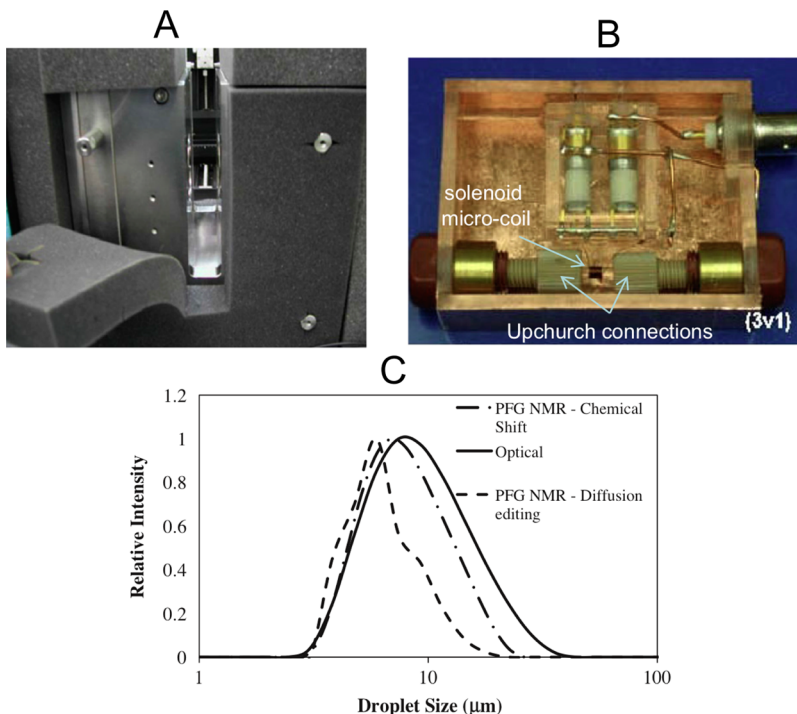


Figure 68. Determination of droplet size distributions with diffusion-resolved NMR spectroscopy: (A) benchtop 1.1 T 20 kg NdFeB permanent magnet; (B) interior of the RF probe where a 2 mm microcoil and tuning and matching capacitors can be seen; and (C) droplet size distributions of a decane-in-water emulsion obtained by PFG-NMR using spectral separation and diffusion editing, as well as an optical method. Reprinted with permission from ref 313. Copyright 2012 Elsevier.

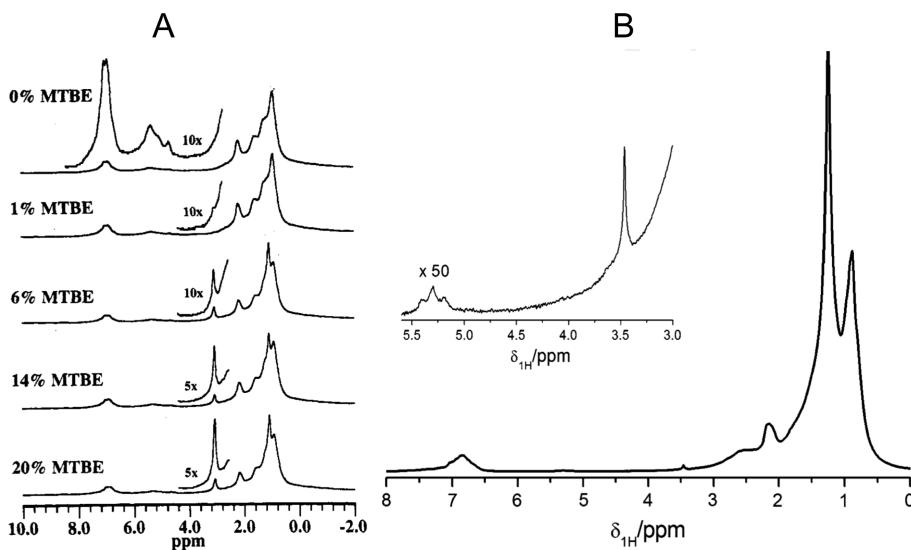


Figure 69. NMR spectra of gasoline and petrodiesel blends: (A) Spectra of a gasoline–MTBE mixture flowing at 2 mL min⁻¹ through the magnet. Reprinted with permission from ref 314. Copyright 1994 American Chemical Society. (B) Single-scan spectrum of petrodiesel containing 2% vol of biodiesel. The enlarged plot illustrates the clearly distinct signals corresponding to the methyl ester (3.6 ppm) and the olefinic protons (5.3 ppm) from biodiesel. Reprinted with permission from ref 315. Copyright 2013 Springer.

sional images measured in the stray field of mobile magnets were also used to follow the evaporation and subsequent curing process in the formation of polymeric films in real time. Reviews of these studies can be found elsewhere.^{322–324}

As of recent, benchtop NMR spectrometers are becoming available by different vendors.^{325–328} The instruments are equipped with permanent magnet producing magnetic fields corresponding to ¹H NMR frequencies from 40 MHz^{325,326} to 60^{327,328} and even 80 MHz.³²⁶ Depending on the magnet field

homogeneity, FWHM less than 1 Hz and detection limits approaching millimolar concentrations in a single scan experiment can be reached in liquids.³²⁵ In addition to measuring routine 1D spectra, simple 2D experiments such as COSY (Figure 73) or J-RES spectroscopy can be executed. The fluid samples are placed into the spectrometer either via injection into a capillary or by means of regular 5 mm diameter sample tubes.

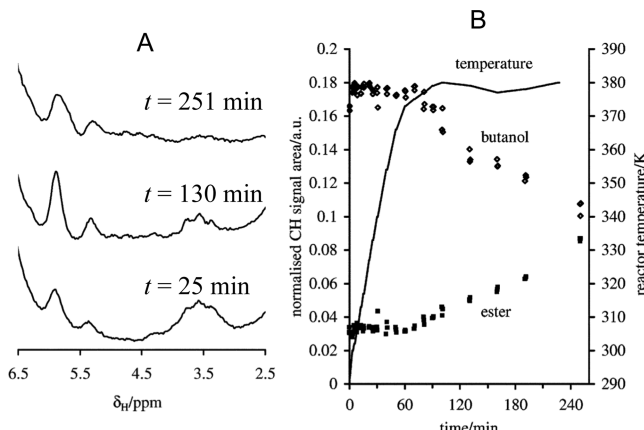


Figure 70. In-line monitoring of an esterification reaction: (A) spectra of a toluene, 2-butanol, and crotonic acid mixture recorded at different times of the reaction; and (B) normalized areas of the CH peak of 2-butanol and crotonic acid. The continuous curve is the temperature of the reactor. Time zero is the time at which the catalyst was added. Reprinted with permission from ref 316. Copyright 2008 Royal Society of Chemistry.

4. CONCLUSIONS

The rapid development of NMR methodology, driven by growing demands and challenges in the areas of biology, pharmacy, chemistry, and nanoscience, is continuously stimulating the construction of novel NMR hardware and instrumentation. The top-of-the-line high-field NMR spec-

trometer operates at 1 GHz and is equipped with a superconducting magnet 5 m tall and 2 m in diameter, weighing about 15 000 kg. Despite their extreme cost and availability only to dedicated research centers, such instruments are of paramount importance at the interface between chemistry and the life sciences to understand the molecular origins of diseases. Highly complex molecules, supramolecular assemblies, and living systems can be studied with structural and functional information revealed at the molecular level. This direction of NMR spectroscopy development is well-known and is widely discussed.

At the other hand of the size distribution of NMR equipment is the miniaturization of NMR, which has experienced amazing technical and methodological progress in recent years. The NMR spectrometer including the permanent magnet can be as small as 50 mm × 30 mm × 15 mm size and weigh less than 100 g. The cost of such an instrument is rather moderate, and it is comparable with the cost of routine laboratory equipment. This opens unprecedented perspectives to integrate NMR analyzers into everyday laboratory practice, materials characterization, and a number of industrial applications.

Bench-top designed NMR spectrometers were constructed to fulfill the gap in structure characterization and to provide flexible solutions to a wide range of research demands in synthesis, catalysis, polymer science, sustainable technologies, and other areas. A valuable direction of NMR miniaturization is the attempt to develop suitable devices for “in flask” or “in tube” operation, that is, a miniature NMR analyzer placed directly into the reaction vessel and connected with a wireless

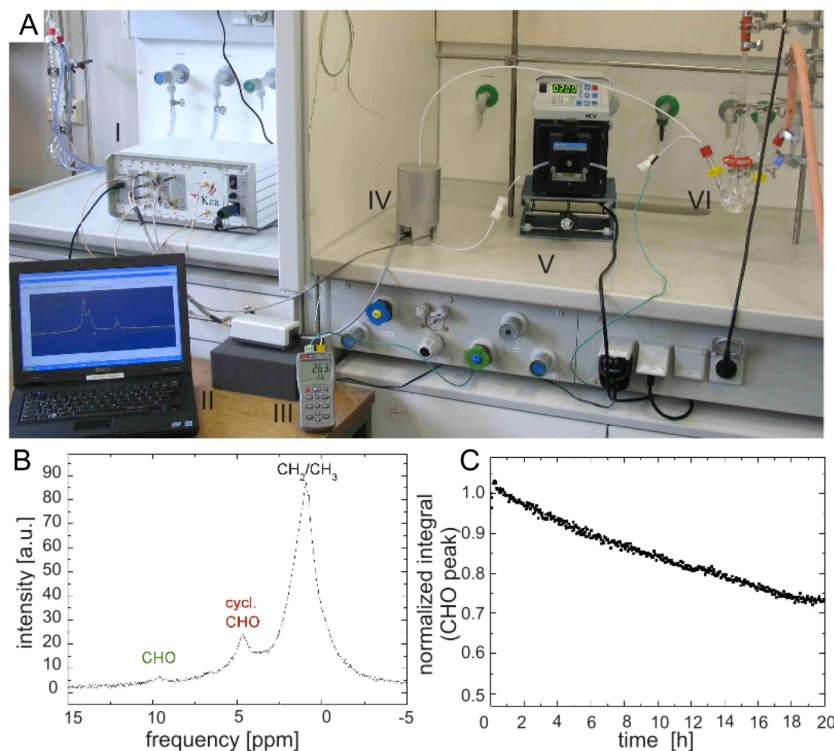


Figure 71. Bench-top NMR applications for routine laboratory practice: (A) NMR under the fume-hood. Experimental setup showing the Kea2 spectrometer (I) connected to a PC (II) used to record the data and also a dual data logger (III) used to monitor the temperature of both the reaction and the fume hood during the complete experiment. Inside of the fume hood one can see the magnet (IV), the peristaltic pump (V), and the glass reactor (VI) equipped with thermocouple, gas inlet, and stirrer. (B) NMR spectrum of the product mixture. (C) Evolution of the reaction monitored by analyzing the aldehyde peak (CHO) of the reactant. Reprinted with permission from ref 317. Copyright 2011 Royal Society of Chemistry.

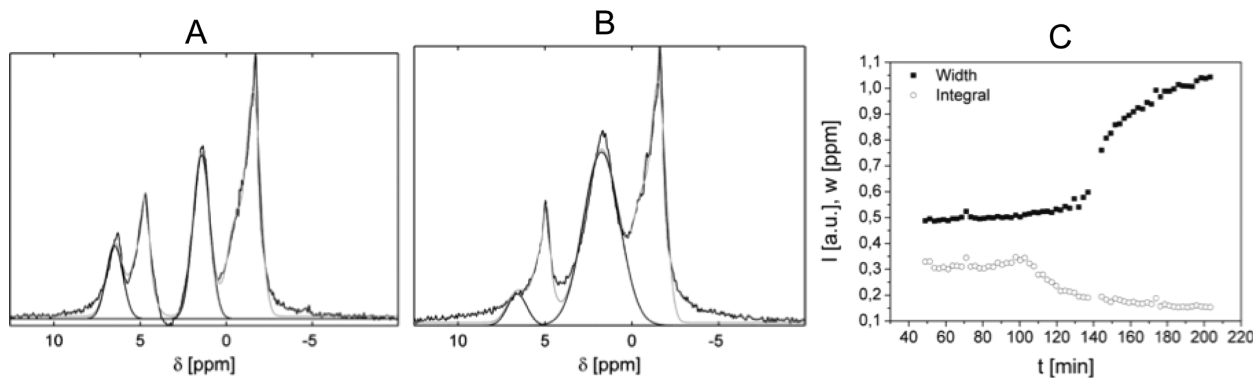


Figure 72. Real-time monitoring of an emulsion polymerization: (A) Initial NMR spectrum of butyl acrylate in D_2O . The relevant signals for the study are at 6.5 and 2.1 ppm. The signal at 4.8 ppm corresponds to water, and the peak at the right is an external reference. (B) NMR spectrum at a later stage of the polymerization. (C) Line width of the aliphatic peak (■) and area of the olefinic peak (○) as a function of the reaction time. Reprinted with permission from ref 318. Copyright 2010 American Chemical Society.

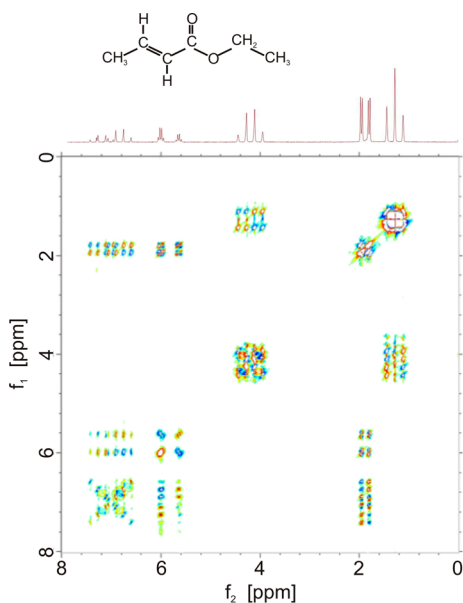


Figure 73. 2D double quantum COSY experiment of 0.4 M ethyl crotonate measured at 40 MHz. 256 increments were acquired in the indirect dimension with 8 scans per step and 4 s relaxation delay. The increment of evolution delay was set to 2 ms. Total experiment time was 2 h. The 1D projection along the direct dimension can be seen on top of the 2D spectrum, as well as a representative sketch of the molecule. Courtesy of Federico Casanova.³²⁵

interface for real-time monitoring of chemical reactions and processes.

When characterizing the examples presented in this review, we can conclude that a wide range of powerful NMR methods has already successfully been applied in various areas with miniature hardware. Rapid growth of this branch of NMR is anticipated, especially, when the information about these powerful techniques becomes more widely known. The interest in structural and mechanistic research based on miniature NMR spectrometers will further be expanded by continuing improvement of the hardware toward better sensitivity and spectral resolution. The NMR studies discussed in this review may be considered to be a collection of representative examples, and many more applications are expected to emerge soon.

AUTHOR INFORMATION

Corresponding Authors

*E-mail: bluemich@mc.rwth-aachen.de.

*Fax: +7 (499) 1355328. E-mail: val@ioc.ac.ru.

Notes

The authors declare no competing financial interest.

Biographies



Sergey Zalesskiy received his B.S. in chemistry from Higher Chemical College of Russian Academy of Sciences in 2010, and his Ph.D. in 2013. He started working with Prof. Ananikov as an undergraduate in 2005, and currently he is doing research in the field of NMR and transition metal catalysis. His research is focused on developing new methodologies for analysis of catalytic reactions with combined physical and chemical approaches as well as development of new catalysts for organic chemistry applications.



Ernesto Danieli was born in 1976, received his M.Sc. in 2001, and his Ph.D. in 2006, Córdoba, Argentina. He joined the group of Prof. Blümich in 2007 as a Humboldt postdoctoral fellow to work in the development of mobile NMR sensors for their application in NMR spectroscopy and imaging. His current research interest is the design and construction of new sensor geometries for mobile low-field MR applications, as well as the development of new NMR/MRI methodologies to be implemented on such devices.



Valentine Ananikov received his Ph.D. degree in 1999, Habilitation in 2003, and in 2005 he was appointed Professor and Laboratory Head of the ND Zelinsky Institute of Organic Chemistry, Russian Academy of Sciences. In 2008 he was elected as a Member of the Russian Academy of Sciences. In 2012 he became Professor of the Chemistry Department of Moscow State University. He was a recipient of the Russian State Prize for Outstanding Achievements in Science and Technology (2004), an Award of the Science Support Foundation (2005), a Medal of the Russian Academy of Sciences (2000), Liebig Lecturer by German Chemical Society (2010), and Balandin Prize for outstanding achievements in the field of catalysis (2010). His research has been supported by grants from the President of Russia. He is a member of the International Advisory Boards of *Advanced Synthesis & Catalysis*, *Organometallics*, and *Chemistry An Asian Journal*. His scientist interests are focused on (i) transition metal and nanoparticle-mediated reactions, (ii) development of new analytic methods, and (iii) mechanistic studies of catalytic reactions.



Bernhard Blümich is a Professor of Macromolecular Chemistry at RWTH Aachen University. He has been working in NMR since his undergraduate studies at Technische Universität Berlin. His expertise is in NMR methodology, solid-state NMR, NMR imaging of materials and processes, and in mobile NMR. He has published around 400 articles in scientific journals, edited a number of books, and authored three books including NMR Imaging of Materials (Oxford University Press, 2000). He has founded the Division of Spatially Magnetic Resonance of the Ampere Society and started the International Conference on Magnetic Resonance Microscopy. His contributions to mobile NMR with the development of the NMR-MOUSE were acknowledged with an honorary Ph.D. degree from the Technical University of Cluj Napoca, the Ampere Prize, and an honorary membership of the Indian Society of Magnetic Resonance. Currently he serves as associate editor of the Journal of Magnetic Resonance and as President of the Ampere Society.

ACKNOWLEDGMENTS

S.S.Z. and V.P.A. acknowledge support from the Russian Foundation for Basic Research (Project nos. 12-03-33127, 13-03-01210), grant MD-4969.2012.3, Ministry of education and science of Russian Federation (Projects 8572, 8453), and Programs of Division of Chemistry and Material Sciences of RAS.

E.D. and B.B. acknowledge support from the Deutsche Forschungsgemeinschaft (DFG) grant CA660/33, Gerätezentrum Pro2NMR: DFG supported joint instrumental NMR facility of RWTH Achen University and KIT Karlsruhe, transregional research project TR32: Patterns in Soil—Vegetation—Atmosphere Systems: Monitoring, Modelling and Data Assimilation, the Virtual Institute for Portable NMR funded by the Helmholtz Association (HGF), the European Community project CHARISMA: Cultural Heritage Advanced Research Infrastructures: Synergy for a Multidisciplinary Approach to Conservation/Restoration, the Allianz Industrie Forschung (AIF) grant IGF-FV:17233N/2, the Alexander von Humboldt Foundation, and the German Academic Exchange Service DAAD.

REFERENCES

- (1) (a) Harada, N. *Chirality* **2008**, *20*, 691. (b) Thiele, C. M. *Eur. J. Org. Chem.* **2008**, *34*, 5673. (c) Kwan, E. E.; Huang, S. G. *Eur. J. Org. Chem.* **2008**, *16*, 2671. (d) March, R.; Brodbelt, J. *J. Mass Spectrom.* **2008**, *43*, 1581. (e) Duddeck, H.; Gomez, E. D. *Chirality* **2009**, *21*, 51. (f) Wenzel, T. J.; Chisholm, C. D. *Chirality* **2011**, *23*, 190.
- (2) (a) Scheuermann, G. M.; Rumi, L.; Steurer, P.; Willi, B.; Muelhaupt, R. *J. Am. Chem. Soc.* **2009**, *131*, 8262. (b) Muniz, K.; Hovelmann, C. H.; Streuff, J. *J. Am. Chem. Soc.* **2008**, *130*, 763.

- (c) Seidel, G.; Mynott, R.; Fuerstner, A. *Angew. Chem., Int. Ed.* **2009**, *48*, 2510. (d) Gnanamgari, D.; Sauer, E. L.; Schley, N. D.; Butler, C.; Incarvito, C. D.; Crabtree, R. H. *Organometallics* **2009**, *28*, 321. (e) Li, X.; Hou, Z. *Coord. Chem. Rev.* **2008**, *252*, 1842. (f) Bhan, A.; Iglesia, E. *Acc. Chem. Res.* **2008**, *41*, 559. (g) Gil, A.; Korili, S. A.; Vicente, M. A. *Catal. Rev.: Sci. Eng.* **2008**, *50*, 153. (h) Lanni, E. L.; McNeil, A. J. *J. Am. Chem. Soc.* **2009**, *131*, 16573. (i) Ananikov, V. P.; Orlov, N. V.; Zalesskiy, S. S.; Beletskaya, I. P.; Khrustalev, V. N.; Morokuma, K.; Musaev, D. G. *J. Am. Chem. Soc.* **2012**, *134*, 6637.
- (3) (a) Salditos, R.; Larive, C. K. *Anal. Bioanal. Chem.* **2012**, *404*, 1165. (b) Franks, W. T.; Linden, A. H.; Kunert, B.; van Barth-Jan, R.; Oschkinat, H. *Eur. J. Cell Biol.* **2012**, *91*, 340. (c) Mittermaier, A. K.; Kay, L. E. *Trends Biochem. Sci.* **2009**, *34*, 601. (d) Zhang, B.; Powers, R. *Future Med. Chem.* **2012**, *4*, 1273. (e) Coen, M.; Holmes, E.; Lindon, J. C.; Jeremy, N. *Chem. Res. Toxicol.* **2008**, *21*, 9.
- (4) (a) Barba, I.; Fernandez-Montesinos, R.; Garcia-Dorado, D.; Pozo, D. *J. Cell. Mol. Med.* **2008**, *12*, 1477. (b) Pichler, B. J.; Wehr, H. F.; Judenhofer, M. S. *J. Nucl. Med.* **2008**, *49*, 5S. (c) Ala-Korpela, M. *Clin. Chem. Lab. Med.* **2008**, *46*, 27. (d) de Vos, P.; Bucko, M.; Gemeiner, P.; Navratil, M.; Svitel, J.; Faas, M.; Strand, B. L.; Skjak-Braek, G.; Morsch, Y. A.; Vikartovska, A.; Igor, L.; Kollarikova, G.; Orive, G.; Poncelet, D.; Pedraz, J. L.; Ansorge-Schumacher, M. B. *Biomaterials* **2009**, *30*, 2559. (e) Fernandez-Busquets, X.; de Groot, N. S.; Daniel, F.; Ventura, S. *Curr. Med. Chem.* **2008**, *15*, 1336.
- (5) (a) Sanchez, C.; Boissiere, C.; Grosso, D.; Christel, L.; Nicole, L. *Chem. Mater.* **2008**, *20*, 682. (b) Colnago, L. A.; Azereedo, R. B.; Netto, A. M.; Andrade, F.; Venancio, T. *Magn. Reson. Chem.* **2011**, *49*, S113. (c) Ito, H. *J. Photopolym. Sci. Technol.* **2008**, *21*, 475. (d) Yeh, J.; Chang, K. *J. Ind. Eng. Chem.* **2008**, *14*, 275. (e) Cerqueira, H. S.; Caeiro, G.; Costa, L.; Ribeiro, F. R. *J. Mol. Catal. A: Chem.* **2008**, *292*, 1. (f) Siro, I.; Plackett, D. *Cellulose* **2010**, *17*, 459.
- (6) Raman, S.; Lange, O. F.; Rossi, P.; Tyka, M.; Wang, X.; Aramini, J.; Liu, G.; Ramelot, T. A.; Eletsky, A.; Szyperski, T.; Kennedy, M. A.; Prestegard, J.; Montelione, G. T.; Baker, D. *Science* **2010**, *327*, 1014.
- (7) (a) Novoa-Carballal, R.; Fernandez-Megia, E.; Jimenez, C.; Riguera, R. *Nat. Prod. Rep.* **2011**, *28*, 78. (b) Zalesskiy, S. S.; Ananikov, V. P. *Organometallics* **2012**, *31*, 2302. (c) Ananikov, V. P.; Gayduk, K. A.; Beletskaya, I. P.; Khrustalev, V. N.; Antipin, M. Yu. *Eur. J. Inorg. Chem.* **2009**, *9*, 1149.
- (8) Casarini, D.; Lunazzi, L.; Mazzanti, A. *Eur. J. Org. Chem.* **2010**, *11*, 2035.
- (9) Zhou, C.; Plashkevych, O.; Chattopadhyaya, J. *Org. Biomol. Chem.* **2008**, *6*, 4627.
- (10) Valiullin, R.; Kaerger, J.; Glaeser, R. *Phys. Chem. Chem. Phys.* **2009**, *11*, 2833.
- (11) (a) Ananikov, V. P. *Chem. Rev.* **2011**, *111*, 418. (b) Khokhlova, E. A.; Kachala, V. V.; Ananikov, V. P. *ChemSusChem* **2012**, *5*, 783.
- (12) (a) Kanellopoulos, J.; Gottert, C.; Schneider, D.; Knorr, B.; Prager, D.; Ernst, H.; Freude, D. *J. Catal.* **2008**, *255*, 68. (b) Ananikov, V. P.; Zalesskiy, S. S.; Kachala, V. V.; Beletskaya, I. P. *J. Organomet. Chem.* **2011**, *696*, 400.
- (13) Jones, D. K. *Cortex* **2008**, *44*, 936.
- (14) For examples of enantiodiscrimination by NMR, see: (a) Seco, J. M.; Quinoa, E.; Riguera, R. *Chem. Rev.* **2004**, *104*, 17. (b) Wenzel, T. J.; Chisholm, C. D. *Prog. Nucl. Magn. Reson. Spectrosc.* **2011**, *59*, 1. (c) Orlov, N. V.; Ananikov, V. P. *Chem. Commun.* **2010**, *46*, 3212. (d) Orlov, N. V.; Ananikov, V. P. *Green Chem.* **2011**, *13*, 1735.
- (15) For applications for NMR in catalysis and nanoparticles science, see: (a) Tedsree, K.; Kong, A. S.; Tsang, S. *Angew. Chem., Int. Ed.* **2009**, *48*, 1443. (b) Mayer, C. *Annu. Rep. NMR Spectrosc.* **2005**, *55*, 205. (c) Kobayashi, H. *ENC 2008 Inorganic Solids & Materials Session; Pacific Grove: CA, March 9–14, 2008*. (d) Gomez, M. V.; Guerra, J.; Velders, A. H.; Crooks, R. M. *J. Am. Chem. Soc.* **2009**, *131*, 341. (e) Durand, J.; Fernández, F.; Barrière, C.; Teuma, E.; Gómez, K.; González, G.; Gómez, M. *Magn. Reson. Chem.* **2008**, *46*, 739. (f) Ananikov, V. P.; Orlov, N. V.; Beletskaya, I. P.; Khrustalev, V. N.; Antipin, M. Yu.; Timofeeva, T. V. *J. Am. Chem. Soc.* **2007**, *129*, 7252.
- (16) (a) Robinette, S. L.; Brueschweiler, R.; Schroeder, F. C.; Edison, A. S. *Acc. Chem. Res.* **2012**, *45*, 288. (b) Price, K. E.; Vandaveer, S. S.; Lunte, C. E.; Larive, C. K. *J. Pharm. Biomed. Anal.* **2005**, *38*, 904. (c) Limtiaco, J. F. K.; Beni, S.; Jones, C. J.; Langeslay, D. J.; Larive, C. K. *Carbohydr. Res.* **2011**, *346*, 2244.
- (17) (a) Felli, I. C.; Pierattelli, R. *IUBMB Life* **2012**, *64*, 473. (b) Markwick, P. R.; Malliavin, T.; Nilges, M. *PLoS Comput. Biol.* **2008**, *4*, e1000168. (c) McDermott, A. *Annu. Rev. Biophys.* **2009**, *38*, 385.
- (18) (a) Inomata, K.; Ohno, A.; Tochio, H.; Isogai, S.; Tenno, T.; Nakase, I.; Takeuchi, T.; Futaki, S.; Ito, Y.; Hiroaki, H.; Masahiro, S. *Nature* **2009**, *458*, 106. (b) Sakakibara, D.; Sasaki, A.; Ikeya, T.; Junpei, H.; Hanashima, T.; Mishima, M.; Masatoshi, Y.; Hayashi, N.; Mikawa, T.; Waelchli, M.; Smith, B. O.; Shirakawa, M.; Guentert, P.; Yutaka, I. *Nature* **2009**, *458*, 102.
- (19) Krohn, K. A.; Link, J. M.; Mason, R. P. *J. Nucl. Med.* **2008**, *49*, 129S.
- (20) Reid, D. G.; Murphy, P. S. *Drug Discovery Today* **2008**, *13*, 473.
- (21) van der Kooy, F.; Maltese, F.; Choi, Y. H.; Kyong, K. H.; Verpoorte, R. *Planta Med.* **2009**, *75*, 763.
- (22) Belyakov, P. A.; Kadentsev, V. I.; Chizhov, A. O.; Kolotyrkina, N. G.; Shashkov, A. S.; Ananikov, V. P. *Mendeleev Commun.* **2010**, *20*, 125.
- (23) High sensitivity detection up to a single molecule is discussed, see, for example: (a) Twerenbold, D. *Cryogenic Detectors: Detection of Single Molecules. Encyclopedia of Life Sciences*; John Wiley & Sons Ltd.: New York, 2006; DOI: 10.1002/9780470015902.a0006203. (b) Soni, M.; Bauer, S.; Amy, J. W.; Wong, P.; Cooks, R. G. *Anal. Chem.* **1995**, *67*, 1409. (c) Robertson, J. W.; Rodrigues, C. G.; Stanford, M. V.; Robinson, K. A.; Krasilnikov, O. V.; Kasianowicz, J. J. *Proc. Natl. Acad. Sci. U.S.A.* **2007**, *104*, 8207. (d) Naik, A. K.; Hanay, M. S.; Hiebert, W. K.; Feng, X. L.; Roukes, M. L. *Nat. Nanotechnol.* **2009**, *4*, 445. (e) McLafferty, F. W. *Annu. Rev. Anal. Chem.* **2011**, *4*, 1.
- (f) Hanay, M. S.; Kelber, S.; Naik, A. K.; Chi, D.; Hertz, S.; Bullard, E. C.; Colinet, E.; Duraffourg, L.; Roukes, M. L. *Nat. Nanotechnol.* **2012**, *7*, 602.
- (24) Fratila, R. M.; Velders, A. H. *Annu. Rev. Anal. Chem.* **2011**, *4*, 227.
- (25) Jones, C. J.; Larive, C. K. *Anal. Bioanal. Chem.* **2012**, *402*, 61.
- (26) Badilita, V.; Meier, R. C.; Spengler, N.; Wallrabe, U.; Utz, M.; Korvink, J. G. *Soft Matter* **2012**, *8*, 10583.
- (27) Blümich, B.; Perlo, J.; Casanova, F. *Prog. Nucl. Magn. Reson. Spectrosc.* **2008**, *52*, 197.
- (28) Danieli, E.; Blümich, B.; Casanova, F. *Mobile Nuclear Magnetic Resonance. Encyclopedia of Magnetic Resonance*; John Wiley & Sons, Ltd.: New York, 2012; DOI: 10.1002/9780470034590.emrstm1287.
- (29) Prado, P. J.; Demas, V. *Concepts Magn. Reson., Part A* **2009**, *34*, 48.
- (30) *Single-Sided NMR*; Casanova, F., Perlo, J., Blümich, B., Eds.; Springer: Manheim, 2011.
- (31) Blümich, B.; Appelt, S. J.; Casanova, F. *Chem. Phys. Lett.* **2009**, *477*, 231.
- (32) Lacey, M. E.; Subramanian, R.; Olson, D. L.; Webb, A. G.; Sweedler, J. V. *Chem. Rev.* **1999**, *99*, 3133.
- (33) Wu, W.; Yu, H.; Chen, D.; Lu, R.; Yean, T.; Chen, J.; Ni, Z. *Microsyst. Technol.* **2014**, *20*, 419.
- (34) Webb, A. *Anal. Bioanal. Chem.* **2007**, *388*, 525.
- (35) van Bentum, P. J.; Janssen, J. W.; Kentgens, A. P. *Analyst* **2004**, *129*, 793.
- (36) Schroeder, F. C.; Gronquist, M. *Angew. Chem., Int. Ed.* **2006**, *45*, 7122.
- (37) Gökyay, O.; Albert, K. *Anal. Bioanal. Chem.* **2012**, *402*, 647.
- (38) (a) Heyn, C.; Ronald, J. A.; Mackenzie, L. T.; MacDonald, I. C.; Chambers, A. F.; Rutt, B. K.; Foster, P. J. *Magn. Reson. Med.* **2006**, *55*, 23. (b) Shapiro, E. M. *Proc. Natl. Acad. Sci. U.S.A.* **2004**, *101*, 10901. (c) Lee, N.; Kim, H.; Choi, S. H.; Park, M.; Kim, D.; Kim, H.-C.; Choi, Y.; Lin, S.; Kim, B. H.; Jung, H. S.; Park, K. S.; Moon, W. K.; Hyeon, T. *Proc. Natl. Acad. Sci. U.S.A.* **2011**, *108*, 2662. (d) Shapiro, E. M.; Sharer, K.; Skrtic, S.; Koretsky, A. P. *Magn. Reson. Med.* **2006**, *55*, 242.

- (e) Smirnov, P.; Poirier-Quinot, M.; Wilhelm, C.; Lavergne, E.; Ginefri, J.; Combadière, B.; Clément, O.; Darrasse, L.; Gazeau, F. *Magn. Reson. Med.* **2008**, *60*, 1292.
 (39) Takeda, K. *Rev. Sci. Instrum.* **2007**, *78*, 033103.
 (40) Takeda, K. *J. Magn. Reson.* **2008**, *192*, 218.
 (41) Lee, H.; Sun, E.; Ham, D.; Weissleder, R. *Nat. Med.* **2008**, *14*, 869.
 (42) (a) Fukushima, E.; Roeder, S. B. W. *Experimental Pulse NMR*; Addison-Wesley: New York, 1981. (b) Derome, A. E. *Modern NMR Techniques for Chemistry Research*; Pergamon Press: Oxford, 1987.
 (c) Abragam, A. *The Principles of Nuclear Magnetism*; Clarendon Press: Oxford, 1961. (d) Chen, C.-N.; Hoult, D. I. *Biomedical Magnetic Resonance Technology*; A. Hilger Ltd.: England, 1989.
 (43) Roth, G. *Spin Rep.* **2003**, *156*, 14.
 (44) Kiyoshi, T.; Sato, A.; Wada, H.; Hayashi, S.; Shimada, M.; Kawate, Y. *IEEE Trans. Appl. Supercond.* **1999**, *9*, 559.
 (45) Kiyoshi, T.; Sato, A.; Takeuchi, T.; Itoh, K.; Matsumoto, S.; Ozaki, O.; Wada, H.; Yoshikawa, M.; Kamikado, T.; Ito, S.; Miki, T.; Hase, T.; Hamada, M.; Hayashi, S.; Kawate, Y.; Hirose, R. *IEEE Trans. Appl. Supercond.* **2001**, *11*, 2347.
 (46) Kiyoshi, T.; Choi, S.; Matsumoto, S.; Zaitsu, K.; Hase, T.; Miyazaki, T.; Otsuka, A.; Yoshikawa, M.; Hamada, M.; Hosono, M.; Yanagisawa, Y.; Nakagome, H.; Takahashi, M.; Yamazaki, T.; Maeda, H. *IEEE Trans. Appl. Supercond.* **2010**, *20*, 714.
 (47) Yanagisawa, Y.; Nakagome, H.; Hosono, M.; Hamada, M.; Kiyoshi, T.; Hobo, F.; Takahashi, M.; Yamazaki, T.; Maeda, H. *J. Magn. Reson.* **2008**, *192*, 329.
 (48) Hahn, S.; Bascuñán, J.; Lee, H.; Bobrov, E. S.; Kim, W.; Iwasa, Y. *Rev. Sci. Instrum.* **2008**, *79*, 026105.
 (49) Hahn, S.; Bascuñán, J.; Lee, H.; Bobrov, E. S.; Kim, W.; Ahn, M. C.; Iwasa, Y. *J. Appl. Phys.* **2009**, *105*, 024501.
 (50) (a) Bascuñán, J.; Hahn, S.; Park, D. K.; Iwasa, Y. *IEEE Trans. Appl. Supercond.* **2011**, *21*, 2092. (b) Gagnon, B.; Hahn, S.; Park, D. K.; Voccio, J.; Kim, K.; Bascuñán, J.; Iwasa, Y. *Phys. C (Amsterdam, Neth.)* **2013**, *486*, 26.
 (51) Matsumoto, S.; Kiyoshi, T.; Otsuka, A.; Hamada, M.; Maeda, H.; Yanagisawa, Y.; Nakagome, H.; Suematsu, H. *Supercond. Sci. Technol.* **2012**, *25*, 025017.
 (52) Bruker Avance 1000 Installed. <http://www.bruker-biospin.com/pr091202.html>, 2009.
 (53) Kitagawa, I.; Tanaka, H.; Okada, M.; Kitaguchi, H.; Kohzuma, T. *Rev. Sci. Instrum.* **2008**, *79*, 123109.
 (54) Saho, N.; Matsuda, K.; Nishijima, N. *Cryogenics* **2012**, *52*, 604.
 (55) Luy, B. *Angew. Chem., Int. Ed.* **2011**, *50*, 354.
 (56) (a) Pake, G. P. *J. Chem. Phys.* **1948**, *16*, 327. (b) Pound, R. V. *Phys. Rev.* **1950**, *79*, 685. (c) Gutowsky, H. S.; Hoffman, C. J. *J. Chem. Phys.* **1951**, *19*, 1259.
 (57) (a) Roméo, F.; Hoult, D. I. *Magn. Reson. Med.* **1984**, *1*, 44. (b) Hoult, D. I.; Lee, D. *Rev. Sci. Instrum.* **1985**, *56*, 131.
 (58) Halbach, K. *Nucl. Instrum. Methods* **1980**, *169*, 1.
 (59) Moresi, G.; Magin, R. *Concepts Magn. Reson., Part B* **2003**, *19B*, 35.
 (60) Raich, H.; Blümller, P. *Concepts Magn. Reson.* **2004**, *23B*, 16.
 (61) Soltner, H.; Blümller, P. *Concepts Magn. Reson.* **2010**, *36A*, 211.
 (62) Cattin, V.; Jeandey, C.; Locatelli, M. EU Patent EP 1063534 A1, 1999.
 (63) Demas, V.; Herberg, J. L.; Malba, V.; Bernhardt, A.; Evans, L.; Harvey, C.; Chinn, S. C.; Maxwell, R. S.; Reimer, J. *J. Magn. Reson.* **2007**, *189*, 121.
 (64) Jachmann, R. C.; Trease, D. R.; Bouchard, L.-S.; Sakellariou, D.; Martin, R. W.; Schlueter, R. D.; Budinger, T. F.; Pines, A. *Rev. Sci. Instrum.* **2007**, *78*, 035115.
 (65) (a) Golay, M. J. E. *Rev. Sci. Instrum.* **1958**, *29*, 313. (b) Anderson, W. A. *Rev. Sci. Instrum.* **1961**, *32*, 241.
 (66) Windt, C. W.; Soltner, H.; van Dusschoten, D.; Blümller, P. J. *Magn. Reson.* **2011**, *208*, 27.
 (67) Danieli, E.; Mauler, J.; Perlo, J.; Blümich, B.; Casanova, F. *J. Magn. Reson.* **2009**, *198*, 80.
 (68) Danieli, E.; Perlo, J.; Blümich, B.; Casanova, F. *Angew. Chem., Int. Ed.* **2010**, *49*, 4133.
 (69) McDowell, A.; Fukushima, E. *Appl. Magn. Reson.* **2008**, *35*, 185.
 (70) (a) Aubert, G. U.S. Patent 5014032, 1991. (b) Armstrong, B. D.; Lingwood, M. D.; McCarney, E. R.; Brown, E. R.; Blümller, P.; Han, S. *J. Magn. Reson.* **2008**, *191*, 273. (c) Hugon, C.; DiAmico, F.; Aubert, G.; Sakellariou, D. *J. Magn. Reson.* **2010**, *205*, 75.
 (71) Manz, B.; Benecke, M.; Volke, F. *J. Magn. Reson.* **2008**, *192*, 131.
 (72) Leupold, H. A.; Potenziani, E., II; Abele, M. G. *J. Appl. Phys.* **1988**, *64*, 5994.
 (73) Potenziani, E., II; Leupold, H. A. *IEEE Trans. Magn.* **1986**, *22*, 1078.
 (74) Aoki, M.; Tsuzaki, T. U.S. Patent US7084633, 2006.
 (75) Fukushima, E. Musings on Hardware Advances and New Directions. In *Magnetic Resonance Microscopy Spatially Resolved NMR Techniques and Applications*; Codd, S. L., Seymour, J. D., Eds.; Wiley-VCH: Weinheim, 2008; pp 1–11.
 (76) (a) Jackson, J. A.; Burnett, L. J.; Harmon, J. F. *J. Magn. Reson.* **1980**, *41*, 411. (b) Kleinberg, R. L. Well logging. *Encyclopedia of NMR*; Wiley-Liss: New York, 1996. (c) Knight, R.; Grunewald, E.; Irons, T.; Dlubac, K.; Song, Y.; Bachman, H. N.; Grau, B.; Walsh, D.; Abraham, J. D.; Cannia, J. *Geophys. Res. Lett.* **2012**, *39*, L03304. (d) Perlo, J.; Danieli, E.; Perlo, J.; Blümich, B.; Casanova, F. *J. Magn. Reson.* **2013**, *233*, 74.
 (77) (a) Eidmann, G.; Savelsberg, R.; Blümller, P.; Blümich, B. *J. Magn. Reson., Ser. A* **1996**, *122*, 104. (b) Blümich, B.; Blümller, P.; Eidmann, G.; Guthausen, A.; Haken, R.; Schmitz, U.; Saito, K.; Zimmer, G. *Magn. Reson. Imaging* **1998**, *16*, 479.
 (78) (a) Prado, P. J.; Blümich, B.; Schmitz, U. *J. Magn. Reson., Ser. A* **2000**, *144*, 200. (b) Casanova, F.; Blümich, B. *J. Magn. Reson., Ser. A* **2003**, *163*, 38. (c) Prado, P. J. *Magn. Reson. Imaging* **2003**, *21*, 397. (d) Perlo, J.; Casanova, F.; Blümich, B. *J. Magn. Reson.* **2004**, *166*, 228.
 (79) (a) Casanova, F.; Perlo, J.; Blümich, B. *J. Magn. Reson.* **2004**, *171*, 124. (b) Perlo, J.; Casanova, F.; Blümich, B. *J. Magn. Reson.* **2005**, *173*, 254.
 (80) Perlo, J.; Casanova, F.; Blümich, B. *J. Magn. Reson.* **2005**, *176*, 64.
 (81) Glover, P. M.; Aptaker, P. S.; Bowler, J. R.; Ciampi, E.; McDonald, P. J. *J. Magn. Reson.* **1999**, *139*, 90.
 (82) McDonald, P. J. *Prog. Nucl. Magn. Reson. Spectrosc.* **1997**, *30*, 69.
 (83) Blank, A.; Alexandrowicz, G.; Muchnik, L.; Tidhar, G.; Schneiderman, J.; Virmani, R.; Golan, E. *Magn. Reson. Med.* **2005**, *54*, 105.
 (84) (a) Haken, R. J. Entwicklung und Anwendung mobiler NMR-sonden. Ph.D. Thesis, RWTH Aachen University, 2001. (b) Blank, A.; Ish-Shalom, S.; Shtirberg, L.; Zur, Y. *Magn. Reson. Med.* **2009**, *62*, 1585.
 (85) (a) Marble, A. E.; Mastikhin, I. V.; Colpitts, B. G.; Balcom, B. J. *J. Magn. Reson.* **2005**, *174*, 78. (b) Balcom, B. J.; Colpitts, B.; Marble, A. E.; Mastikhin, I. V. EU Patent EP2102674 A1, 2006. (c) Manz, B.; Coy, A.; Dykstra, R.; Eccles, C. D.; Hunter, M. W.; Parkinson, B. J.; Callaghan, P. T. *J. Magn. Reson.* **2006**, *183*, 25.
 (86) Fukushima, E.; Jackson, J. A. U.S. Patent US6489872, 2002.
 (87) Perlo, J.; Casanova, F.; Blümich, B. *Science* **2007**, *315*, 1110.
 (88) Paulsen, J. L.; Bouchard, L. S.; Graziani, D.; Blümich, B.; Pines, A. *Proc. Natl. Acad. Sci. U.S.A.* **2008**, *105*, 20601.
 (89) Woods, R.; McAllister, J.; Lightbody, G.; Yi, Y. *FPGA-Based Implementation of Signal Processing Systems*; John Wiley & Sons, Ltd.: Chichester, UK, 2009.
 (90) Sulaiman, N.; Obaid, Z. A.; Marhaban, M. H.; Hamidon, M. N. *Aust. J. Basic Appl. Sci.* **2009**, *3*, 3575.
 (91) Kim, J.; Hammer, B.; Harjani, R. A 5–300 MHz CMOS Transceiver for Multi-Nuclear NMR Spectroscopy. IEEE Custom Integrated Circuits Conference, 2012.
 (92) Murphy, E.; Slattery, C. *Analog Dialogue* **2004**, *38*, 1.
 (93) Surber, J.; McHugh, L. *Analog Dialogue* **1996**, *30*, 12.
 (94) Gengying, L.; Haibin, X. *Rev. Sci. Instrum.* **1999**, *70*, 1511.
 (95) Liang, X.; Weimin, W. *Rev. Sci. Instrum.* **2009**, *80*, 124703.

- (96) Yun, J.; Yu, J.; Hongyan, T.; Gengying, L. *Rev. Sci. Instrum.* **2002**, *73*, 3329.
- (97) Memis, O. G.; Eryaman, Y.; Aytur, O.; Atalar, E. *Magn. Reson. Med.* **2008**, *59*, 165.
- (98) Cherifi, T.; Abouchi, N.; Lu, G.-N.; Bouchet-Fakri, L.; Quiquerez, L.; Sorli, B.; Chateaux, J.-F.; Pitaval, M.; Morin, P. *IEEE Trans. Circuits Syst. I: Regular Papers* **2005**, *52*, 2576.
- (99) Blümich, B.; Gong, Q.; Byrne, E.; Greferath, M. *J. Magn. Reson.* **2009**, *199*, 18.
- (100) (a) Marion, D. J.-Y.; Desvaux, H. *J. Magn. Reson.* **2008**, *193*, 153. (b) Mandal, S.; Utsuzawa, S.; Cory, D. G.; Hürlimann, M.; Poizsch, M.; Song, Y.-Q. *J. Magn. Reson.* **2014**, *242*, 113.
- (101) Nausner, M.; Goger, M.; Bendet-Taicher, E.; Schlaglgnitweit, J.; Jerschow, A.; Müller, N. *J. Biomol. NMR* **2010**, *48*, 157.
- (102) Ogawa, K.; Yokouchi, Y.; Haishi, T.; Ito, K. *J. Magn. Reson.* **2013**, *234*, 147.
- (103) (a) Martin, G. E. *Annu. Rep. NMR Spectrosc.* **2005**, *56*, 1. (b) Schlotterbeck, G.; Ross, A.; Hochstrasser, R.; Senn, H.; Kühn, T.; Marek, D.; Schett, O. *Anal. Chem.* **2002**, *74*, 4464.
- (104) Koskela, H.; Vanninen, P. *Anal. Chem.* **2008**, *80*, 5556.
- (105) Takeda, K. *Solid State Nucl. Magn. Reson.* **2012**, *47*–48, 1.
- (106) Kentgens, A. P. M.; Bart, J.; van Bentum, P. J. M.; Brinkmann, A.; van Eck, E. R. H.; Gardeniers, J. G. E.; Janssen, J. W. G.; Knijn, P.; Vasa, S.; Verkuijlen, M. H. W. *J. Chem. Phys.* **2008**, *128*, 052202.
- (107) Webb, A. G. *J. Magn. Reson.* **2013**, *229*, 55.
- (108) Wright, A. C.; Neideen, T. A.; Magin, R. L.; Norcross, J. A. *Rev. Sci. Instrum.* **1998**, *69*, 3938.
- (109) Olson, D.; Peck, T.; Webb, A.; Magin, R.; Sweedler, J. *Science* **1995**, *270*, 1967.
- (110) (a) Wu, N.; Peck, T. L.; Webb, A. G.; Magin, R. L.; Sweedler, J. V. *J. Am. Chem. Soc.* **1994**, *116*, 7929. (b) Wu, N.; Peck, T. L.; Webb, A. G.; Magin, R. L.; Sweedler, J. V. *Anal. Chem.* **1994**, *66*, 3849.
- (111) Wu, N.; Webb, A.; Peck, T. L.; Sweedler, J. V. *Anal. Chem.* **1995**, *67*, 3101.
- (112) Subramanian, R.; Kelley, W. P.; Floyd, P. D.; Tan, Z. J.; Webb, A. G.; Sweedler, J. V. *Anal. Chem.* **1999**, *71*, 5335.
- (113) Krivic, P. *Adv. Mater. Res.* **2013**, *685*, 362.
- (114) Seeber, D. A.; Hoftiezer, J. H.; Pennington, C. H. *Rev. Sci. Instrum.* **2000**, *71*, 2908.
- (115) Jacquinot, J.-F.; Sakellariou, D. *Concepts Magn. Reson., Ser. A* **2011**, *38*, 33.
- (116) (a) Sakellariou, D.; Le Goff, G. L.; Jacquinot, J.-F. *Nature* **2007**, *447*, 694. (b) Wong, A.; Li, X.; Sakellariou, D. *Anal. Chem.* **2013**, *85*, 2021.
- (117) Raimann, M.; Peter, A.; Mager, D.; Wallrabe, U.; Korvink, J. G. *IEEE Trans. Power* **2012**, *27*, 3996.
- (118) Brinkmann, A.; Vasa, S. K.; Janssen, H.; Kentgens, A. P. M. *Chem. Phys. Lett.* **2010**, *485*, 275.
- (119) Elena, B.; de Paëpe, G.; Emsley, L. *Chem. Phys. Lett.* **2004**, *398*, 532.
- (120) Badilita, V.; Fassbender, B.; Kratt, K.; Wong, A.; Bonhomme, C.; Sakellariou, D.; Korvink, J. G.; Wallrabe, U. *PLoS One* **2012**, *7*, e42848.
- (121) Ryan, H.; Song, S.-H.; Zaß, A.; Korvink, J.; Utz, M. *Anal. Chem.* **2012**, *84*, 3696.
- (122) Aguiar, P. M.; Jacquinot, J.-F.; Sakellariou, D. *Chem. Commun.* **2011**, *47*, 2119.
- (123) McDowell, A. F.; Adolphi, N. L. *J. Magn. Reson.* **2007**, *188*, 74.
- (124) Sillerud, L. O.; McDowell, A. F.; Adolphi, N. L.; Serda, R. E.; Adams, D. P.; Vasile, M. J.; Alam, T. M. *J. Magn. Reson.* **2006**, *181*, 181.
- (125) Haukanes, B.; Kvam, C. *Nat. Biotechnol.* **1993**, *11*, 60.
- (126) Seeber, D. A.; Cooper, R. L.; Ciobanu, L.; Pennington, C. H. *Rev. Sci. Instrum.* **2001**, *72*, 2171.
- (127) Anzenbacher, P.; Palacios, M. A. *Nat. Chem.* **2009**, *11*, 80.
- (128) However, concurrent solenoid designs generating perpendicular B_0 field are known: (a) Gerald, R. E., II; Rathke, J. W. U.S. Patent US7486078, 2009. (b) Alonso, J.; Soleilhavoup, A.; Wong, A.; Guiga, A.; Sakellariou, D. *J. Magn. Reson.* **2013**, *235*, 32.
- (129) An alternative approach based on the split-type superconducting magnet was recently demonstrated: Wakuda, T.; Park, M.; Kawasaki, K.; Tanaka, H.; Fukuda, Y.; Okada, M.; Kitaguchi, H. *Concepts Magn. Reson., Part B* **2013**, *43*, 79.
- (130) (a) Glenat, H. U.S. Patent US5528143, 1996. (b) Glenat, H. U.S. Patent US5198767, 1993.
- (131) Harel, E. *Prog. Nucl. Magn. Reson. Spectrosc.* **2010**, *57*, 293.
- (132) Massin, C.; Vincent, F.; Homys, A.; Ehrmann, K.; Boero, G.; Besse, P.-A.; Daridon, A.; Verpoorte, E.; de de Rooij, N. F.; Popovic, R. S. *J. Magn. Reson.* **2003**, *164*, 242.
- (133) Ehrmann, K.; Saillen, N.; Vincent, F.; Stettler, M.; Jordan, M.; Wurm, F. M.; Besse, P.; Popovic, R. *Lab Chip* **2007**, *7*, 373.
- (134) Carver, K.; Mink, J. *IEEE Trans. Antennas Propag.* **1981**, *29*, 2.
- (135) Zhang, X.; Ugurbil, K.; Chen, W. *Magn. Reson. Med.* **2001**, *46*, 443.
- (136) Maguire, Y.; Chuang, I. L.; Zhang, S.; Gershenfeld, N. *Proc. Natl. Acad. Sci. U.S.A.* **2007**, *104*, 9198.
- (137) van Bentum, P. J. M.; Janssen, J. W. G.; Kentgens, A. P. M.; Bart, J.; Gardeniers, J. G. E. *J. Magn. Reson.* **2007**, *189*, 104.
- (138) Bart, J.; Janssen, J. W. G.; van Bentum, P. J. M.; Kentgens, A. P. M.; Gardeniers, J. G. E. *J. Magn. Reson.* **2008**, *201*, 175.
- (139) Bart, J.; Kolkman, A. J.; de Vries, A. J.; Koch, K.; Nieuwland, P. J.; Janssen, H.; van Bentum, J.; Ampt, K. A.; Rutjes, F. P.; Wijmenga, S. S.; Gardeniers, H.; Kentgens, A. P. J. *Am. Chem. Soc.* **2009**, *131*, 5014.
- (140) Markley, J. *Nat. Biotechnol.* **2007**, *25*, 750.
- (141) Leidich, S.; Braun, M.; Gessner, T.; Riemer, T. *Concepts Magn. Reson., Part B* **2009**, *35B*, 11.
- (142) Watzlaw, J.; Glöggler, S.; Blümich, B.; Mokwa, W.; Schnakenberg, U. *J. Magn. Reson.* **2013**, *230*, 176.
- (143) Walton, J. H.; de Ropp, J. S.; Shutov, M. V.; Goloshevsky, A. G.; McCarthy, M. J.; Smith, R. L.; Collins, S. D. *Anal. Chem.* **2003**, *75*, 5030.
- (144) Norcross, J. A.; Milling, C. T.; Olson, D. L.; Xu, D.; Audrieth, A.; Albrecht, R.; Ruan, K.; Likos, J.; Jones, C.; Peck, T. L. *Anal. Chem.* **2010**, *82*, 7227.
- (145) Peti, W.; Page, R.; Moy, K.; O'Neil-Johnson, M.; Wilson, I. A.; Stevens, R. C.; Wüthrich, K. *J. Struct. Funct. Genomics* **2006**, *6*, 259.
- (146) Aramini, J. M.; Rossi, P.; Anklin, C.; Xiao, R.; Montelione, G. T. *Nat. Methods* **2007**, *4*, 491.
- (147) (a) Horst, R.; Stanczak, P.; Stevens, R. C.; Wüthrich, K. *Angew. Chem., Int. Ed.* **2013**, *52*, 331. (b) Stanczak, P.; Horst, R.; Serrano, P.; Wüthrich, K. *J. Am. Chem. Soc.* **2009**, *131*, 18450.
- (148) Dechow, J.; Lanz, T.; Stumber, M.; Forchel, A.; Haase, A. *Rev. Sci. Instrum.* **2003**, *74*, 4855.
- (149) Boero, G.; Frounchi, J.; Furrer, B.; Besse, P.-A.; Popovic, R. S. *Rev. Sci. Instrum.* **2001**, *72*, 2764.
- (150) Magin, R. L.; Webb, A. G.; Peck, T. L. *IEEE Spectrum* **1997**, *34*, 51.
- (151) Narasimhan, P.; Jacobs, R. *Annu. Rep. NMR Spectrosc.* **2005**, *55*, 259.
- (152) Denoth, S.; Fey, M.; Massin, C.; Vincent, F. EU Patent EP1895314 B1, 2006.
- (153) Seeber, D. A.; Hoftiezer, J. H.; Daniel, W. B.; Rutgers, M. A.; Pennington, C. H. *Rev. Sci. Instrum.* **2000**, *71*, 4263.
- (154) Weiger, M.; Schmidig, D.; Denoth, S.; Massin, C.; Vincent, F.; Schenkel, M.; Fey, M. *Concepts Magn. Reson., Ser. B* **2008**, *33B*, 84.
- (155) Fan, L.; Hsu, S. S.; Jin, J.; Hsieh, C.; Lin, W.; Hao, H. C.; Cheng, H.; Hsueh, K.; Lee, C. *IEEE Int. Conf. Solid-State Circuits* **2007**, *166*.
- (156) Jasiński, K.; Mlynarczyk, A.; Latta, P.; Volotovskyy, V.; Weglarz, W. P.; Tomanek, B. *Magn. Reson. Imaging* **2012**, *30*, 70.
- (157) Sahebjavaher, R. S.; Walus, K.; Stoeber, B. *Rev. Sci. Instrum.* **2010**, *81*, 023706.
- (158) Badilita, V.; Kratt, K.; Baxan, N.; Mohmmadzadeh, M.; Burger, T.; Weber, H.; von Elverfeldt, D. V.; Hennig, J.; Korvink, J. G.; Wallrabe, U. *Lab Chip* **2010**, *10*, 1387.
- (159) Mohmmadzadeh, M.; Baxan, N.; Badilita, V.; Kratt, K.; Weber, H.; Korvink, J. G.; Wallrabe, U.; Henning, J.; von Elverfeldt, D. J. *Magn. Reson.* **2011**, *208*, 20.

- (160) Keil, B.; Wald, L. L. *J. Magn. Reson.* **2013**, 229, 75.
- (161) Barmet, C.; de Zanche, N.; Wilm, B. J.; Pruessmann, K. P. *Magn. Reson. Med.* **2009**, 62, 269.
- (162) Barmet, C.; de Zanche, N. D.; Pruessmann, K. P. *Magn. Reson. Med.* **2008**, 60, 187.
- (163) Atlar, E.; Bottomley, P. A.; Ocali, O.; Correia, L. C.; Kelemen, M. D.; Lima, J. A.; Zerhouni, E. A. *Magn. Reson. Med.* **1996**, 36, 596.
- (164) (a) Dumoulin, C. L.; Souza, S. P.; Darrow, R. D. *Magn. Reson. Med.* **1993**, 29, 411. (b) Haken, R.; Blümller, B.; Blümich, B. The NMR endoscope. In *Spatially Resolved Magnetic Resonance*; Blümller, P., Blümich, B., Botto, R., Fukushima, E., Eds.; Wiley-VCH Verlag: Weinheim, 1998.
- (165) Quick, H. H.; Zenge, M. O.; Kuehl, H.; Kaiser, G.; Aker, S.; Massing, S.; Bosk, S.; Ladd, M. E. *Magn. Reson. Med.* **2005**, 53, 446.
- (166) Atalar, E. Catheter Coils. *Encyclopedia of Magnetic Resonance* [Online]; 2011; DOI: 10.1002/9780470034590.emrstm1135.
- (167) Sidles, J. A. *Appl. Phys. Lett.* **1991**, 58, 2854.
- (168) Madsen, L. A. *Proc. Natl. Acad. Sci. U.S.A.* **2004**, 101, 12804.
- (169) Barbic, M.; Barrett, C. P.; Vltava, L.; Emery, T. H.; Walker, C.; Scherer, A. *Concepts Magn. Reson., Part B* **2008**, 1, 33B.
- (170) Xu, S.; Harel, E.; Michalak, D. J.; Crawford, C. W.; Budker, D.; Pines, A. *J. Magn. Reson. Imaging* **2008**, 28, 1299.
- (171) Mamin, H. J.; Poggio, M.; Degen, C. L.; Rugar, D. *Nat. Nanotechnol.* **2007**, 2, 301.
- (172) Mamin, H. J.; Kim, M.; Sherwood, M. H.; Rettner, C. T.; Ohno, K.; Awschalom, D. D.; Rugar, D. *Science* **2013**, 339, 557.
- (173) Hemmer, P. *Science* **2013**, 339, 529.
- (174) Staudacher, T.; Shi, F.; Pezzagna, S.; Meijer, J.; Meriles, C. A.; Reinhard, F.; Wrachtrup, J. *Science* **2013**, 339, 561.
- (175) Greenberg, Y. *Rev. Mod. Phys.* **1998**, 70, 175.
- (176) Levitin, L. V.; Bennett, R. G.; Casey, A.; Cowan, B. P.; Lusher, C. P.; Saunders, J.; Drung, D.; Schurig, T. *Appl. Phys. Lett.* **2007**, 91, 262507.
- (177) (a) Espy, M.; Matlashov, A.; Volegov, P. J. *Magn. Reson.* **2013**, 229, 127. (b) Liao, S.-H.; Chen, H.-H.; Deng, Y.-S.; Wang, M.-W.; Chen, K. L.; Liu, C. W.; Liu, C. I.; Yang, H.-C.; Horng, H.-E.; Chieh, J. J.; Yang, S. Y. *IEEE Trans. Appl. Supercond.* **2013**, 23, 1602404.
- (178) Granata, C.; Esposito, E.; Vettoliere, A.; Petti, L.; Russo, M. *Nanotechnology* **2008**, 19, 275501.
- (179) Qian, C.; Zabow, G.; Koretsky, A. *J. Magn. Reson.* **2013**, 229, 67.
- (180) Harel, E.; Schröder, L.; Xu, S.; Schröder, L. *Annu. Rev. Anal. Chem.* **2008**, 1, 133.
- (181) McDonnell, E. E.; Han, S.; Hilty, C.; Pierce, K. L.; Pines, A. *Anal. Chem.* **2005**, 77, 8109.
- (182) Han, S.; Granwehr, J.; Garcia, S.; McDonnell, E. E.; Pines, A. *J. Magn. Reson.* **2006**, 182, 260.
- (183) Hilty, C.; McDonnell, E. E.; Granwehr, J.; Pierce, K. L.; Han, S.; Pines, A. *Proc. Natl. Acad. Sci. U.S.A.* **2005**, 102, 14960.
- (184) Granwehr, J.; Harel, E.; Han, S.; Garcia, S.; Pines, A.; Song, Y.-Q. *Phys. Rev. Lett.* **2005**, 95, 075503–1.
- (185) Verpillat, F.; Ledbetter, M. P.; Xu, S.; Michalak, D. J.; Hilty, C.; Bouchard, L. S.; Antonijevic, S.; Budker, D.; Pines, A. *Proc. Natl. Acad. Sci. U.S.A.* **2008**, 105, 2271.
- (186) (a) Kominis, I. K.; Kornack, T. W.; Allred, J. C.; Romalis, M. V. *Nature* **2003**, 422, 596. (b) Cho, A. *Science* **2005**, 307, 1855.
- (187) Harel, E.; Pines, A. *J. Magn. Reson.* **2008**, 193, 199.
- (188) Harel, E. *Lab Chip* **2009**, 9, 17.
- (189) Bajaj, V. S.; Paulsen, J.; Harel, E.; Pines, A. *Science* **2010**, 330, 1078.
- (190) Teisseire, T. Z.; Urban, J.; Halpern-Manners, N. W.; Chambers, S. D.; Bajaj, V. S.; Svec, F.; Pines, A. *Anal. Chem.* **2011**, 83, 6004.
- (191) Danieli, E.; Perlo, J.; Blümich, B.; Casanova, F. *Phys. Rev. Lett.* **2013**, 110, 180801.
- (192) (a) Andrew, E. R.; Bradbury, A.; Eades, R. G. *Nature* **1958**, 182, 1659. (b) Lowe, I. J. *Phys. Rev. Lett.* **1959**, 2, 285.
- (193) Sørensen, M. K.; Bakharev, O.; Jensen, O.; Jakobsen, H. J.; Skibsted, J.; Nielsen, N. Chr. *J. Magn. Reson.* **2013**, 238, 20.
- (194) Sakellariou, D.; Hugon, C.; Guiga, A.; Aubert, G.; Cazaux, S.; Hardy, P. *Magn. Reson. Chem.* **2010**, 48, 903.
- (195) Hugon, C. Rotating permanent magnets: Towards MAS NMR/MRI on a static sample. *ICMRM11*, Beijing, China, August, 2011.
- (196) Styles, P.; Soffe, N. F.; Scott, C. A. *J. Magn. Reson.* **1989**, 84, 376.
- (197) Kovacs, H.; Moskau, D.; Spraul, M. P. *Prog. Nucl. Magn. Reson. Spectrosc.* **2005**, 46, 131.
- (198) Russel, D. J.; Hadden, C. E.; Martin, G. E.; Gibson, A. A.; Zens, A. P.; Carolan, J. L. *J. Nat. Prod.* **2000**, 63, 1047.
- (199) (a) Flynn, P. F.; Matiello, D. L.; Hill, H. D. W.; Wand, A. J. *J. Am. Chem. Soc.* **2000**, 122, 4823. (b) Hajdu, P. J.; Gerfin, T.; Boehlen, J.-M.; Häberli, M.; Marek, D.; Fesik, S. W. *J. Med. Chem.* **1999**, 42, 2315.
- (200) (a) Keun, H. C.; Beckonert, O.; Griffin, J. L.; Richter, C.; Moskau, D.; Lindon, J. C.; Nicholson, J. K. *Anal. Chem.* **2002**, 74, 4588. (b) Spraul, M.; Freund, A. S.; Nast, R. E.; Withers, R. S.; Maas, W. E.; Corcoran, O. *Anal. Chem.* **2003**, 75, 1546. (c) Hobo, F.; Takahashi, M.; Maeda, H. *Rev. Sci. Instrum.* **2009**, 80, 036106.
- (201) Darrase, L.; Ginefri, J.-C. *Biochimie* **2003**, 85, 915.
- (202) (a) Colell, J.; Türschmann, P.; Glöggler, St.; Schleker, P.; Theis, T.; Ledbetter, M.; Budker, D.; Pines, A.; Blümich, B.; Appelt, St. *Phys. Rev. Lett.* **2013**, 110, 137602. (b) Hövener, J.-B.; Schwaderlapp, N.; Lickert, T.; Duckett, S. B.; Mewis, R. E.; Highton, L. A. R.; Kenny, S. M.; Green, G. G. R.; Leibfritz, D.; Korvink, J. G.; Hennig, J.; von Elverfeldt, D. *Nat. Commun.* **2013**, 4, 2946.
- (203) Schröder, L.; Lowery, T. J.; Hilty, C.; Wemmer, D. E.; Pines, A. *Science* **2006**, 314, 446.
- (204) (a) Fey, M.; Massin, C. EU Patent EP1918730 A1, 2006. (b) Avizonis, D.; Haner, L. R.; Michelin, G. M. EU Patent EP1680683 B1, 2003.
- (205) Eldridge, S. L.; Korir, A. K.; Merrywell, C. E.; Larive, C. K. *Adv. Chromatogr.* **2008**, 46, 351.
- (206) Silva Elipe, M. V. *Anal. Chim. Acta* **2003**, 497, 1.
- (207) (a) Kühnle, M.; Holtin, K.; Albert, K. *J. Sep. Sci.* **2009**, 32, 719. (b) Albert, K. NMR as a Chromatography Detector. In *Handbook of Spectroscopy*; Gauglitz, G., Vo-Dinh, T., Moore, D. S., Eds.; Wiley-VCH: Weinheim, 2010.
- (208) Kühnle, M.; Kreidler, D.; Holtin, K.; Czesla, H.; Schuler, P.; Schaal, W.; Schurig, V.; Albert, K. *Anal. Chem.* **2008**, 80, 5481.
- (209) Lindon, J. C.; Nicholson, J. K.; Wilson, I. D. *Prog. Nucl. Magn. Reson. Spectrosc.* **1996**, 29, 1.
- (210) Wilson, I. D.; Morgan, E. D.; Lafont, R.; Shockcor, J. P.; Lindon, J. C.; Nicholson, J. K.; Wright, B. *Chromatographia* **1999**, 49, 374.
- (211) Smallcombe, S. H.; Patt, S. L.; Keifer, P. A. *J. Magn. Reson., Ser. A* **1995**, 117, 295.
- (212) Bringmann, G.; Messer, K.; Wohlfarth, M.; Kraus, J.; Dumbuya, K.; Rückert, M. *Anal. Chem.* **1999**, 71, 2678.
- (213) Kim, H. K.; Choi, Y. H.; Verpoorte, R. *Trends Biotechnol.* **2011**, 29, 267.
- (214) Daykin, C. A.; Corcoran, O.; Hansen, S. H.; Björnsdottir, I.; Cornett, C.; Connor, S. C.; Lindon, J. C.; Nicholson, J. K. *Anal. Chem.* **2001**, 73, 1084.
- (215) Lin, Y.; Schiavo, S.; Orjala, J.; Vouros, P.; Kautz, R. *Anal. Chem.* **2008**, 80, 8045.
- (216) Glauser, G.; Guillarme, D.; Grata, E.; Boccard, J.; Thiocone, A.; Carrupt, P.; Veuthey, J.; Rudaz, S.; Wolfender, J. *J. Chromatogr., A* **2008**, 1180, 90.
- (217) (a) McGarry, J. F.; Ogle, C. A.; Brich, Z.; Loosli, H. R. *J. Am. Chem. Soc.* **1985**, 107, 1810. (b) Perrin, C. L.; Rivero, I. A. *Rev. Sci. Instrum.* **1999**, 70, 2173.
- (218) Khajeh, M.; Bernstein, M. A.; Morris, G. A. *Magn. Reson. Chem.* **2010**, 48, 516.
- (219) Hentschel, P.; Holtin, K.; Steinhauser, L.; Albert, K. *Chirality* **2012**, 24, 1074.
- (220) (a) Keifer, P. A.; Smallcombe, S. H.; Williams, E. H.; Salomon, K. E.; Mendez, G.; Belletire, J. L.; Moore, C. D. *J. Comb. Chem.* **2000**,

- 2, 151. (b) Brächer, A.; Hoch, S.; Albert, K.; Kost, H. J.; Werner, B.; von Harbou, E.; Hasse, H. *J. Magn. Reson.* **2014**, 242, 155.
- (221) Maiwald, M.; Fischer, H. H.; Kim, Y.; Albert, K.; Hasse, H. *J. Magn. Reson.* **2004**, 166, 135.
- (222) Dalitz, F.; Cudaj, M.; Maiwald, M.; Guthausen, G. *Prog. Nucl. Magn. Reson. Spectrosc.* **2012**, 60, 52.
- (223) Vilkner, T.; Janasek, D.; Manz, A. *Anal. Chem.* **2004**, 76, 3373.
- (224) Dittrich, P. S.; Tachikawa, K.; Manz, A. *Anal. Chem.* **2006**, 78, 3887.
- (225) West, J.; Becker, M.; Tombrink, S.; Manz, A. *Anal. Chem.* **2008**, 80, 4403.
- (226) Wensink, H.; Benito-Lopez, F.; Hermes, D. C.; Verboom, W.; Gardeniers, H. J. G. E.; Reinhoudt, D. N.; van den Berg, A. *Lab Chip* **2005**, 5, 280.
- (227) Ahola, S.; Casanova, F.; Perlo, J.; Münnemann, K.; Blümich, B.; Stafp, S. *Lab Chip* **2006**, 6, 90.
- (228) Harel, E.; Hilty, C.; Koen, K.; McDonnell, E.; Pines, A. *Phys. Rev. Lett.* **2007**, 98, 017601.
- (229) Ehrmann, K.; Pataky, K.; Stettler, M.; Wurm, F. M.; Brugger, J.; Besse, P.-A.; Popovic, R. S. *Lab Chip* **2007**, 7, 381.
- (230) (a) Victoria Gómez, M.; Reinhoudt, D. N.; Velders, A. H. *Small* **2008**, 4, 3179–1293. (b) Fratila, R. M.; Victoria Gómez, M.; Sýkora, S.; Velders, A. H. *Nat. Commun.* **2014**, 5, 3025.
- (231) Anders, J.; Chiaramonte, G.; SanGiorgio, P.; Boero, G. *J. Magn. Reson.* **2009**, 201, 239.
- (232) Anders, J.; SanGiorgio, P.; Deligianni, X.; Santini, F.; Scheffler, K.; Boero, G. *Magn. Reson. Med.* **2012**, 67, 290.
- (233) Anders, J.; SanGiorgio, P.; Boero, G. *J. Magn. Reson.* **2011**, 209, 1.
- (234) Trumbull, J. D.; Glasgow, I. K.; Beebe, D. J.; Magin, R. L. *IEEE Trans. Biomed. Eng.* **2011**, 47, 3.
- (235) (a) Sun, N.; Liu, Y.; Lee, H.; Weissleder, R.; Ham, D. *IEEE J. Solid-State Circuits* **2009**, 44, 1629. (b) Sun, N.; Yoon, T.; Lee, H.; Andress, W.; Weissleder, R.; Ham, D. *IEEE J. Solid-State Circuits* **2011**, 46, 342.
- (236) Sun, N.; Liu, Y.; Qin, L.; Lee, H.; Weissleder, R.; Ham, D. *Solid-State Electron.* **2013**, 84, 13.
- (237) (a) Tycko, R. *Nature* **2005**, 434, 966. (b) Yusa, G.; Muraki, K.; Takashina, K.; Hashimoto, K.; Hirayama, Y. *Nature* **2005**, 434, 1001.
- (238) “Even more portable NMR”: <http://www.spectroscopynow.com/details/ezine/sepspec11387ezine/Even-more-portable-NMR.html>.
- (239) Ciobanu, L.; Webb, A. G.; Pennington, C. H. *Prog. Nucl. Magn. Reson. Spectrosc.* **2003**, 42, 69.
- (240) Reckel, S.; Hänsel, R.; Löhr, F.; Dötsch, V. *Prog. Nucl. Magn. Reson. Spectrosc.* **2007**, 51, 91.
- (241) (a) Serber, Z.; Keatinge-Clay, A. T.; Ledwidge, R.; Kelly, A. E.; Miller, S. M.; Dötsch, V. *J. Am. Chem. Soc.* **2001**, 123, 2446. (b) Wieruszkeski, J.-M.; Bohin, A.; Bohin, J.-P.; Lippens, G. *J. Magn. Reson.* **2001**, 151, 118.
- (242) Serber, Z.; Dötsch, V. *Biochemistry* **2001**, 40, 14317.
- (243) (a) Burz, D. S.; Dutta, K.; Cowburn, D.; Shekhtman, A. *Nat. Methods* **2006**, 3, 91. (b) Philipp, S.; Wagner, G. *Nat. Methods* **2006**, 3, 80.
- (244) Inomata, K.; Ohno, A.; Tochio, H.; Isogai, S.; Tenno, T.; Nakase, I.; Takeuchi, T.; Futaki, S.; Ito, Y.; Hiroaki, H.; Shirakawa, M. *Nature* **2009**, 458, 106.
- (245) Maldonado, A. Y.; Burz, D. S.; Shekhtman, A. *Prog. Nucl. Magn. Reson. Spectrosc.* **2011**, 59, 197.
- (246) Issadore, D.; Min, C.; Liang, M.; Chung, J.; Weissleder, R.; Lee, H. *Lab Chip* **2011**, 11, 2282.
- (247) Renault, M.; Boxtel, R. T.; Bos, M. P.; Post, J. A.; Tommassen, J.; Baldus, M. *Proc. Natl. Acad. Sci. U.S.A.* **2012**, 109, 4863.
- (248) Reckel, S.; Lopez, J. J.; Löhr, F.; Glaubitz, C.; Dötsch, V. *ChemBioChem* **2012**, 13, 534.
- (249) (a) Terada, Y.; Kono, S.; Tamada, D.; Uchiumi, T.; Kose, K.; Miyagi, R.; Yamabe, E.; Yoshioka, H. *Magn. Reson. Med.* **2013**; DOI: 10.1002/mrm.24439. (b) Terada, Y.; Kono, S.; Ishizawa, K.; Inamura, S.; Uchiumi, T.; Tamada, D.; Kose, K. *J. Magn. Reson.* **2013**, 230, 125.
- (250) Shirai, T.; Haishi, T.; Utsuzawa, S.; Matsuda, Y.; Kose, K. *Magn. Reson. Med. Sci.* **2005**, 4, 137.
- (251) Besheer, A.; Caysa, H.; Metz, H.; Müller, T.; Kressler, J.; Mader, K. *Int. J. Pharm.* **2011**, 417, 196.
- (252) McDonald, P. J.; Akhmerov, A.; Backhouse, L. J.; Pitts, S. *J. Pharm. Sci.* **2005**, 94, 1850.
- (253) Casanova, F.; Perlo, J.; Blümich, B. Depth profiling by single-sided NMR. In *NMR Imaging in Chemical Engineering*; Stafp, S., Han, S.-I., Eds.; Wiley-VCH Verlag: Weinheim, 2006; pp 107–123.
- (254) Ciampi, E.; van Ginkel, M.; McDonald, P. J.; Pitts, S.; Bonnist, E. Y. M.; Singleton, S.; Williamson, A.-M. *NMR Biomed.* **2011**, 24, 134.
- (255) van Landeghem, V.; Danieli, E.; Perlo, J.; Blümich, B.; Casanova, F. *J. Magn. Reson.* **2012**, 215, 74.
- (256) Rata, D. G.; Casanova, F.; Perlo, J.; Demco, D. E.; Blümich, B. *J. Magn. Reson.* **2006**, 180, 229.
- (257) Rössler, E.; Mattea, C.; Mollova, A.; Stafp, S. *J. Magn. Reson.* **2011**, 213, 112.
- (258) Haken, R.; Blümich, B. *J. Magn. Reson.* **2000**, 144, 195.
- (259) Fechete, R.; Demco, D. E.; Blümich, B.; Eliav, E.; Navon, G. *J. Magn. Reson.* **2003**, 162, 166.
- (260) Fullerton, G. D.; Cameron, I. L.; Ord, V. A. *Radiology* **1985**, 155, 433.
- (261) Blümich, B.; Kölker, C.; Casanova, F.; Perlo, J.; Felder, J. *Phys. Unserer Zeit* **2005**, 36, 236.
- (262) Dalitz, F.; Cudaj, M.; Maiwald, M.; Guthausen, G. *Prog. Nucl. Magn. Spectrosc.* **2012**, 60, 52.
- (263) (a) Mitchell, J.; Gladden, L. F.; Chandrasekera, T. C.; Fordham, E. *J. Prog. Nucl. Magn. Spectrosc.* **2013**, 76, 1. (b) Blümich, B.; Haber-Pohlmeier, S.; Zia, W. *Compact NMR*; Walter de Gruyter GmbH: Berlin/Boston, 2014. (c) Chen, J. J.; Kong, X.; Sumida, K.; Manumpil, M. A.; Long, J. R.; Reimer, J. A. *Angew. Chem. Int. Ed.* **2013**, 52, 12043. (d) Process NMR Associates, LLC, <http://www.process-nmr.com/process.htm>.
- (264) Blümller, P.; Blümich, B. *Rubber Chem. Technol.* **1997**, 70, 468.
- (265) Zimmer, G.; Guthausen, A.; Blümich, B. *Solid State Nucl. Magn. Reson.* **1998**, 12, 183.
- (266) Guthausen, G.; Guthausen, A.; Balibau, F.; Eymael, R.; Hailu, K.; Schmitz, U.; Blümich, B. *Macromol. Mater. Eng.* **2000**, 276/277, 25.
- (267) (a) Fechete, R.; Demco, D. E.; Blümich, B. *Macromolecules* **2002**, 35, 6083. (b) Voda, M. A.; Demco, D. E.; Perlo, J.; Orza, R. A.; Blümich, B. *J. Magn. Reson.* **2005**, 172, 78. (c) Valentín, J. L.; Mora-Barrantes, I.; Carretero-González, J.; López-Manchado, M. A.; Sotta, P.; Long, D. R.; Saalwächter, K. *Macromolecules* **2010**, 43, 334.
- (268) Kölz, J.; Martins, J.; Kremer, K.; Mang, T.; Blümich, B. *Kautsch. Gummi Kunstst.* **2007**, 60, 179.
- (269) Zimmer, G.; Guthausen, A.; Schmitz, U.; Saito, K.; Blümich, B. *Adv. Mater.* **1997**, 9, 987.
- (270) Gottwald, A.; Scheler, U. *Macromol. Mater. Eng.* **2005**, 290, 438.
- (271) Ratzsch, K.-F.; Kádár, R.; Naue, I. F. C.; Wilhelm, M. *Macromol. Mater. Eng.* **2013**, 298, 1124.
- (272) Danieli, E.; Berdel, K.; Perlo, J.; Michaeli, W.; Masberg, U.; Blümich, B.; Casanova, F. *J. Magn. Reson.* **2010**, 207, 53.
- (273) Blümich, B.; Casanova, F.; Perlo, J.; Anferova, S.; Anferov, V.; Kremer, K.; Goga, N.; Kupferschläger, K.; Adams, M. *Magn. Reson. Imaging* **2005**, 23, 197.
- (274) Blümich, B.; Adams-Buda, A.; Baias, M. *GWF, Gas/Erdgas* **2007**, 148, 95.
- (275) Adams, A.; Adams, M.; Blümich, B.; Kocks, H.-J.; Hilgert, O.; Zimmermann, S. *3R Int. Conf.* **2010**, 49, 216.
- (276) Blümich, B.; Casanova, F.; Buda, A.; Kremer, K.; Wegener, T. *Acta Phys. Pol. A* **2005**, 108, 13.
- (277) Kwamen, R.; Blümich, B.; Adams, A. *Macromol. Rapid Commun.* **2012**, 33, 943.
- (278) *Nuclear Magnetic Resonance Spectroscopy of Cement-Based Materials*; Colombet, P., Grimmer, A.-R., Zanni, H., Eds.; Springer-Verlag: Berlin, Heidelberg, 1998.
- (279) Marko, A.; Wolter, B.; Arnold, W. *J. Magn. Reson.* **2007**, 185, 19.

- (280) Blümich, B.; Haber, A.; Casanova, F.; Del Federico, E.; Boardman, V.; Wahl, G.; Stilliano, A.; Isolani, L. *Anal. Bioanal. Chem.* **2010**, *397*, 3117.
- (281) McDonald, P. J.; Aptaker, P. S.; Mitchell, J.; Mulheron, M. J. *Magn. Reson. 2007*, *185*, 1.
- (282) Prado, P. J. *Magn. Reson. Imaging* **2001**, *19*, 505.
- (283) Díaz-Díaz, F.; de J. Cano-Barrita, P. F.; Balcom, B. J.; Solís-Nájera, S. E.; Rodríguez, A. O. *Sensors* **2013**, *13*, 15985–15999.
- (284) de J. Cano-Barrita, P. F.; Marble, A. E.; Balcom, B. J.; Garcia, J. C.; Mastikhin, I. V.; Thomas, M. D. A.; Bremner, T. W. *Cem. Concr. Res.* **2009**, *39*, 324.
- (285) Sharma, S.; Casanova, F.; Wache, W.; Segre, A.; Blümich, B. *Magn. Reson. Imaging* **2003**, *21*, 249.
- (286) McDonald, P. J.; Mitchell, J.; Mulheron, M.; Aptaker, P. S.; Korb, J. P.; Monteilhet, L. *Cem. Concr. Res.* **2007**, *37*, 303.
- (287) Marble, A. E.; Young, J. J.; Mastikhin, I. V.; Colpitts, B. G.; Balcom, B. J. U.S. Patent US7733091, 2010.
- (288) Capitani, D.; Di Tullio, V.; Proietti, N. *Prog. Nucl. Magn. Reson. Spectrosc.* **2012**, *64*, 29.
- (289) Blümich, B.; Casanova, F.; Perlo, J.; Presciutti, F.; Anselmi, C.; Doherty, B. *Acc. Chem. Res.* **2010**, *43*, 761.
- (290) Proietti, N.; Capitani, D.; Rossi, E.; Cozzolio, S.; Segre, A. L. *J. Magn. Reson.* **2007**, *186*, 311.
- (291) Rühli, F. J.; Böni, T.; Perlo, J.; Casanova, F.; Baias, M.; Egarter, E.; Blümich, B. *J. Cult. Heritage* **2007**, *8*, 257.
- (292) Rascher, U.; Blossfeld, S.; Fiorani, F.; Jahnke, S.; Jansen, M.; Kuhn, A. J.; Matsubara, S.; Märtin, L. L.; Merchant, A.; Metzner, R.; Müller-Linow, M.; Nagel, K. A.; Pieruschka, R.; Pinto, F.; Schreiber, C. M.; Temperton, V. M.; Thorpe, M. R.; van Dusschoten, D.; van Volkenburgh, E.; Windt, C. W.; Schurr, U. *Funct. Plant Biol.* **2011**, *38*, 968.
- (293) Geya, Y.; Kimura, T.; Fujisaki, H.; Terada, Y.; Kose, K.; Haishi, T.; Gemma, H.; Sekozawa, Y. *J. Magn. Reson.* **2013**, *226*, 45.
- (294) Jones, M.; Aptaker, P. S.; Cox, J.; Gardiner, B. A.; McDonald, P. J. *J. Magn. Reson.* **2012**, *218*, 133.
- (295) van As, H.; Reinders, J. E. A.; de Jager, P. A.; van de Sanden, P. A. C. M.; Schaafsma, T. J. *J. Exp. Bot.* **1994**, *45*, 61.
- (296) Metz, H.; Mäder, K. *Int. J. Pharm.* **2008**, *364*, 170.
- (297) Malaterre, V.; Metz, H.; Ogorka, J.; Gurny, R.; Loggia, N.; Mäder, K. *J. Controlled Release* **2009**, *133*, 31.
- (298) (a) Guthausen, G.; Kamrowski, A. Developments in time domain and single sided NMR, review. In *9th International Conference on Applications of Magnetic Resonance in Food Science*; Guojonsdottir, M., Belton, P., Webb, G. A., Eds.; RSC Publisher: Nordic House, Reykjavik, Iceland, 2008; p 46. (b) Corver, J.; Guthausen, G.; Kamrowski, A. *Pharm. Eng.* **2005**, *25*, 18.
- (299) Kloza, M.; Schmalbein, D.; Maier, D. U.S. Patent US7397247, 2008.
- (300) Hills, B. *Magnetic Resonance Imaging in Food Science*; Wiley: New York, 1998.
- (301) McCarthy, M. J. *Magnetic Resonance Imaging in Foods*; Chapman & Hall: New York, 1995.
- (302) *Modern Magnetic Resonance Part 3: Application to Materials Science and Food Science*; Webb, G. A., Ed.; Springer: Dordrecht, 2006.
- (303) *Magnetic Resonance in Food Science: An Exciting Future*; Renou, J. P., Belton, P. S., Webb, G. A., Eds.; The Royal Society of Chemistry: Cambridge, 2011.
- (304) Maciel, G. A. NMR in Industrial Process Control and Quality Control. In *Nuclear Magnetic Resonance in Modern Technology*; Maciel, G. A., Ed.; Springer: Netherlands, 1994; pp 225–275.
- (305) van Duynhoven, J. P. M.; Goudappel, G. J. W.; van Dalen, G.; van Bruggen, P. C.; Blonk, J. C. G.; Eijkelenboom, A. P. A. M. *Magn. Reson. Chem.* **2002**, *40*, S51.
- (306) van Duynhoven, J.; Voda, A.; Witek, M.; van As, H. *Annu. Rep. NMR Spectrosc.* **2010**, *69*, 145.
- (307) Milczarek, R. R.; McCarthy, M. J. Low-Field MR Sensors for Fruit Inspection. In *Magnetic Resonance Microscopy Spatially Resolved NMR Techniques and Applications*; Codd, S. L., Seymour, J. D., Eds.; Wiley-VCH: Weinheim, 2008; pp 289–301.
- (308) Voda, M. A.; van Duynhoven, J. *Trends Food Sci. Technol.* **2009**, *20*, 533.
- (309) Tanner, J. E.; Stejskal, E. O. *J. Chem. Phys.* **1968**, *49*, 1768.
- (310) Murday, J. S.; Cotts, R. M. *J. Chem. Phys.* **1968**, *48*, 4938.
- (311) Manz, B.; Gladden, L. F.; Warren, P. B. *AIChE J.* **1999**, *45*, 1845.
- (312) Barzykin, V. *J. Magn. Reson.* **1999**, *139*, 342.
- (313) Lingwood, I. A.; Chandrasekera, T. C.; Kölz, J.; Fridjonsson, E. O.; Johns, M. L. *J. Magn. Reson.* **2012**, *214*, 281.
- (314) Skloss, T. W.; Kim, A. J.; Haw, J. F. *Anal. Chem.* **1994**, *66*, 536.
- (315) Linck, Y. G.; Killner, M. H. M.; Danieli, E.; Blümich, B. *Appl. Magn. Reson.* **2013**, *44*, 41.
- (316) Nordon, A.; Diez-Lazaro, A.; Wong, C. W. L.; McGill, C. A.; Littlejohn, D.; Weerasinghe, M.; Mamman, D. A.; Hitchman, M. L.; Wilkie, J. *Analyst* **2008**, *133*, 339.
- (317) Küster, S. K.; Danieli, E.; Blümich, B.; Casanova, F. *Phys. Chem. Chem. Phys.* **2011**, *13*, 13172.
- (318) Vargas, M. A.; Cudaj, M.; Hailu, K.; Sachsenheimer, K.; Guthausen, G. *Macromolecules* **2010**, *43*, 5561.
- (319) Hailu, K.; Guthausen, G.; Becker, W.; König, A.; Bendfeld, A.; Geissler, E. *Polym. Test.* **2010**, *29*, 513.
- (320) (a) Vargas, M. A.; Sachsenheimer, K.; Guthausen, G. *Polym. Test.* **2012**, *31*, 127. (b) Cudaj, M.; Guthausen, G.; Hofe, T.; Wilhelm, M. *Macromol. Chem. Phys.* **2012**, *213*, 1933.
- (321) Litvinov, V.; Dias, A. A. *Macromol. Symp.* **2005**, *230*, 20.
- (322) Mitchell, J.; Blümler, P.; McDonald, P. J. *Prog. Nucl. Magn. Reson. Spectrosc.* **2006**, *48*, 161.
- (323) Danieli, E.; Blümich, B. *J. Magn. Reson.* **2013**, *229*, 142.
- (324) Litvinov, V. M.; De, P. P. *Spectroscopy of Rubbers and Rubbery Materials*; Rapra Technology Ltd.: Shawbury, UK, 2002.
- (325) Magritek Spinsolve benchtop NMR spectrometer, <http://www.magritek.com/products-spinsolve>.
- (326) Thermo Scientific picoSpin NMR Spectrometer, <http://www.picospin.com>.
- (327) Nanalysis NMReady benchtop NMR spectrometer, <http://www.nanalysis.com>.
- (328) Oxford Instruments, <http://www.oxford-instruments.com/pulsarnmr>.